NASA Contractor Report 3975

Natural Laminar Flow Flight Experiments on a Swept Wing Business Jet—Boundary Layer Stability Analyses

R. A. Rozendaal

GRANT NAG1-401
MAY 1986

NASA Contractor Report 3975

Natural Laminar Flow Flight Experiments on a Swept Wing Business Jet—Boundary Layer Stability Analyses

R. A. Rozendaal
Boeing Commercial Airplane Company
Seattle, Washington

Prepared by Boeing Commercial Airplane Company
for Wichita State University for
NASA Langley Research Center
under Grant NAG1-401

National Aeronautics
and Space Administration

**Scientific and Technical
Information Branch**

1986

CONTENTS

FIGURES

FIGURES

1.0 SUMMARY

An important question facing the designers of efficient, high performance aircraft is whether the potential advantage of laminar flow can be realized. Advances in materials technology, most notable the maturing of composite applications, indicate that the surface smoothness requirements for laminar flow are now attainable. However, there are only limited data available on the effects of wing sweep, Reynolds number, Mach number, and pressure distribution shape on transition behavior and location.

The objective of this experiment was to develop and use hot film devices to measure transition on a Cessna Citation III business jet at various flight conditions and correlate the results with linear boundary layer stability analyses. These results would provide valuable additional data in establishing criteria for use in designing high-performance swept wings that promote long runs of laminar flow.

This document describes the method and gives the results of the boundary layer stability analyses of 18 conditions flown during the flight tests. The transition point varied from 5% to 35% chord for these conditions, and both upper and lower wing surfaces were included. Altitude varied from 10,000 to 43,000 ft and Mach number from 0.3 to 0.8. Four cases were at nonzero sideslip.

Although there is much scatter in the results, the analyses of boundary layer stability at the 18 conditions led to some of the same conclusions as those from the earlier F-111 laminar flow glove flight tests. The three upper surface cases that involved sideslip showed that crossflow and Tollmien-Schlichting disturbances may interact and reduce the maximum amplification of either isolated disturbance that can be tolerated without causing transition. However, the majority of the results indicated that crossflow instabilities were the primary cause of transition in these tests; the crossflow amplification factors were scattered around 5 at transition while Tollmien-Schlichting amplification factors varied from 0 to 8. The lower surface shows much lower Tollmien-Schlichting amplification at transition than the upper surface, but similar crossflow amplifications. No relationship between Mach number and disturbance amplification at transition could be found. The quality of these results is uncertain because of questionable wing surface quality, inadequate density of transition sensors on the wing upper surface, and an unresolved pressure shift in the wing pressure data.

The results of this study show the need for careful preparation for transition experiments. Preparation should include flow analyses of the test surface, boundary layer disturbance amplification analyses, and assurance of adequate surface quality in the test area. The placement of necessary instruments and usefulness of the resulting data could largely be determined during the pretest phase.

2.0 INTRODUCTION

2.1 BACKGROUND AND OBJECTIVES

An important question facing the designers of efficient, high-performance aircraft is whether the potential advantage of laminar flow can be realized. Advances in materials technology, most notable the maturing of composite applications, indicate that the surface smoothness requirements for laminar flow are now attainable. However, there are only limited data available on the effects of wing sweep, Reynolds number, Mach number, and pressure distribution shape on transition behavior and location. Reference 1 reports results of a study of sweep effect on transition location for a range of Reynolds numbers, but at a Mach number less than 0.3. Transition locations from several general aviation aircraft flight tests are reported in reference 2 and include a good range of Mach, Reynolds number, and wing sweep. Neither of these references involves a correlation of actual transition locations obtained with the anticipated growth of boundary layer instabilities. This connection was made in a NASA EET sponsored flight test of a natural laminar flow glove on the F-111 TACT aircraft. Linear stability analyses were correlated with transition locations inferred from boundary layer measurements in an attempt to establish transition criteria which could be used for Natural Laminar Flow (NLF) wing design. Reference 3 explains the results and methods used in that program. However, the determination of transition location by measuring the boundary layer profile after transition introduces an uncertainty into the work of reference 3. Recently, experimentation with hot film devices has provided a new tool for sensing transition.

The objective of this experiment was to develop and use hot film devices to measure transition on a high-performance business jet at various flight conditions and correlate the results with linear stability analyses such as those used in reference 3. These results would provide valuable additional data in establishing criteria for use in designing high-performance swept wings which promote long runs of laminar flow.

2.2 APPROACH

The aircraft used in this experiment was the Cessna Citation III (Model 650). This aircraft has a quarter chord sweep of 25 deg and is capable of operation up to Mach 0.8 and altitudes over 45,000 ft. A wing area 5 ft in span and 60% in chord was smoothed with fiberglass and filler to eliminate the roughness of fasteners and joints. No attempt was made to alter the shape of the wing sections.

To determine the pressure distribution on the test area, flights were made with three pressure belts: one on each side of the test area and one in the center. On later flights, the center belt was removed and replaced with a series of hot film transition-sensing gages. The correlation of the pressure distributions from the outer belts with the middle belt distribution was used to infer the pressure distribution over the transition sensors for the second series of flights. The flight test conditions ranged from 10,000 to 43,000 ft and from Mach 0.3 to 0.8, and positive and negative sideslip was also flown.

The flight conditions and wing pressure data were recorded on Cessna Aircraft digital flight-recording equipment. The hot film signals were also recorded on the same magnetic tape on analog tracks. Signals from several of the hot films could be monitored simultaneously in flight with oscillographs. Data reduction and hot film signal processing occurred at a ground station.

Examination of the hot film data led to the selection of conditions which received detailed analysis. The transition location and corresponding wing pressure distributions for the selected flight condition were used to determine the boundary layer instability growth up to the transition point. A finite-element infinite swept wing boundary layer analysis code was used in this process. These boundary layer parameters were then used in a linear stability analysis code, which calculated the growth of both Tollmien-Schlichting and crossflow disturbance modes. Plots of the disturbance growth that occurred before transition give an indication of the amount of growth which could occur on other wings (new designs) before transition occurred (i.e., a transition criterion).

3.0 SYMBOLS AND ABBREVIATIONS

Acronyms

CF	crossflow
NLF	natural laminar flow
TS	Tollmien-Schlichting
WBL	wing butt line

Symbols

A	disturbance amplitude
A_o	disturbance amplitude at neutral stability point
c	chord
C_p	wing streamwise pressure coefficient
c_f	surface friction coefficient
c_l	section lift coefficient
c_n	section normal force coefficient
c_p	section pressure coefficient
H	altitude
h	height of surface above mean profile
M	Mach number
N	disturbance amplification factor ($\ln A/A_o$)
Re_1	unit Reynolds number
$Re_{\theta_{a.l.}}$	attachment line Reynolds number based on boundary layer momentum thickness
$r_{l.e.}$	leading-edge radius of a wing section
S	estimate of standard deviation
s	distance measured along a surface
W	aircraft weight
x	distance measured along the chord line
z	distance measured perpendicular to the chord line
$\alpha^*_{r_s}$	component of dimensional wavenumber in the direction of wing sweep
δ	boundary layer thickness
Λ	wing sweep angle
λ	wavelength

$\tau_{ell.}$	thickness ratio of the ellipse that best fits the wing section shape at the leading edge
ψ	disturbance propagation angle, relative to local potential flow direction, positive toward wing outboard
ω	disturbance frequency

Subscripts

a	average
c	chordwise
n	normal to the sweep
T	at boundary layer transition
∞	freestream conditions

4.0 FLIGHT TEST PRESSURE DATA ANALYSES

4.1 METHOD OF ANALYSIS

The boundary layer stability analysis of the flight test data in the present study requires a detailed knowledge of the boundary layer parameters on the wing section of interest, especially near the leading edge. Since these could not be measured practically, they were calculated by a boundary layer code. The boundary layer code used a finite difference formulation to calculate laminar or turbulent boundary layers on two-dimensional, axisymmetric, or infinite swept bodies. As input, the program requires certain freestream and geometry parameters and the pressure distribution on the body or wing. Since a foundation of the stability analysis is the pressure distribution, an accurate and detailed knowledge of the pressure distribution was important in this study.

As mentioned previously, the first series of test flights measured pressure distributions at three sections in the test area: WBL 111, 141, and 171. The primary section of interest, 141, was bracketed by the other two so that when the middle pressure belt was removed for the transition-sensing flights, the two outside belts could give an indication of the pressure at the primary section. At each flight condition of interest, several complete pressure distributions for each section were taken. These data were reduced to pressure coefficients, and all distributions for each flight condition and wing section were plotted together. Any obviously incorrect data points were apparent on these plots; after eliminating them, the remaining points from each wing pressure orifice were averaged. This resulted in one pressure distribution per flight condition for each wing section, as well as an indication of the variation in the distribution that might occur while trying to hold the flight condition. The relationship between the pressure distributions of the two outside sections (WBL 111 and 171) and that of the primary section (WBL 141) was one of the guides in determining the pressure distributions for the primary section during the later transition-sensing flights. The pressure measured on the primary section during the pressure flights could not be used directly on the later transition-sensing flights because the flight weights were not the same and the accuracy and detail of the measured distribution was not adequate.

A general layout of the instrumentation arrangement for this study is shown in figure 1. Three scanivalves were used to measure wing section pressures, and a detailed description of the components and their function is in reference 4.

Another guide to determining the pressure distributions of the primary section was two-dimensional transonic flow analyses of the primary section's airfoil shape. The forward 60% of this airfoil was determined by careful measurements taken after the flight test. Since transition occurred near the leading edge for almost all flight conditions, it was important to have a fine resolution of the pressures near the leading edge. The computer analysis was a better method of finding these details than interpolating from the measured wing pressures on the sides of the test area.

Using these theoretical results and the measured pressure distributions from the outside sections during the transition-sensing flights led to the pressure distributions to be used for the boundary layer analyses.

4.2 PRESSURE DATA RESULTS

The method of taking wing pressure data during this study resulted in a large amount of data. As many as 25 individual pressure distributions for each of the three wing sections at one flight condition were obtained. Averaging these distributions was appropriate in order to reduce the volume of data and because of the small degree of scatter in the pressures at each flight condition. Figure 2 shows a set of pressure distribution data consisting of 10 samplings for one of the flight conditions and each of the three wing sections. These data were taken in about 45 sec (10 pressure readings per second per scanivalve). The small amount of scatter is readily apparent. Estimates of standard deviation of pressure coefficient, S_{Cp}, at a given test condition, which were calculated during the pressure averaging process, were generally less than 0.005. In areas where the pressure was very sensitive to flight condition, such as near the wing leading edge and near shocks, the S_{Cp} rose to about 0.02. The few cases of interruption of the flow of data, due to reasons which were not determined, were easily spotted by looking at the estimates of standard deviation. Those few points were then averaged manually. There were a few pressure orifices on the wing belts which gave incorrect readings (fig.2), and these were omitted from further processing. Figure 3 shows the averaged pressure coefficient data for wing sections 111, 141, and 171 from the pressure-measuring flights. These graphs were used as a guide to establish the difference in pressure distributions between the test section (WBL 141) and the outside sections.

The three-dimensional boundary layer and stability codes are set up to operate on a *normal* (perpendicular to the sweep) section of the wing. Therefore, the streamwise pressure data from the transition-sensing flights were transformed into normal pressure coefficients by dividing the averaged C_p's by the cosine squared of the local wing sweep angle (simple sweep theory). Figures 4 to 21 show the resulting averaged, then "normalized", pressure coefficient data from wing sections 111 and 171 for all cases analyzed during the transition-sensing flights. Table 1 outlines the streamwise conditions for each of the 18 cases selected for stability analysis.

A two-dimensional transonic viscous airfoil analysis code (ref. 5) also played an important part in determining the pressure distribution to be used in the boundary layer stability analyses. The airfoil coordinates to use with the two-dimensional analyses came from two sources. Over the front 60% of the chord, a detailed and accurate measurement of the wing at WBL 141 was made after the flight tests. Aft of this area the coordinates of the wing design loft were used initially. These two sets of coordinates were combined smoothly, and this airfoil was then scaled up by $1/\cos \Lambda$ to account for the streamwise to normal transformation (simple sweep theory). The sweep used here and later for the stability analyses was 26.6 deg, which is the wing sweep at about 7.5% chord. This value was chosen because most of the transition points during this study were between 5% and 15% chord. This scaled up airfoil could now be analyzed by the two-dimensional code using *normal* Mach number and lift coefficient for any of the cases and the results compared to the "normalized" flight data for that case. This procedure showed that the airfoil first used for the analyses had too much aft camber, resulting in too little lift being carried forward. Several variations in the airfoil shape were tried, some of which had extended chords to simulate a separation bubble, since wing pressures near the trailing edge are low, indicating separation. The one that was most successful and used for the remainder of the study was the first airfoil used with a small amount of the lower surface cusp filled in, but no extended chord. Figure 22 shows a trace of this airfoil. Even after the airfoil was found which gave a chordwise lift distribution that compared well to the data, there was a pressure coefficient level shift between the theoretical analysis and data. This shift was similar to that which would arise from using an incorrect static pressure measurement during data reduction, but a careful review of the data acquisition and reduction procedure did not locate any errors. This shift in pressure coefficients was also evident when comparing the flight data with unpublished wind tunnel data from NASA Langley Research Center 8-ft Pressure Tunnel Test 795. The closest comparison possible

with the wind tunnel data was pressures from WBL 160 at $M_\infty = 0.70$. Figures 3m and 3n both show the comparison, since $M_\infty = 0.70$ falls between the Mach 0.68 and 0.725 flown during this program and shown on those figures. The sectional lift coefficient of the flight and wind tunnel data were within a few percent. The wind tunnel configuration did include the nacelles, so the shift was probably not caused by the presence of the nacelles or engine power setting, and an estimate of the body pressure field indicates a much smaller effect than the observed discrepancy. The c_p level shift was also not likely to be caused by translating the measured wing pressure coefficients to equivalent normal section pressure coefficients, which comes only from simple sweep theory. This procedure is used often at Boeing on wings of this class of sweep and taper with good results. Since no definite cause for the c_p discrepancy could be found, the theoretical pressures were shifted to best match the data for each of the 18 cases analyzed. This is illustrated in figure 4. Thus, the theory was only really used for interpolating the experimental pressure data.

To summarize, the "normal" section conditions used to calculate the theoretical pressure distributions to compare to the data were defined as:

- $M_n = M_\infty \cos(26.6)$
- $c_{l_n} \sim c_n/\cos^2(26.6)$
- Reynolds number was calculated based on M_n, test altitude, and a normal chord length of 5.42 ft.

Table 2 gives the normal section conditions for the 18 study cases.

Figures 4 to 21 also show the theoretical pressure distributions plotted with the corresponding normal section data for all 18 cases. The value of the shift necessary to match the two is reported for each. The irregularities in the theoretical distributions near the leading edge also appear in the curvature distribution of the WBL 141 airfoil definition. The apparent discrepancies between the data and theory arise because of the influence of the pressure flight data. Reviewing figure 3 points out that the middle section of the test area appears to have a slightly different section shape, and the greater density of pressure orifices also gives greater insight into the details of the rapid pressure decrease near the leading edge, which is a characteristic of this airfoil. The theoretical pressure distributions as shown in figures 4 to 21 are the distributions that were used in the infinite swept wing boundary layer code for the stability analyses.

Figure 23 summarizes the data analysis procedure from flight pressure data through boundary layer stability analysis.

5.0 BOUNDARY LAYER STABILITY ANALYSES

5.1 Stability Analysis Method

The method selected for analyzing boundary layer transition data in this study is based on linear boundary layer stability theory (ref.6 to 13). The basic premise of this method is that transition is caused by the amplification of initially small disturbances in the boundary layer. When the amplitude of the disturbance becomes sufficiently large, nonlinear effects cause transition to turbulent flow. Although the later stages of transition are beyond the scope of the theory, it still provides the best currently available basis for correlating transition data.

The use of stability theory for correlating transition data was first used in detailed calculations by Smith (ref.14), who found that the total theoretical amplification from the neutral point to the transition point was approximately e^9 for a large number of two-dimensional data. In principle, this discovery allowed transition to be predicted for any airfoil by computing the theoretical amplifications. This has been generally confirmed by later research, but the exponent has been found to range from 8 to 15. For swept wings, however, transition can occur much sooner than predicted by the e^9 method. It is now known that there are several types of instability that must be considered.

On a high-speed swept wing there are four basic types of laminar boundary layer instabilities to be considered (refs.1 and 15): (1) Tollmien-Schlichting (TS), (2) crossflow (CF), (3) Taylor-Goertler(TG), and (4) leading-edge attachment line stability.

Tollmien-Schlichting instability relates to the velocity profile in the local freestream direction. Amplification of TS disturbances is usually small or negative in regions of favorable pressure gradient and large in regions of adverse pressure gradient. For incompressible flow, the most unstable disturbance waves propagate in the freestream direction, but for compressible flows the waves may be oblique.

Crossflow instability refers to waves propagating in a direction nearly perpendicular to the local freestream direction. On swept wings, a crossflow develops within the boundary layer so that the profile of a velocity component in directions oblique to the local freestream has an inflection point. Such velocity profiles are highly unstable, so that crossflow instabilities may be dominant on swept wings. Boundary layer crossflow is most severe in the wing leading-edge and trailing-edge regions, where pressure gradients are largest.

Taylor-Goertler instability occurs in the flow over concave surfaces. Because the Cessna natural laminar flow (NLF) glove did not have concave surfaces in the region designed to have laminar flow, this type of instability was not considered in this study.

Attachment line instability refers to the behavior of the boundary layer along the forward stagnation or attachment line (i.e., the locus of points for which the chordwise velocity is zero). The boundary layer flow along the attachment line can be either laminar or turbulent depending on Reynolds number and environment, as described in reference 15. If the attachment line flow does become turbulent, the flow over the wing will be turbulent also. Detailed stability calculations are not used to assess attachment line instability; previous experimental studies have shown that if the attachment line momentum thickness Reynolds number is less than 100, the leading-edge flow will be laminar. In this study, the attachment line Reynolds number was somewhat below 100 at the transition test section.

The empirical determination of the allowable theoretical amplification factors for swept wings in flight is an objective of the present analysis. The rate by which a disturbance is amplified depends not only on the local flow conditions and boundary layer profile, but also on the disturbance frequency and propagation direction, so there are several possible variations of the process. The process used here is outlined below, and reference 3 contains details of the method as actually applied.

In situations in which both TS and CF instabilities are present, as in the present case, interactions may occur that cause earlier transition than if either was absent. Such interaction was evident in the F-111 laminar flow flight test, reference 3. Following Smith (ref.14), it is more common to work with the natural logarithm of the amplification factors rather than their actual values. The logs of the amplification factors are usually called N-factors. For the F-111 data, amplification factors for both modes were calculated, and each experimental transition point plotted on a the N_{TS} - N_{CF} plane as shown in figure 24. The shaded band representing the data gives an indication of the effect of such interactions. The data band of figure 24 can be used as a transition criterion. The transition data from the present study were analyzed in a similar manner to assess and improve the F-111 criterion.

The boundary layer temperature and velocity profiles, which are the primary output of the boundary layer code, became the primary input to the stability program, which is a Boeing modification of a computer program originated by L. M. Mack (ref. 16). This program solves the boundary layer stability equations for three-dimensional, linearized, parallel flow for a perfect gas and can calculate either Tollmien-Schlichting or crossflow stability. The program was used to calculate disturbance growth curves, such as those shown in figure 24.

The disturbance growth direction used to compute amplification factors was along the local potential flow streamline. Mack (ref. 11) determined that this was a satisfactory approximation to the actual growth direction, which is equal to the real part of the group velocity angle. The stability code can compute either incompressible or compressible stability. In the present study, compressible stability was used for all but one of the calculations. The sixth-order equations (which neglect dissipation) were used instead of the complete eighth-order equations. This use resulted in a significant reduction in computation time, and, as shown by Mack (ref. 11), results given by the sixth-order equations for a transonic swept wing differed from those of the eighth-order equations by only a few percentage points.

TS disturbances were followed downstream, keeping frequency and wave angle fixed. The wave angles changed from one case to the next and were determined by examining the change in amplification for different wave angles for each case. The angle was then chosen for each case to correspond closely to the angle for maximum disturbance amplification. For each case several frequencies were calculated to establish an envelope of TS amplification.

CF disturbances were followed downstream, keeping the frequency fixed and letting the wave angle vary in accordance with the irrotationality condition applied to the wavenumber vector, as proposed by Mack (ref. 11). The result of applying the irrotationality condition to an infinite swept wing analysis is that the spanwise (in the direction of the wing leading edge) component of the dimensional wavenumber, $\alpha^*_{r_s}$, must remain constant as the disturbance propagates downstream. Therefore, in defining the envelope of CF disturbances, disturbances having a range of $\alpha^*_{r_s}$ values are followed downstream. The frequency was kept at zero for this study, although zero frequency waves may not be the most highly amplified. This method of analysis is suggested by flow visualization of swept wing transition, which often shows streamwise striations indicating the presence of uniformly spaced streamwise vortices. The analysis just described corresponds to this flow model.

5.2 STABILITY ANALYSIS RESULTS

Eighteen cases (Table 1) were chosen for stability analysis from the large volume of flight data recorded during the transition flights. Most of the cases are from data taken at 30,000-ft altitude, cases 7 to 18, with four cases from 10,000 ft, cases 1 to 4, and only two from the high altitude of about 43,000 ft, cases 5 and 6. All cases were taken with the aircraft at near zero yaw except the last four cases. Cases 15 and 16 were taken at a negative yaw angle (nose right) and cases 17 and 18 at a positive yaw. Normal chord Reynolds number for the 18 cases ranged from a low of 5.42×10^6 at the high altitude, case 6, to a high of 13.8×10^6 at the low altitude, case 4. Normal Mach number ranged from 0.264 for cases 1 and 2 to 0.715 for case 14. Table 2 summarizes the normal flow conditions and calculated instability growth parameters, N_{TS} and N_{CF}, near the transition point for each of these cases.

The boundary layer analysis of case 1 indicated separation ($c_f = 0$) at a surface distance aft of the attachment line, s/c, of 0.0725. This is not surprising when one considers the strong pressure peak near the leading edge for this condition (fig. 4). The measured transition location for this case was at or ahead of x/c = 0.05, which is very close to an s/c of 0.09 for this condition. Therefore, it is likely that a laminar separation bubble caused the transition in this instance. Linear stability calculations would be of no use in predicting this mode of transition because the extremely adverse pressure gradient causes almost instantaneous growth in TS instability. Therefore, none were made for case 1. It is important to note here the significance of the difference between chordwise distance from the leading edge, x/c, and surface distance aft of the attachment line, s/c. The surface distance was used in the boundary layer analyses and subsequent stability analyses, whereas the transition gage locations were measured chordwise aft of the wing leading edge. Because the instability growth was rapid for many of the cases analyzed, it was important to know the transition gage locations with respect to the attachment line location for each case. Figure 25 shows a plot of s/c versus x/c with attachment line locations for the 18 cases.

For all cases except case 1, the boundary layer code did not predict laminar separation for at least 10% chord beyond the point where the transition was measured. The stability calculations were therefore meaningful for these cases and were carried out, when possible, to a point 5% to 10% chord aft of the point where transition was measured. For several cases, the crossflow instability calculations were difficult and could be completed only to about the point of transition. This occurred on upper surface cases where the pressure peak was followed by a rather strong adverse pressure gradient; figure 6, case 3, is an example. Figures 26 to 42 show instability growth plots for cases 2 through 18. Both Tollmien-Schlichting (TS) and crossflow (CF) disturbance growth factors (N) are plotted for each case in which there was growth. The strong favorable pressure gradient for the lower surface, cases 2 and 7, led to no TS growth before transition, and the other lower surface cases, 5, 6, 9, 13, 16, and 18, showed very little TS amplification. The TS amplification plots show the growth of disturbances of various frequencies, as well as the envelope of the growth. The wave angle used for the TS calculations for each case is noted. This angle was the one which gave the greatest N factors and was determined for each case by calculating the growth for different angles. For crossflow disturbance growth, the range of the value of spanwise wave numbers used in the calculation is noted on the N_{CF} - s/c plots. For crossflow zero frequency was always used (standing waves only), as described above.

The lower surface cases had strong favorable pressure gradients for the first 20% to 30% chord, so TS disturbance growth was insignificant except for cases 5 and 6, which had laminar runs of about 30%. For these lower surface cases, the CF disturbances were the ones to be more highly amplified, precisely because of the strong favorable pressure gradients in combination with the high wing sweep. The upper surface cases showed strong TS growth starting at about 5% to 6% chord. This was the area where the strong favorable gradient at the nose ended in a peak minimum pressure followed by an adverse gradient. For these cases the CF disturbances showed most of their growth in the first 5% to 8% chord and

were generally damped aft of there. Figures 43 and 44 show N_{TS} versus N_{CF} traces for cases 2 to 18 as the boundary layer grows aft of the attachment line. The dramatic growth in TS disturbances aft of s/c = 0.06 for the upper surface cases is easily seen in these plots.

The hot film transition sensors were located at 2.5% and 5% chord and then at every 5% chord back to 70% on the upper surface and 65% on the lower surface. From intermittancy data, which is described in reference 4, transition occurred rapidly, with each gage generally indicating either fully laminar ($\sim$ 15% intermittancy) or fully turbulent ($\sim$ 85% intermittancy) flow. On the traces of N_{TS} - N_{CF}, the location in s/c of the last gage that indicated laminar flow and the first gage that indicated turbulent flow can be noted. It can be said that transition occurs at a combination of TS and CF disturbance growths somewhere between these two points. These two points and the trace between them are plotted for each case in figures 45 and 46. Unfortunately, in general, there was a large difference in N-factors between the last laminar point and the first turbulent point, resulting in a poorly defined transition band. This was basically because transition generally occurred far forward where the N-factors grew rapidly in the short distances between the sensors.

Figure 45 is quite different in character from the F-111 data (fig. 24). One interpretation of this figure would be that crossflow instability was the primary cause of transition, with TS having little influence. For this highly swept wing, this may be the case. Figure 46 also supports that conclusion, but in this case there was almost no TS amplification. The three sideslip cases, 6, 8, and 10, did show some interaction (fig. 47) but much less than the F-111 data. The equivalent lower surface cases, 7, 9, and 11, still show no TS growth and little change of N_{CF} at transition for the different sweep angles. The low TS N-factors are the natural result of the lower surface pressure distribution and not inconsistent with the upper surface data. Transition generally occurs at N_{CF}'s of 4 to 6 for both surfaces.

Apparently low N_{TS} factors at transition for the lower surface were also noticed in the F-111 NLF glove flight test (ref. 3) (fig. 48). Again, the low TS values are due to the pressure distribution, but the real question is why the low N_{CF} at transition. The reason for these low values on the lower surface was not determined for that test, although noise contamination from the F-111 underwing inlet was a possibility.

Since transition generally occurred earlier than anticipated on the basis of the F-111 data, explanations were sought. Potential culprits are waviness and attachment line contamination, or unknown Mach number effects. Figure 49 shows a waviness trace taken from measurements of the wing profile at WBL 141. This trace was calculated by taking the perpendicular distance between the measured coordinates and a smoothed set of the same measured coordinates. The large spike near the leading edge is artificial and due to an error in reference points used during the wing measurement. The other waves shown in figure 49 may or may not present a problem for sustaining laminar flow. From reference 17 an acceptable wave criterion of

$$\frac{2h}{\lambda} \leqslant \left[\frac{59\,000\,(\cos^2\Lambda)}{\lambda\,Re_c^{1.5}} \right]^{1/2}$$

is established for single waves and one-third of this for multiple waves. Note the h as defined herein is half the amplitude as used in reference 17. For the most stringent flight condition (lowest altitude, highest speed), case 4, the allowable wave height, h, for multiple waves is about 0.0017 in for a 2-in wavelength or 0.0025 for a 5-in wavelength. The test surface meets this requirement only very marginally and definitely does not at a few sharp spikes like those at which s equals 50, 53, and 69 in; therefore, surface

waviness cannot be ruled out as a possible adverse influence on laminar flow during this study. If these waves produced initial disturbances in the boundary layer, perhaps the lower speed flow on the lower surface amplified them more, accounting for the low N_{TS} factors at transition on that surface.

As for attachment line contamination, the criterion is summarized in reference 15 as:

$$Re_{\theta_{a.l.}} \sim \frac{0.405 \sin \Lambda}{\sqrt{\cos \Lambda}} \sqrt{\frac{Re_{1_\infty}(r_{l.e._n})}{(1 + \tau_{ell.})}} < 90 \quad .$$

For this study, at the highest Re_{1_∞} (low altitude, high speed), case 4, the $Re_{\theta_{a.l.}}$ is about 90 according to this formula. These calculations indicate little possibility of a problem due to attachment line contamination and transition at the section where transition was measured. If the attachment line boundary layer becomes turbulent ahead of the line of transition gages, one would expect that all gages would register turbulence. However, if disturbances arose near, but on either side of the attachment line inboard of the transition gauge location, they could be convected outboard as they moved downstream. This would be more pronounced on the lower surface where the chordwise component of velocity is lower.

The data in this study were taken from Mach numbers of 0.3 to 0.8, but as shown in figure 50, the N-factors at transition from the boundary layer analyses show no obvious dependence on Mach number. The N_{CF} data show a definite grouping around 4 to 6, independent of Mach number, but the N_{TS} data show no discernable grouping.

6.0 CONCLUSIONS AND RECOMMENDATIONS

6.1 CONCLUSIONS

The analysis of the boundary layers and their stability for the 18 cases supplied to Boeing from the Citation III laminar flow flight test resulted in the following conclusions.

- The quality of the transition data from the hot film sensors during this study seems good. However, there are uncertainties which cloud the usefulness of the stability analyses. First is the lack of measured pressure data on the wing along the section where transition was measured, leading to heavy reliance on theoretically determined pressure distributions for the stability analyses. The shift that was necessary to match analytical and experimental wing section pressures was also never explained and may point to an error in the experimental pressures. Second, the rapid growth of TS disturbances on the upper surface made the 5% chord spacing of the hot films almost too sparse. Third, the quality of the surface in the area where transition was measured was marginal with regard to waviness and was not adequately surveyed. Although the attachment line Reynolds number was probably not too high, it would have been desirable to isolate the inboard leading edge from the leading edge in the test area.

With these reservations, the following results were obtained:

- Transition generally occurred sooner than expected on the basis of the reference 3 data.

- There is little evidence of an interaction between the TS and crossflow instabilities. Since such an interaction is to be expected, the three sideslip cases were examined separately. These data do show an interaction, but much weaker than for the F-111, and most of the cases indicate that crossflow instability apparently caused transition, independently of the magnitude of Tollmien-Schlichting instability growth.

- A wide range of Mach numbers was flown during these tests and no dependence on freestream Mach number could be determined for TS or CF N-factors at transition.

6.2 RECOMMENDATIONS

The results of this study point strongly toward the need for detailed preparation before conducting laminar flow experiments:

- The pressure distributions that will be encountered during the experiment should be determined and verified beforehand. This will influence:

    - whether the experiment will be useful without revisions.

    - whether a change in the wing section shape would make the experiment much more useful (decreasing the "peakiness" of the section in this study would have been very helpful).

    - the density and placement of instrumentation.

- The quality of the surface throughout the area where laminar flow may occur needs to be very high and verified before laminar flow testing begins. If practical, a good way to do this would be to use flow visualization at one or two of the more ambitious (high transition Reynolds number) test conditions.

- It would be very helpful to have pressure and transition measurements on the same surface simultaneously.

- Suitable density of transition sensors is necessary if the results are to be correlated with theoretical stability analyses.

- If a laminar flow experiment may involve high sweep angles, the span of the test area should be considerable, and the attachment line boundary layer inboard of the test area should be diverted so there is a fresh boundary layer on the attachment line in the test area.

- The results of this experiment call into question the existence of a well-defined transition boundary on the N_{TS} vs N_{CF} diagram. Additional analyses should be made of other possible correlations or other methods of applying the stability theory.

7.0 REFERENCES

1. Boltz, F. W., Kenyon, G. C., and Allen, C. Q., "Effects of Sweep Angle on the Boundary-Layer Stability Characteristics of an Untapered Wing at Low Speeds," NASA TN D-338, October 1960.

2. Holmes, B. J., and Obara, C. J., "Observations and Implications of Natural Laminar Flow on Practical Airplane Surfaces," Journal of Aircraft, Vol. 20, No. 12, December 1983.

3. Preliminary Design Dept., BCAC, "F-111 Natural Laminar Flow Glove Flight Test Data Analysis and Boundary Layer Stability Analysis," NASA CR-166051, January 1984.

4. Wentz, W.H., Jr., Ahmed, A., and Nyenhuis, R., Further Results of Natural Laminar Flow Flight Experiments, SAE Paper 850862, April 1985.

5. Bauer, F., Garabedian, P., Korn, D., and Jameson, A., "Supercritical Wing Sections II," Lecture Notes in Economics and Mathematical Systems, Springer-Verlag, New York, 1975.

6. Jaffe, N. A., Okamura, T. T., and Smith, A. M. O., "Determination of Amplification Factors and Their Application to Predicting Transition," AIAA Journal, Vol. 8, pp. 301-308, February 1970.

7. Mack, L. M., "Transition Prediction and Linear Stability Theory," presented at AGARD Fluid Dynamics Panel Symposium on Laminar Turbulent Transition, Copenhagen, Denmark, May 2-4, 1977.

8. Srokowski, A. J., and Orzag, S. A., "Mass Flow Requirements for LFC Wing Design," AIAA Paper 77-1222, AIAA Aircraft Systems and Technology Meeting, Seattle, WA, August 22-24, 1977.

9. Nayfeh, A. H., "Stability of Three-Dimensional Boundary Layers," AIAA Paper 79-0262, AIAA 17th Aerospace Sciences Meeting, New Orleans, LA, January 15-17, 1979.

10. Cebeci, T., and Stewartson, K., "On Stability and Transition in Three-Dimensional Flows," AIAA Paper 79-0263, AIAA 17th Aerospace Sciences Meeting, New Orleans, LA, January 15-17, 1979.

11. Mack, L. M., "On the Stability of the Boundary Layer on a Transonic Swept Wing," AIAA Paper 79-0264, AIAA 17th Aerospace Sciences Meeting, New Orleans, LA, January 15-17, 1979.

12. Lekoudis, S. G., "Stability of Three-Dimensional Compressible Boundary Layers Over Wings With Suction," AIAA Paper 79-0265, AIAA 17th Aerospace Sciences Meeting, New Orleans, LA, January 15-17, 1979.

13. Runyan, L. J. and George-Falvy, D., "Amplification Factors at Transition on an Unswept Wing in Free Flight and on a Swept Wing in Wind Tunnel," AIAA Paper 79-0267, AIAA 17th Aerospace Sciences Meeting, New Orleans, LA, January 15-17, 1979.

14. Smith, A. M. O., "Transition Pressure Gradient and Stability Theory," Proc. of the 9th Inter. Congress of Appl. Mech., Brussels, 1957, Vol. 4, pp. 234.

15. Pfenninger, W., "Flow Problems of Swept Low-Drag Suction Wings of Practical Construction at High Reynolds Numbers," Annals of the N.Y. Academy of Sciences, Vol. 154, Art. 2, pp. 672-703, November 1968.

16. Mack, L. M., "Computation of the Stability of the Laminar Compressible Boundary Layer," Methods in Computational Physics, edited by B. Adler, Academic Press, NY, pp. 247-299, 1965.

17. Northrop Corp., "Final Report on LFC Aircraft Design Data Laminar Flow Control Demonstration Program," NOR 67-136, June 1967.

Table 1 - Flight Conditions For Cases Analyzed

Case	Flight Number	M_∞	Altitude, ft	Weight, lb	Static Temperature, °F	Surface	x/c (First Turbulent Gage)	Sideslip, deg
1	1180	0.295	9965	16765	20	Upper	0.05	0
2	1180	0.295	9965	16765	20	Lower	0.10	0
3	1180	0.491	9980	16576	19	Upper	0.10	0
4	1180	0.538	9976	16060	18	Upper	0.05	0
5	1182	0.442	29918	15133	—	Lower	0.15	0
6	1182	0.632	29837	15411	-53	Upper	0.10	0
7	1182	0.632	29848	15377	-53	Lower	0.10	0
8	1182	0.631	29884	15034	-53	Upper	0.15	-3.2
9	1182	0.635	29848	14981	-52	Lower	0.15	-2.5
10	1182	0.635	29931	15004	-53	Upper	0.05	4.3
11	1182	0.631	29874	14962	-52	Lower	0.05	3.9
12	1182	0.679	29797	16093	-52	Upper	0.15	0
13	1182	0.724	29782	15523	-53	Upper	0.10	0
14	1182	0.771	29679	15863	-52	Upper	0.05	0
15	1182	0.770	29692	15816	-52	Lower	0.05	0
16	1182	0.799	29645	15703	-53	Upper	0.05	0
17	1181	0.581	42696	15871	-56	Lower	0.35	0
18	1181	0.680	42716	15589	-59	Lower	0.30	0

Table 2 - Stability Analysis Conditions and Results

Case	Surface	M_n	$Re_{c_n} \times 10^{-6}$	c_{l_n} (Used in Airfoil Analysis Code)	Λ (Used in Stability Analysis), deg	At First Turbulent Gage	
						N_{TS}	N_{CF}
1	Upper	0.264	7.60	0.850	26.6	—	—
2	Lower	0.264	7.60	0.850	26.6	0	5.1
3	Upper	0.439	12.60	0.406	26.6	8.65	6.0
4	Upper	0.482	13.80	0.338	26.6	1.75	6.05
5	Lower	0.396	6.10	0.840	26.6	0	6.05
6	Upper	0.566	8.67	0.475	26.6	7.15	3.15
7	Lower	0.566	8.67	0.475	26.6	0	4.6
8	Upper	0.579	8.89	0.448	23.4	8.05	2.3
9	Lower	0.579	8.89	0.448	24.1	0	4.35
10	Upper	0.544	8.40	0.514	30.9	2.25	5.4
11	Lower	0.544	8.40	0.450	30.5	0	4.4
12	Upper	0.601	10.90	0.450	26.6	7.4	3.8
13	Upper	0.648	9.92	0.388	26.6	3.75	5.35
14	Upper	0.689	10.57	0.350	26.6	0.25	4.65
15	Lower	0.689	10.57	0.350	26.6	0.4	5.2
16	Upper	0.715	10.80	0.353	26.6	0.2	4.9
17	Lower	0.520	4.82	0.944	26.6	0.8	7.85
18	Lower	0.609	5.40	0.722	26.6	0.5	6.05

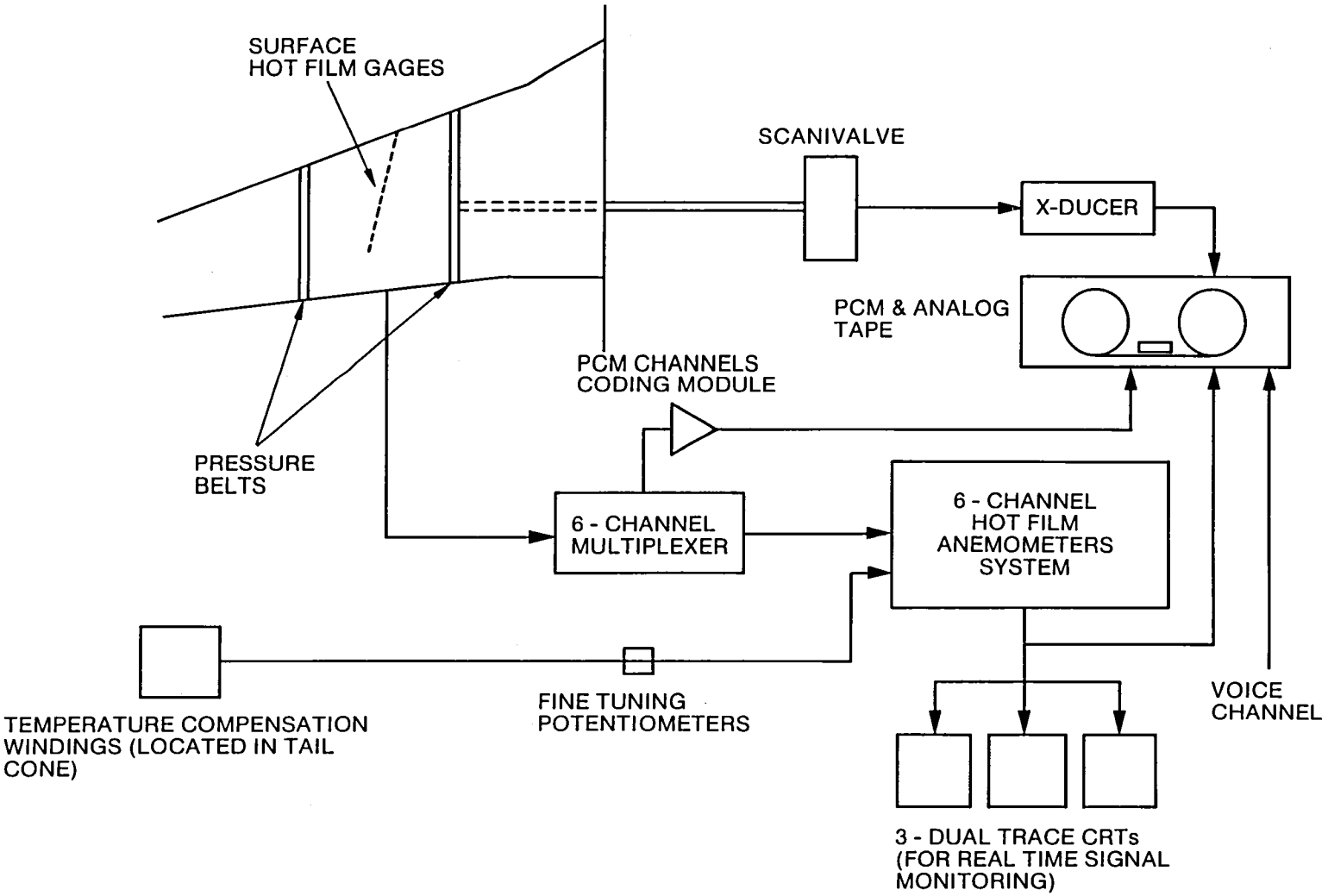

Figure 1 Instrumentation Layout

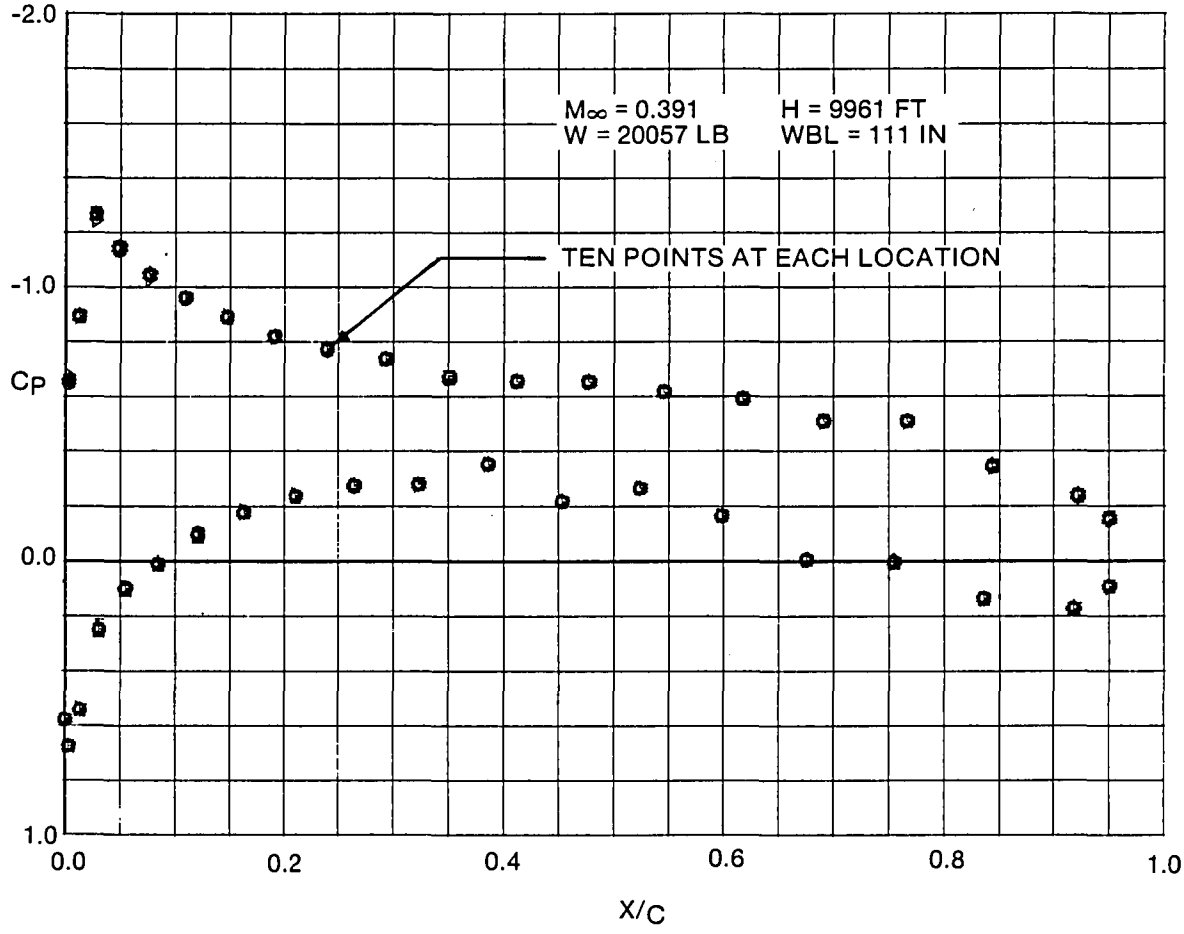

Figure 2a - Example of Citation III Wing Pressures

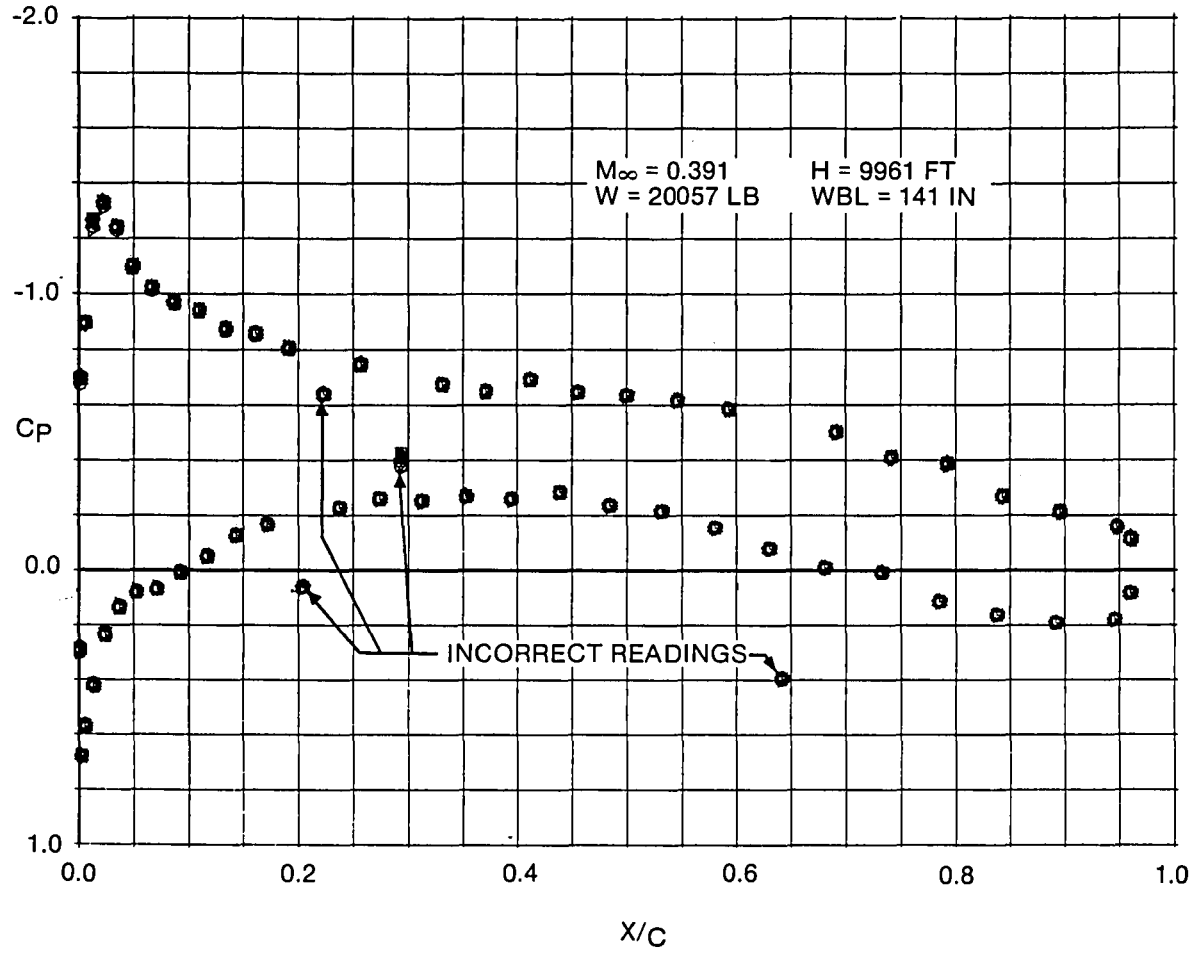

Figure 2b - Example of Citation III Wing Pressures

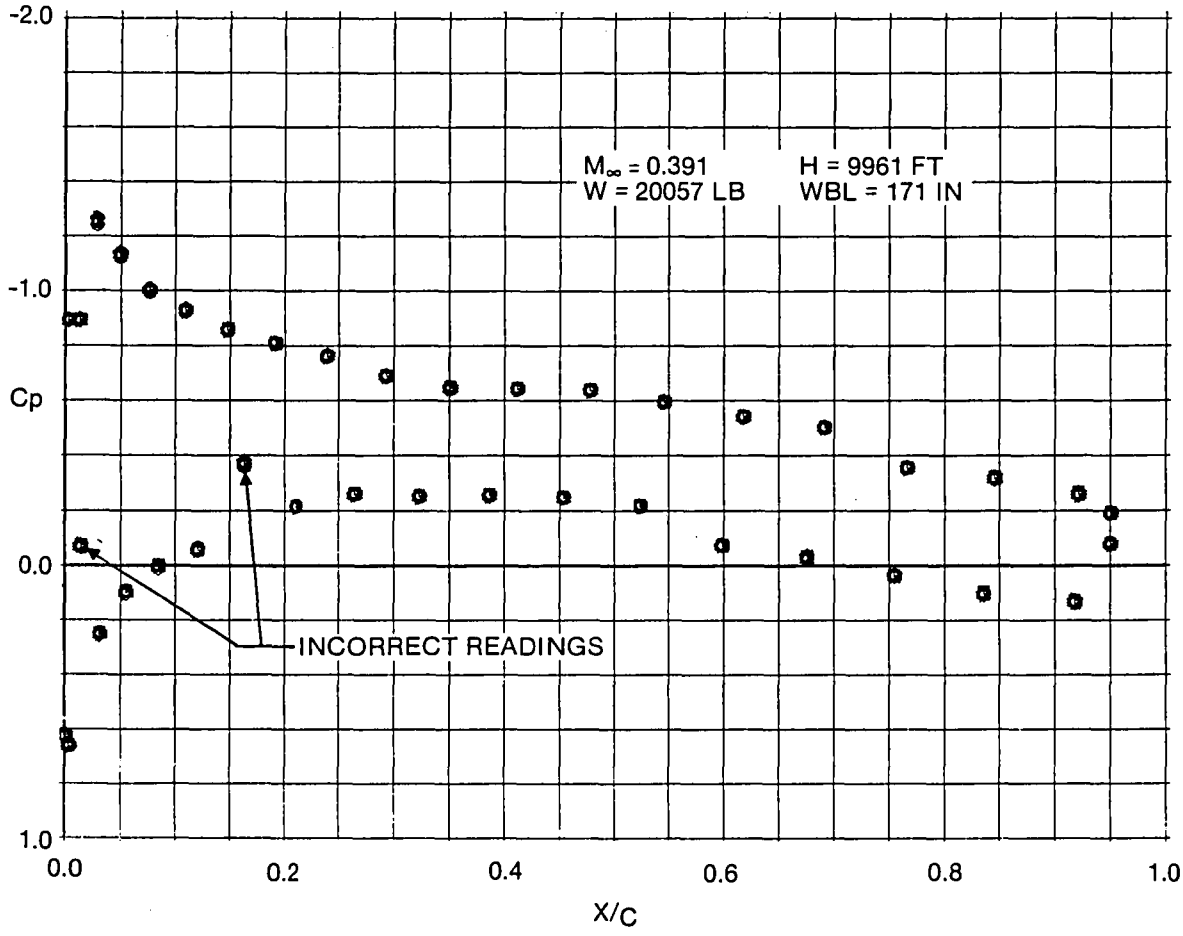

Figure 2c - Example of Citation III Wing Pressures

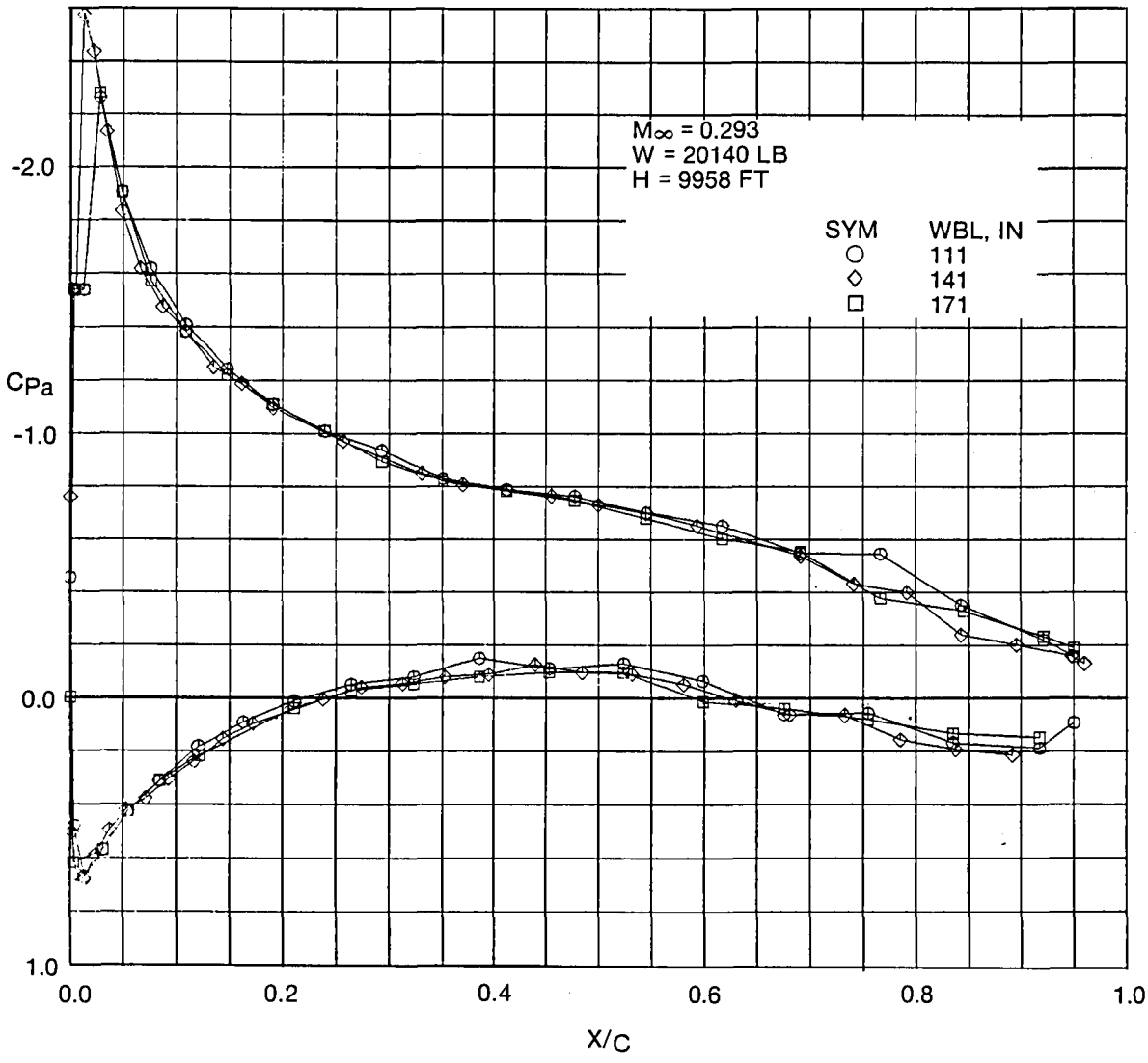

Fig. 3a Citation III Averaged Wing Pressures - Pressure Flights

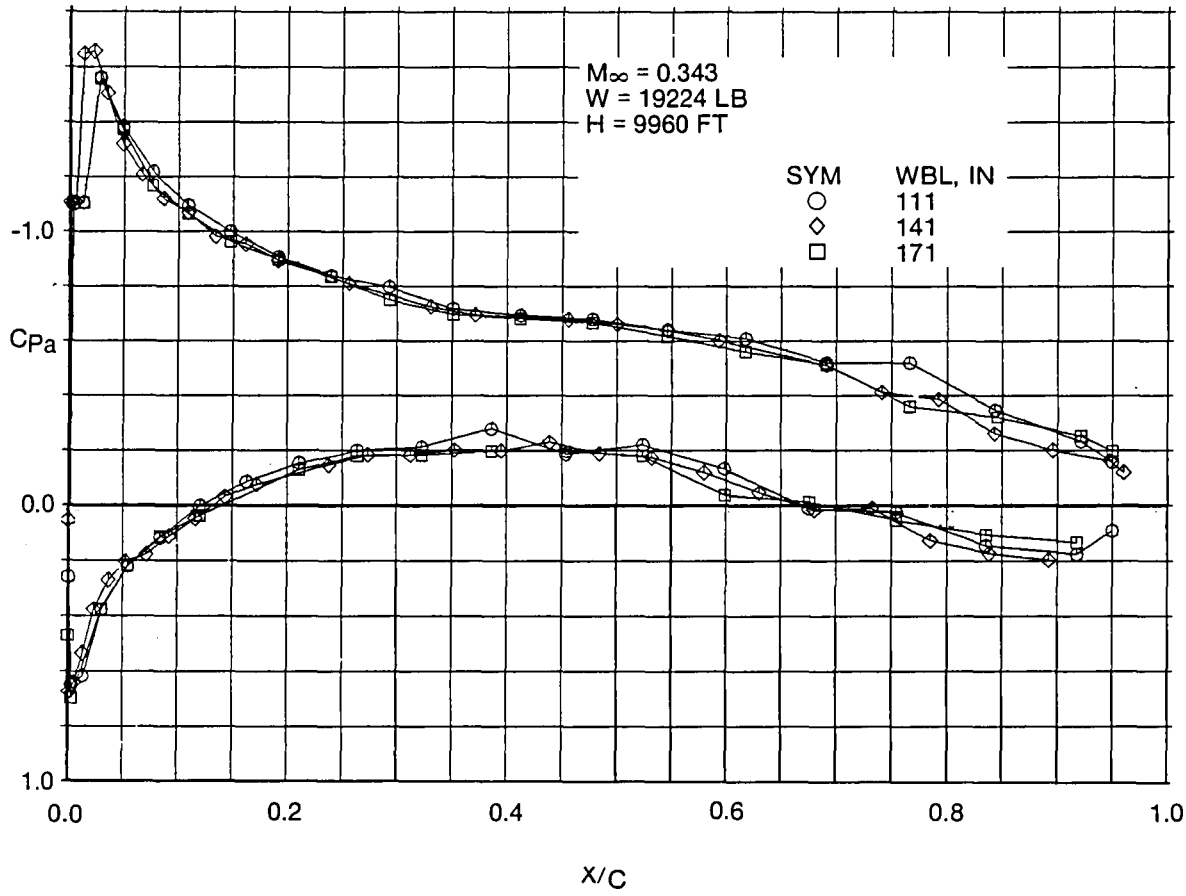

Fig. 3b Citation III Averaged Wing Pressures - Pressure Flights (continued)

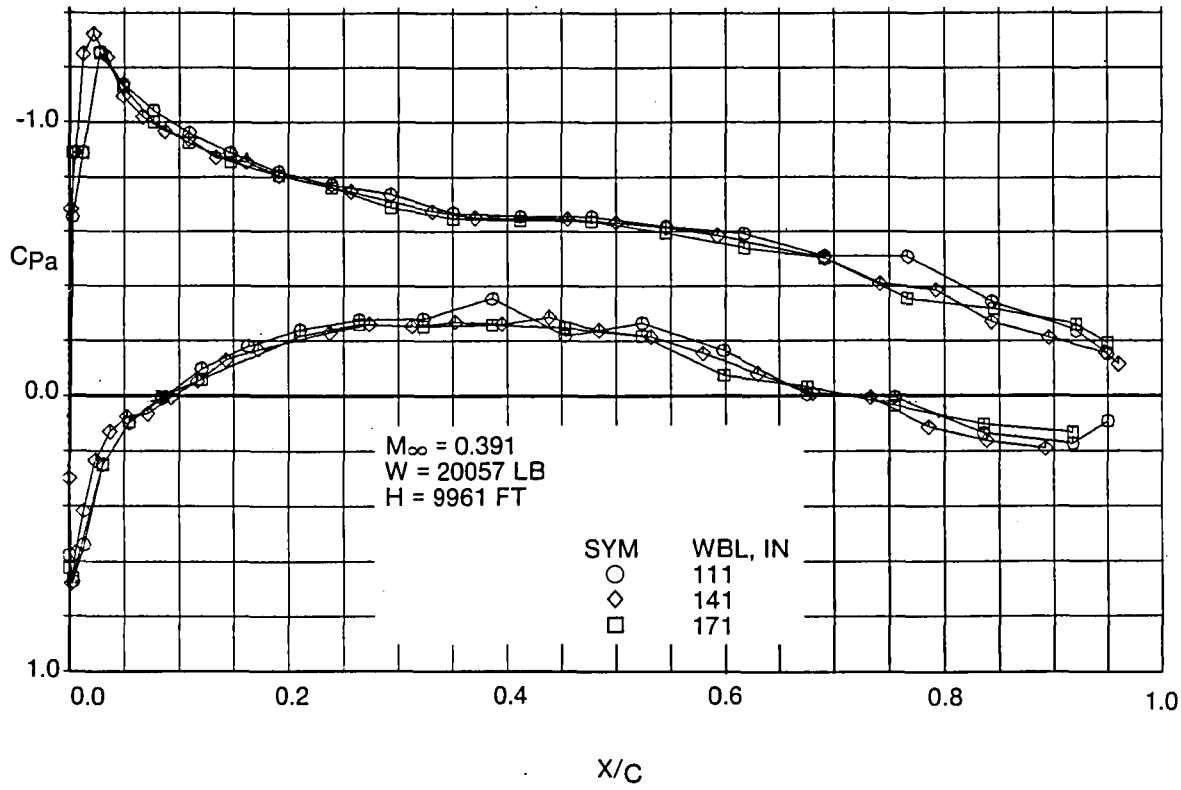

Fig. 3c Citation III Averaged Wing Pressures - Pressure Flights (continued)

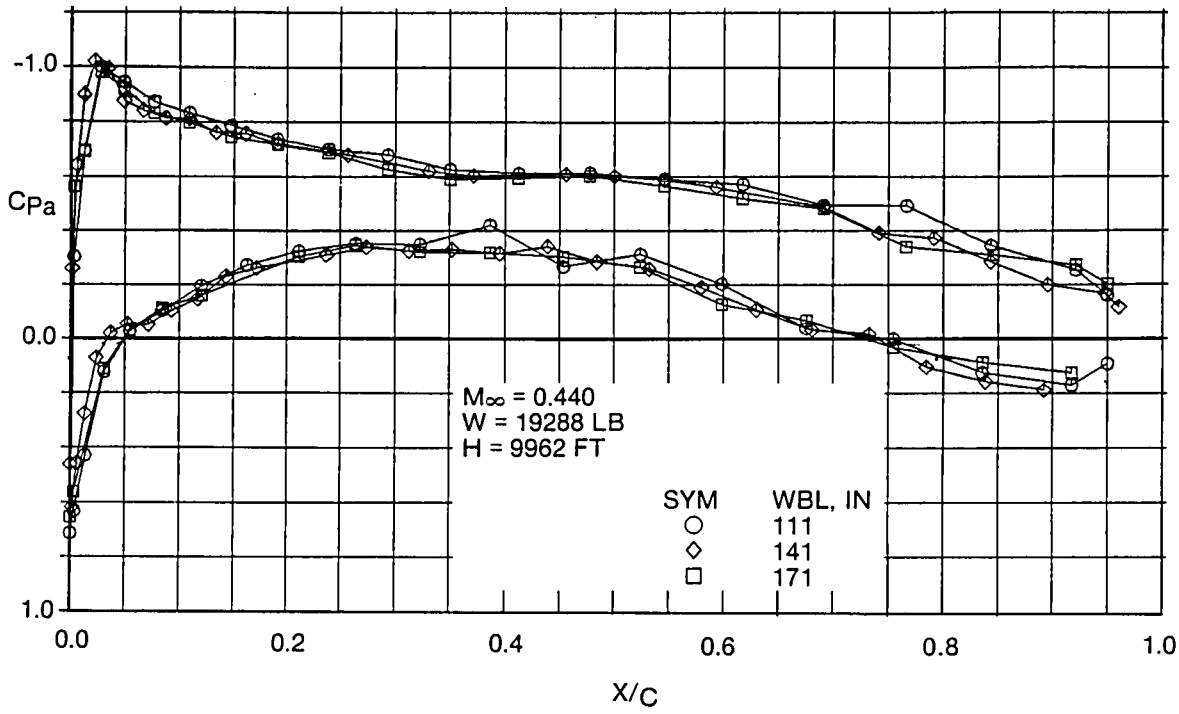

Fig. 3d Citation III Averaged Wing Pressures - Pressure Flights (continued)

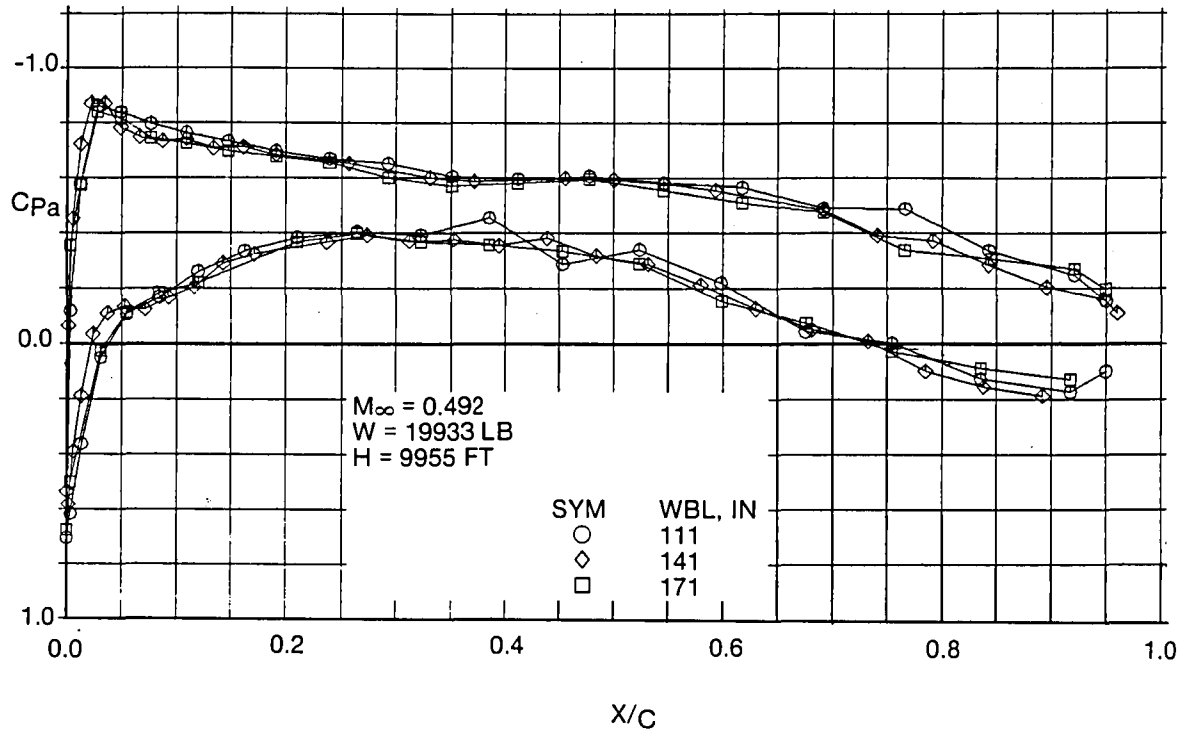

Fig. 3e Citation III Averaged Wing Pressures - Pressure Flights (continued)

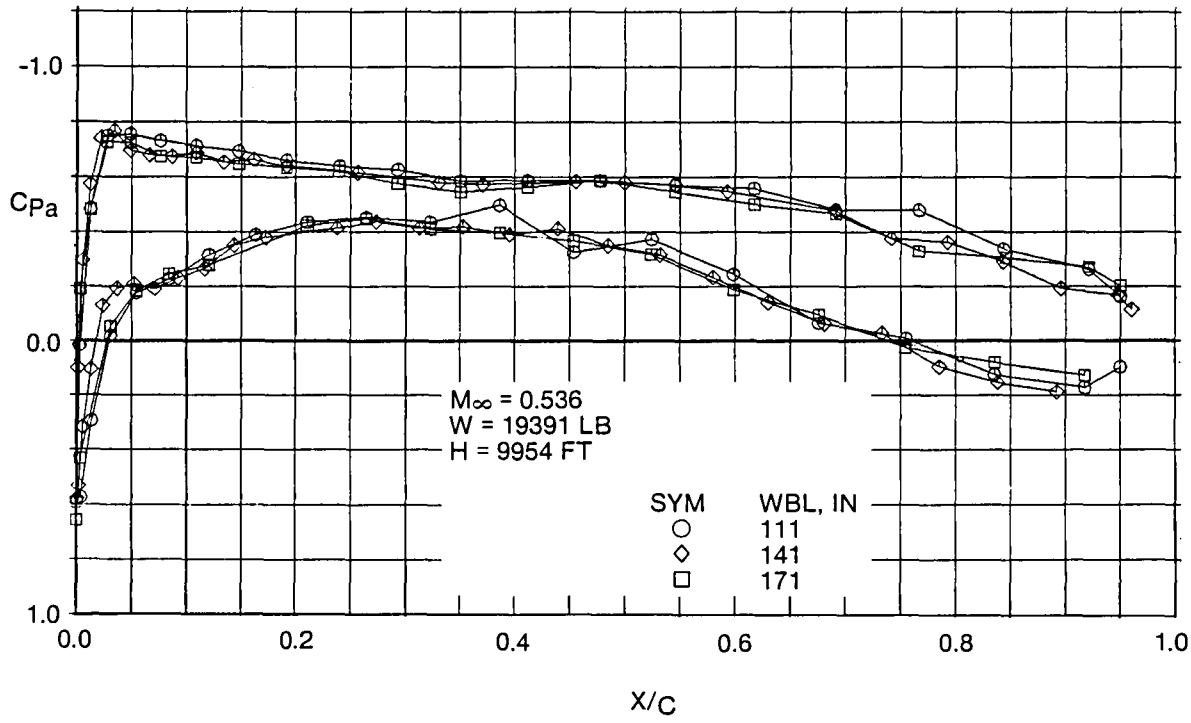

Fig. 3f Citation III Averaged Wing Pressures - Pressure Flights (continued)

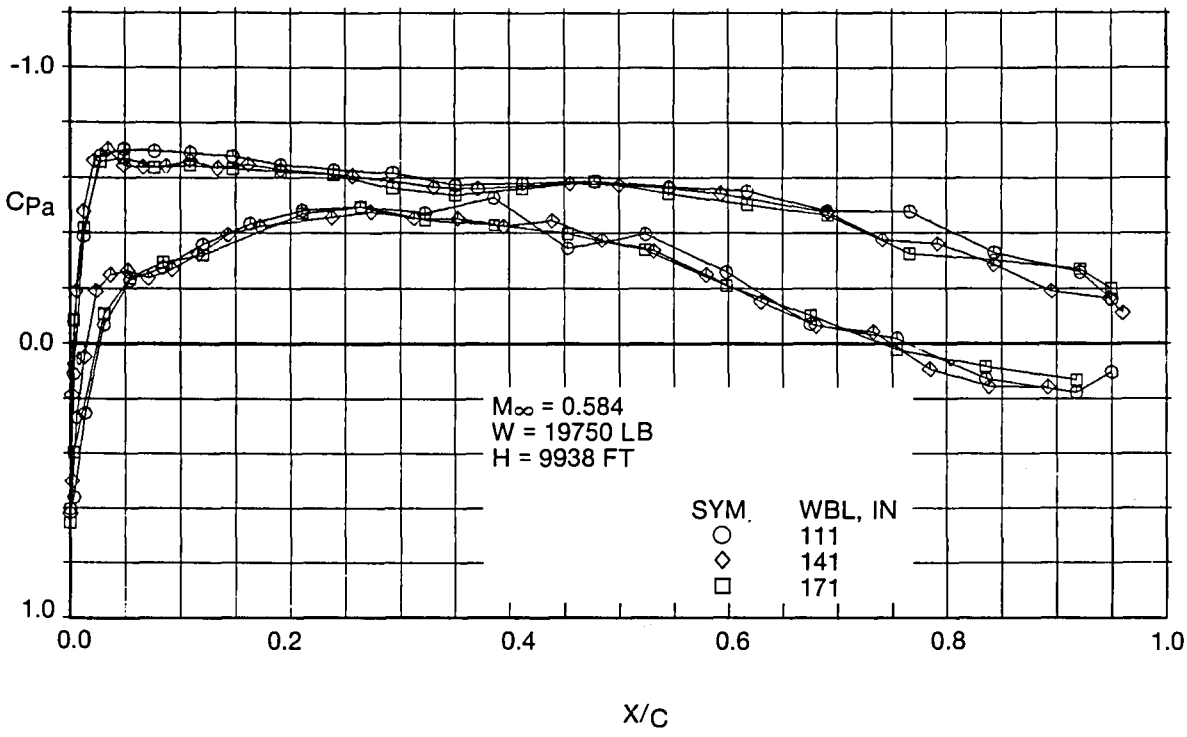

Fig. 3g Citation III Averaged Wing Pressures -Pressure Flights (continued)

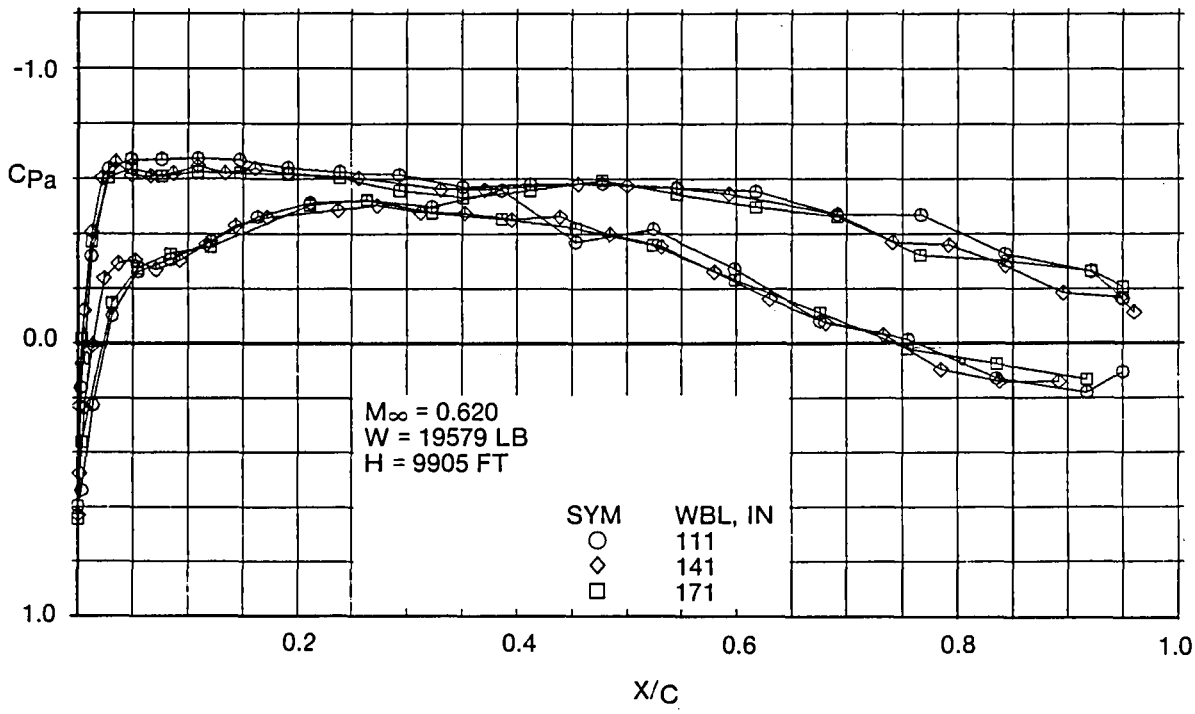

Fig. 3h Citation III Averaged Wing Pressures -Pressure Flights (continued)

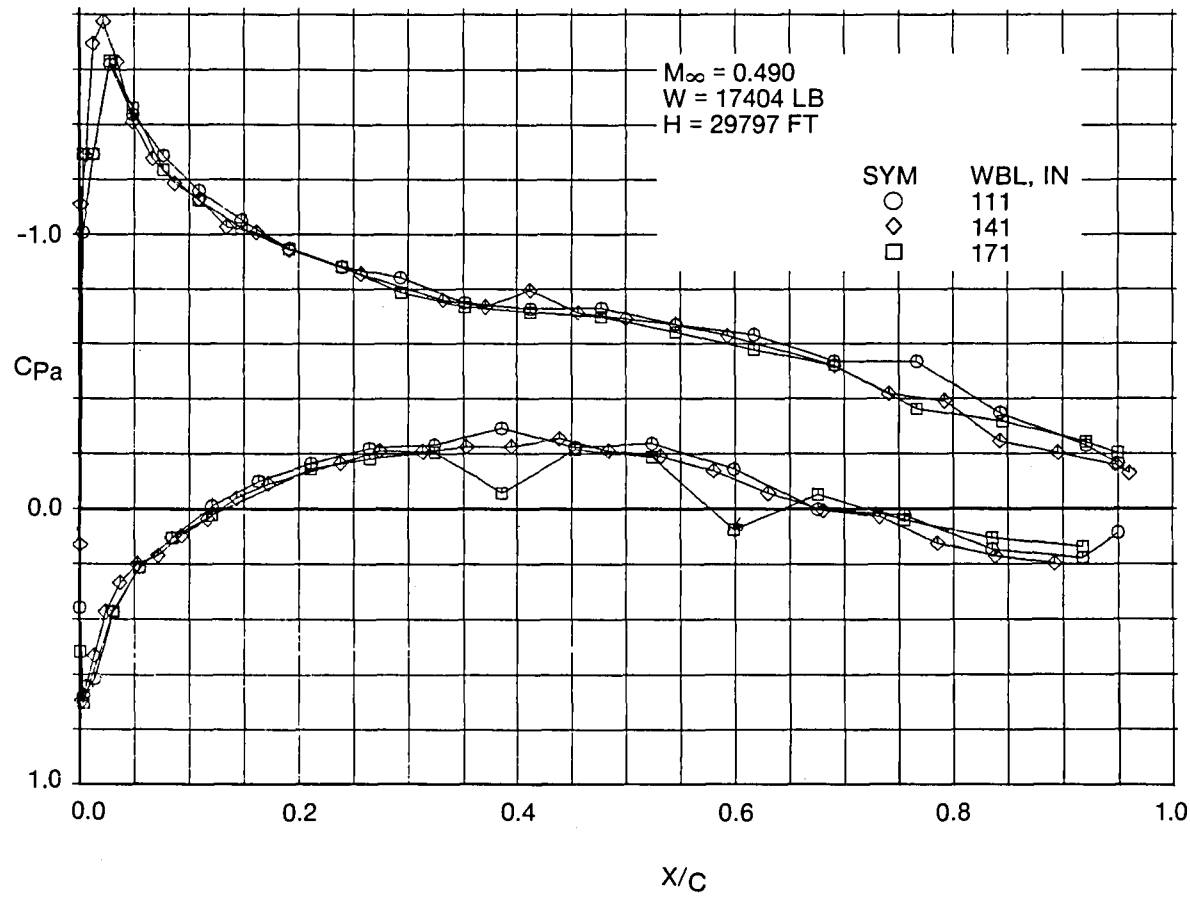

Fig. 3i Citation III Averaged Wing Pressures -Pressure Flights (continued)

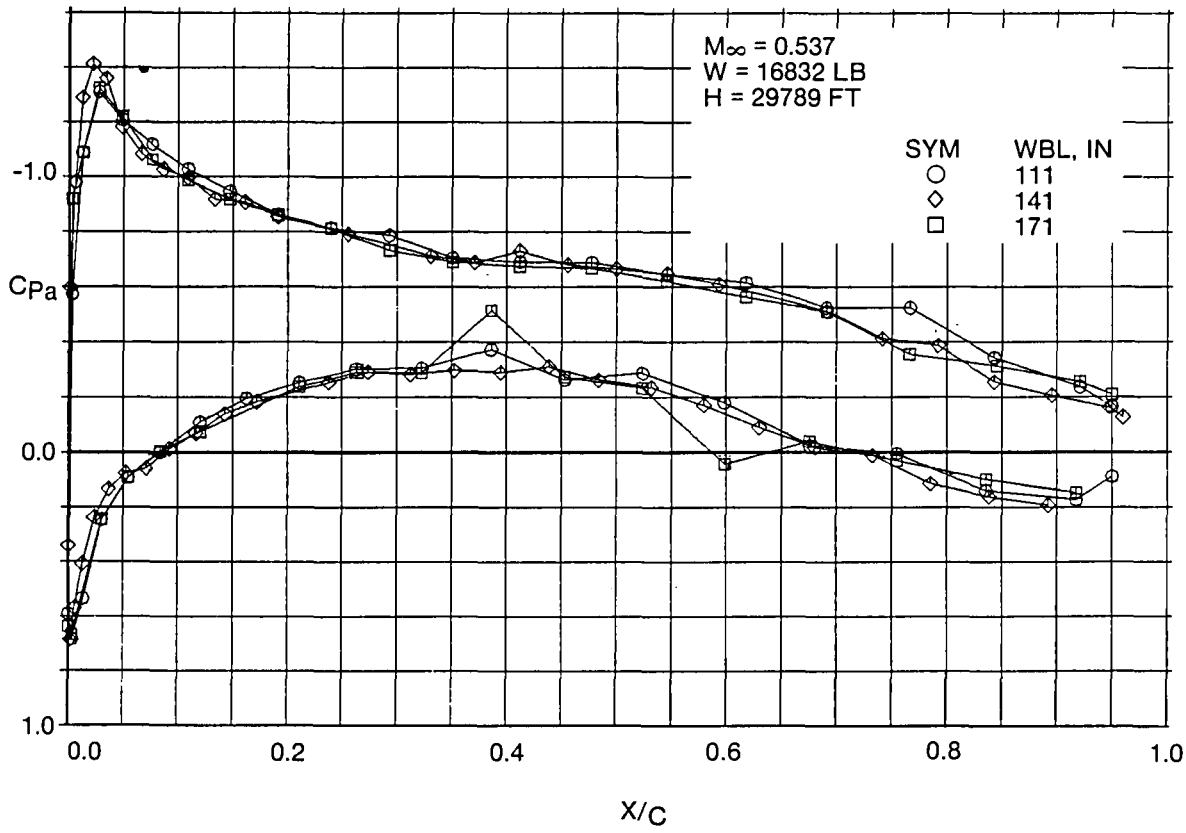

Fig. 3j Citation III Averaged Wing Pressures -Pressure Flights (continued)

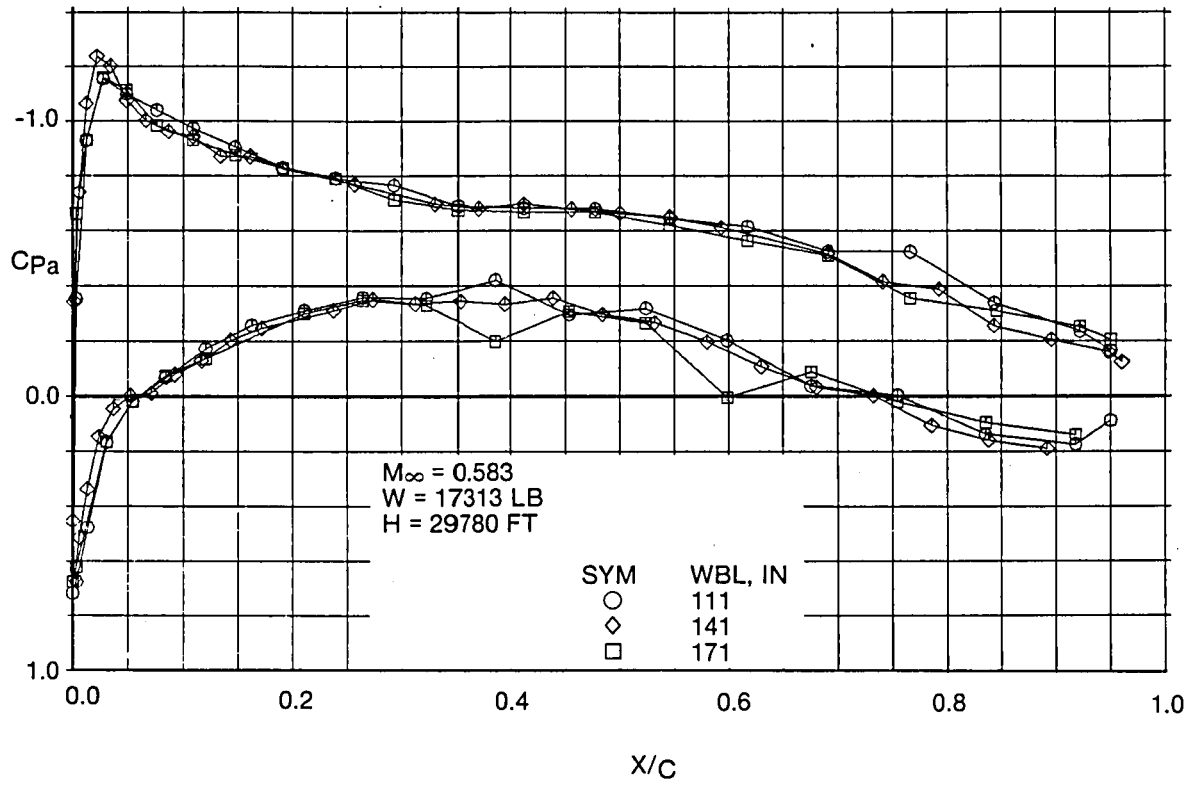

Fig. 3k Citation III Averaged Wing Pressures -Pressure Flights (continued)

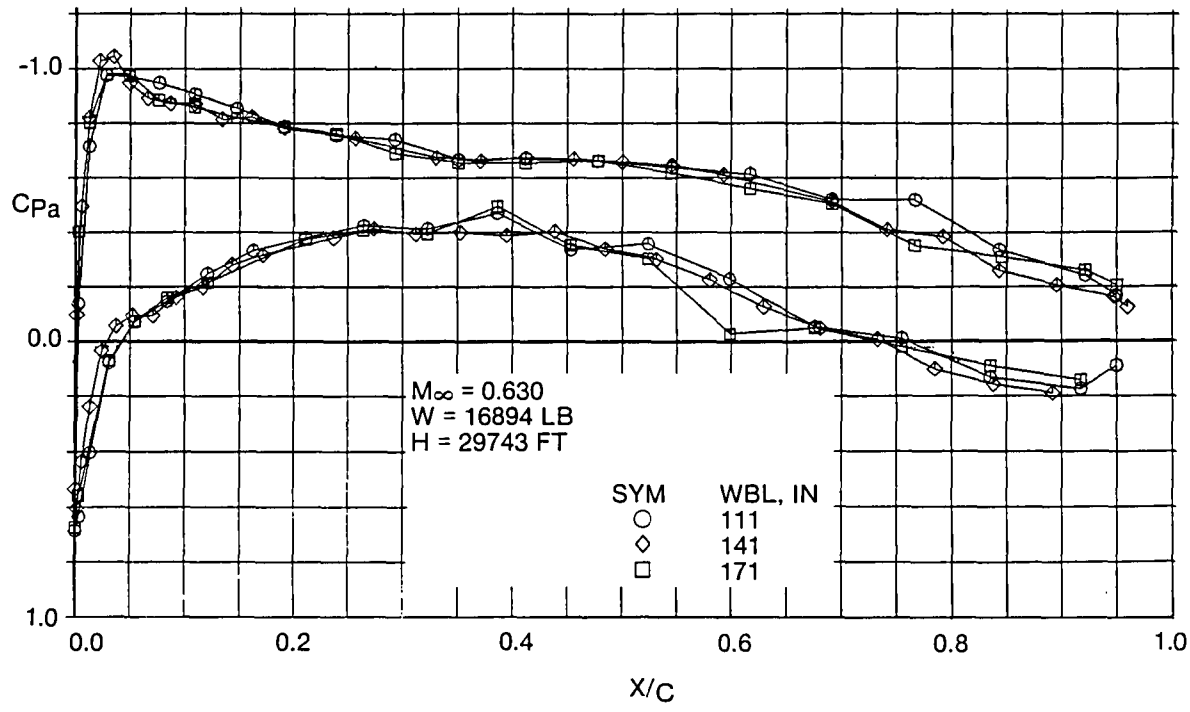

Fig. 3l Citation III Averaged Wing Pressures -Pressure Flights (continued)

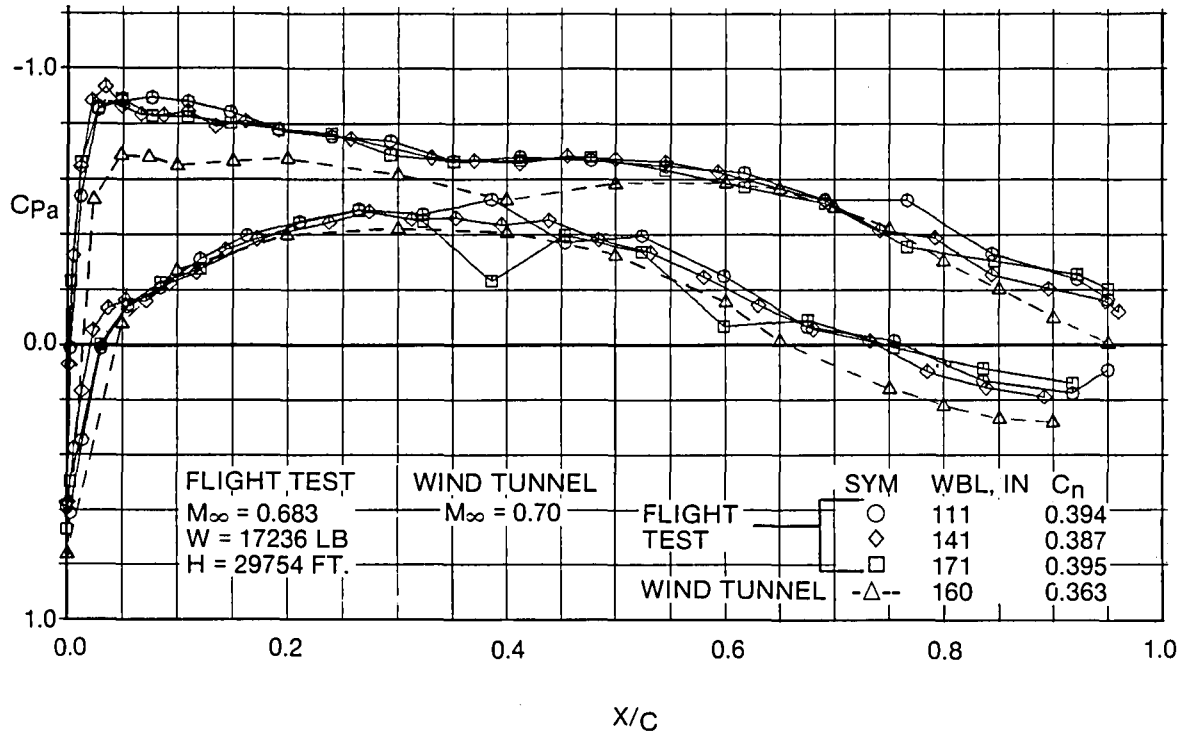

Fig. 3m Citation III Averaged Wing Pressure - Pressure Flights (continued)

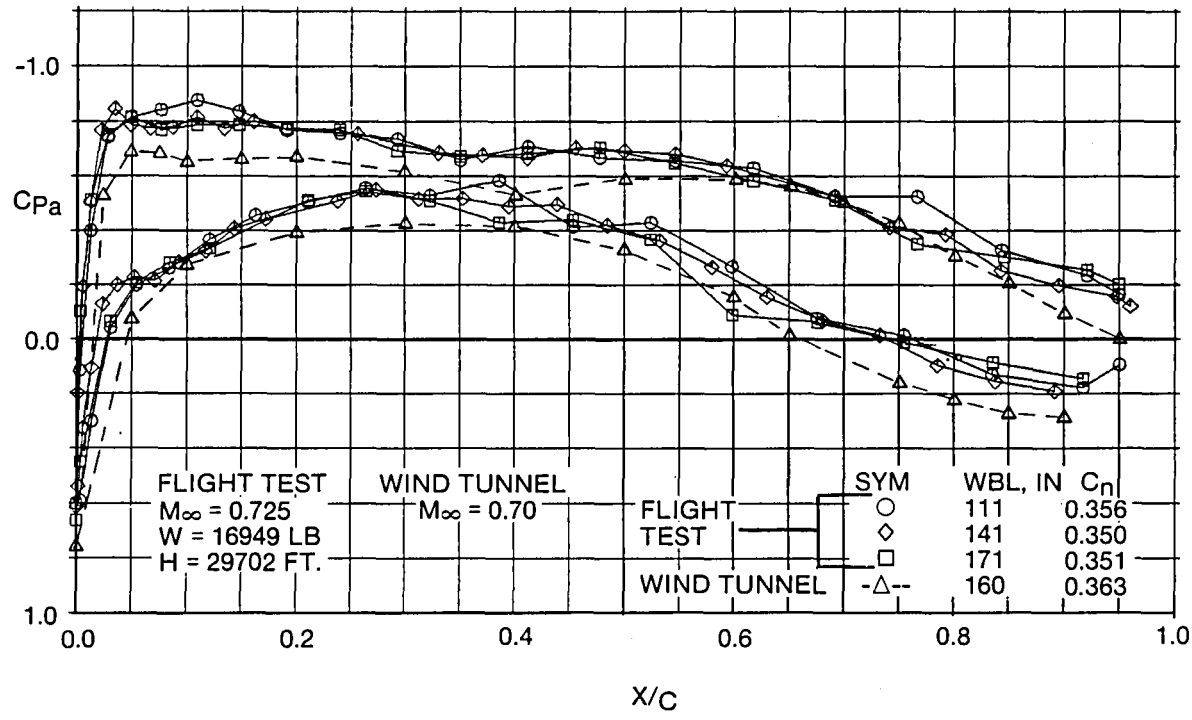

Fig. 3n Citation III Averaged Wing Pressures - Pressure Flights (continued)

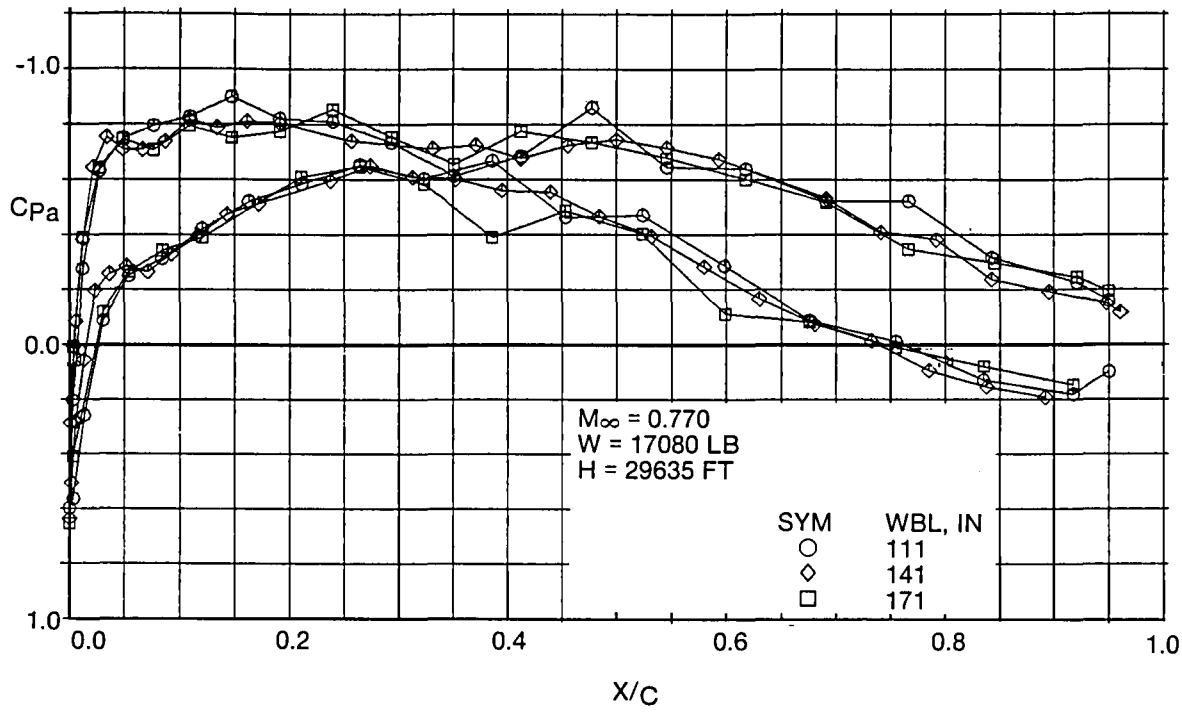

Fig. 3o Citation III Averaged Wing Pressures -Pressure Flights (continued)

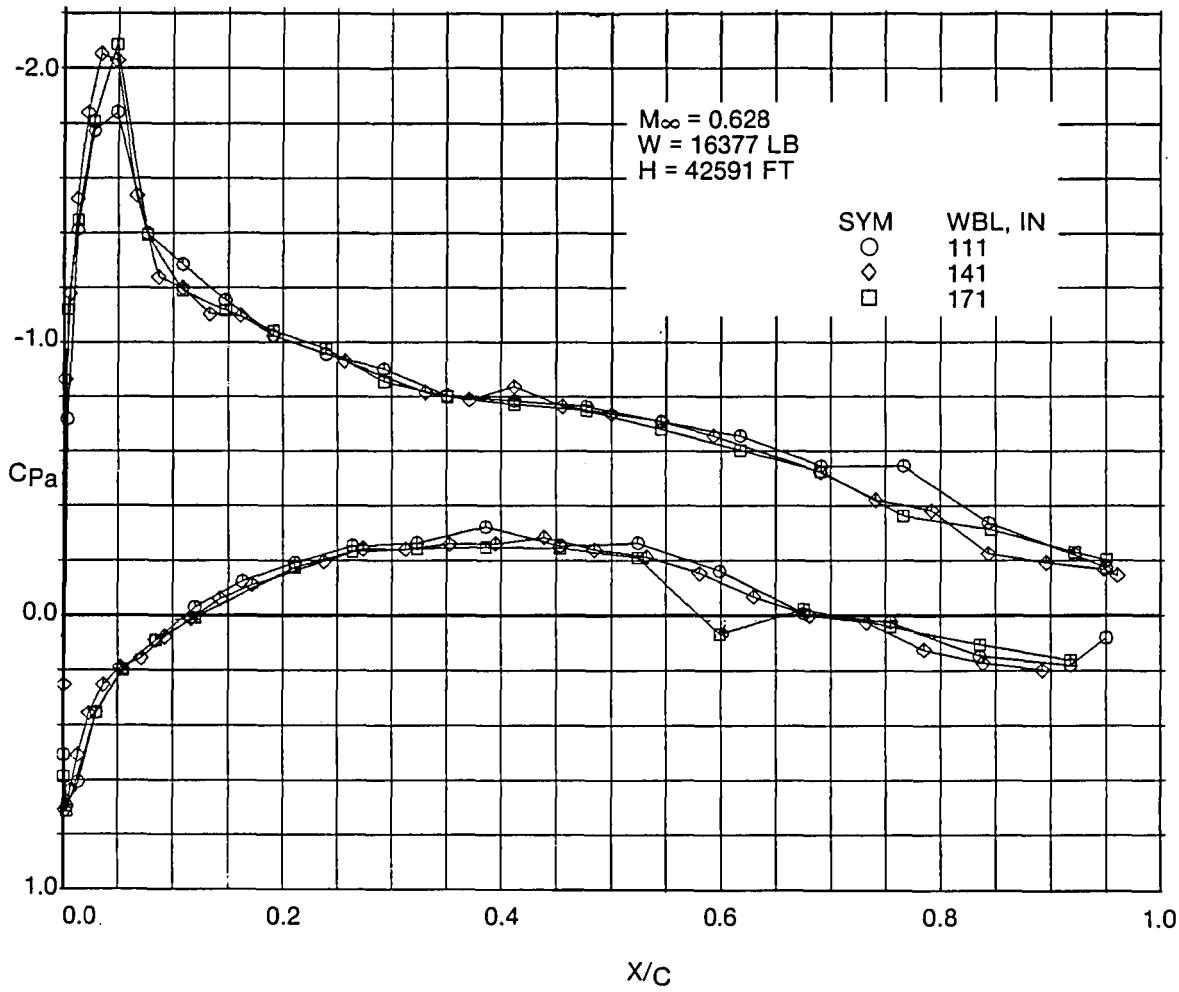

Fig. 3p Citation III Averaged Wing Pressures - Pressure Flights (continued)

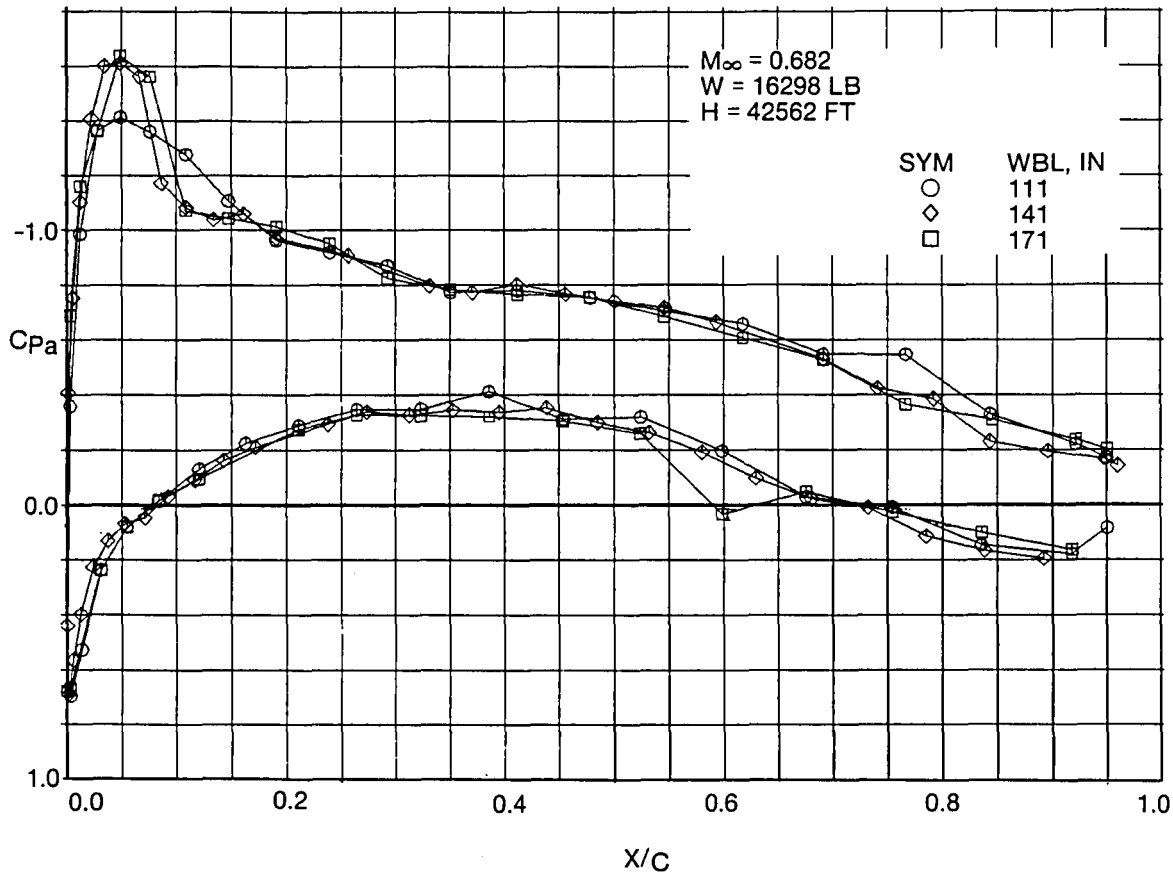

Fig. 3q Citation III Averaged Wing Pressures -Pressure Flights (continued)

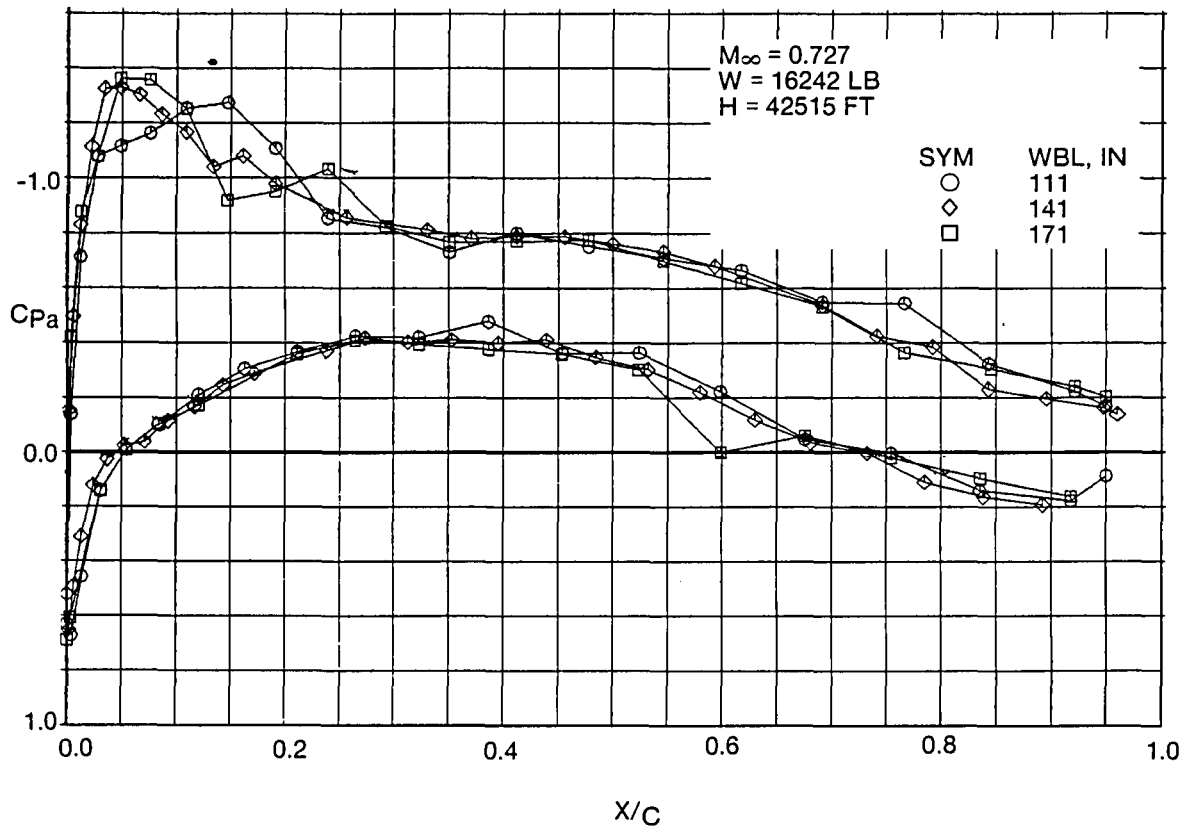

Fig. 3r Citation III Averaged Wing Pressures -Pressure Flights (continued)

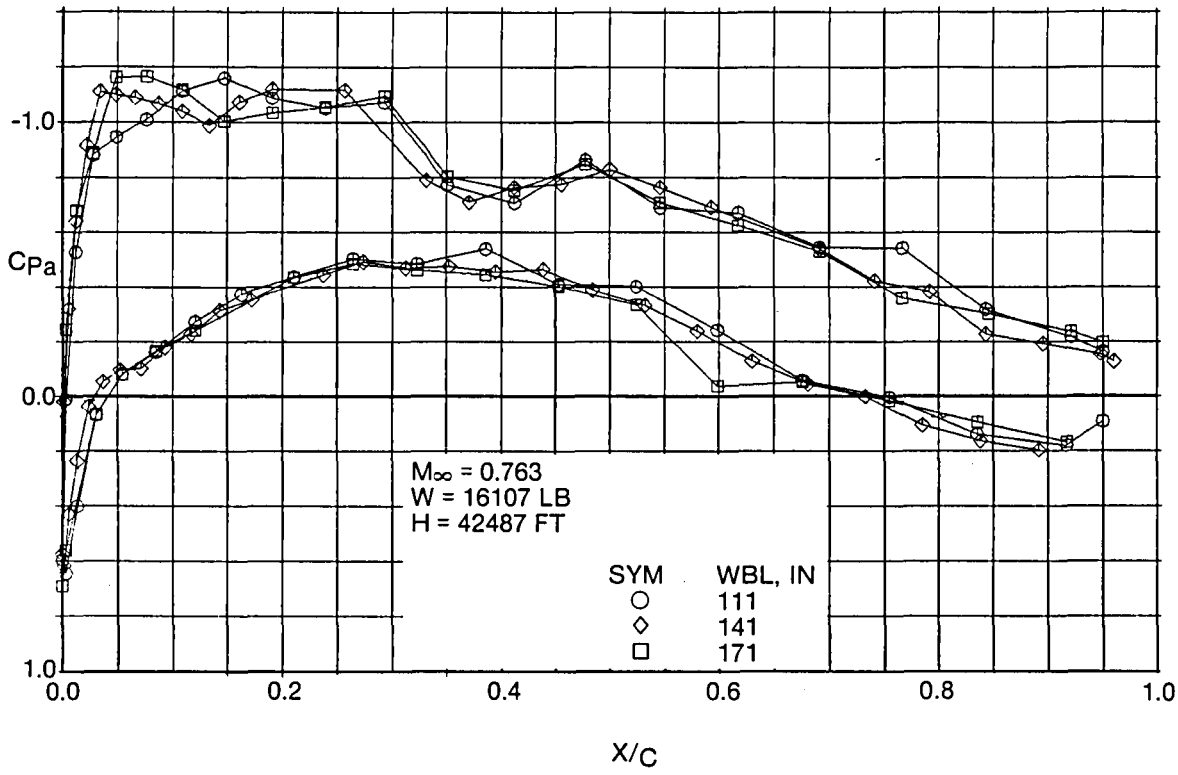

Fig. 3s Citation III Averaged Wing Pressures -Pressure Flights (continued)

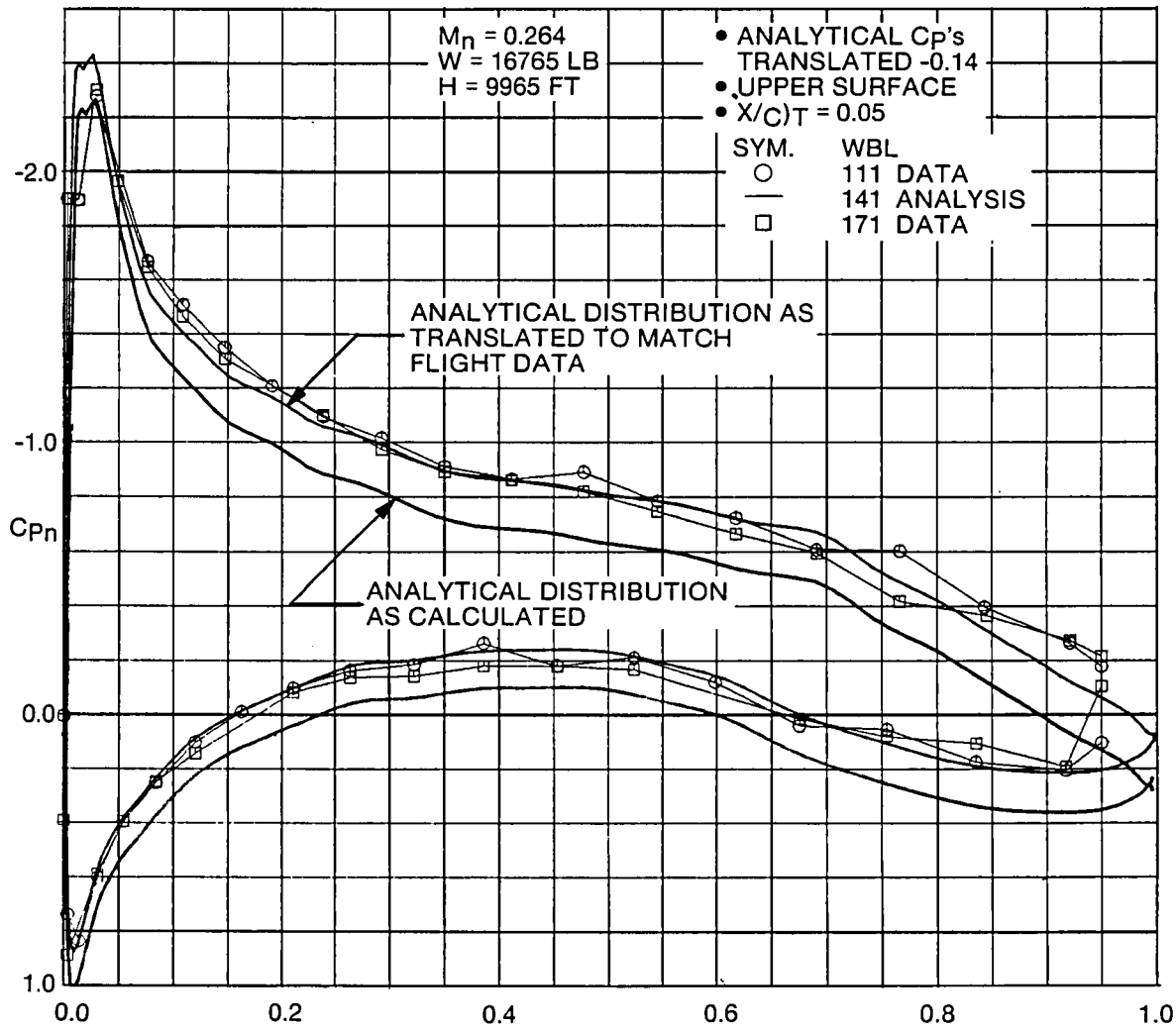

Fig. 4 Citation III Normal Wing Pressures -Transition Flight, Case 1

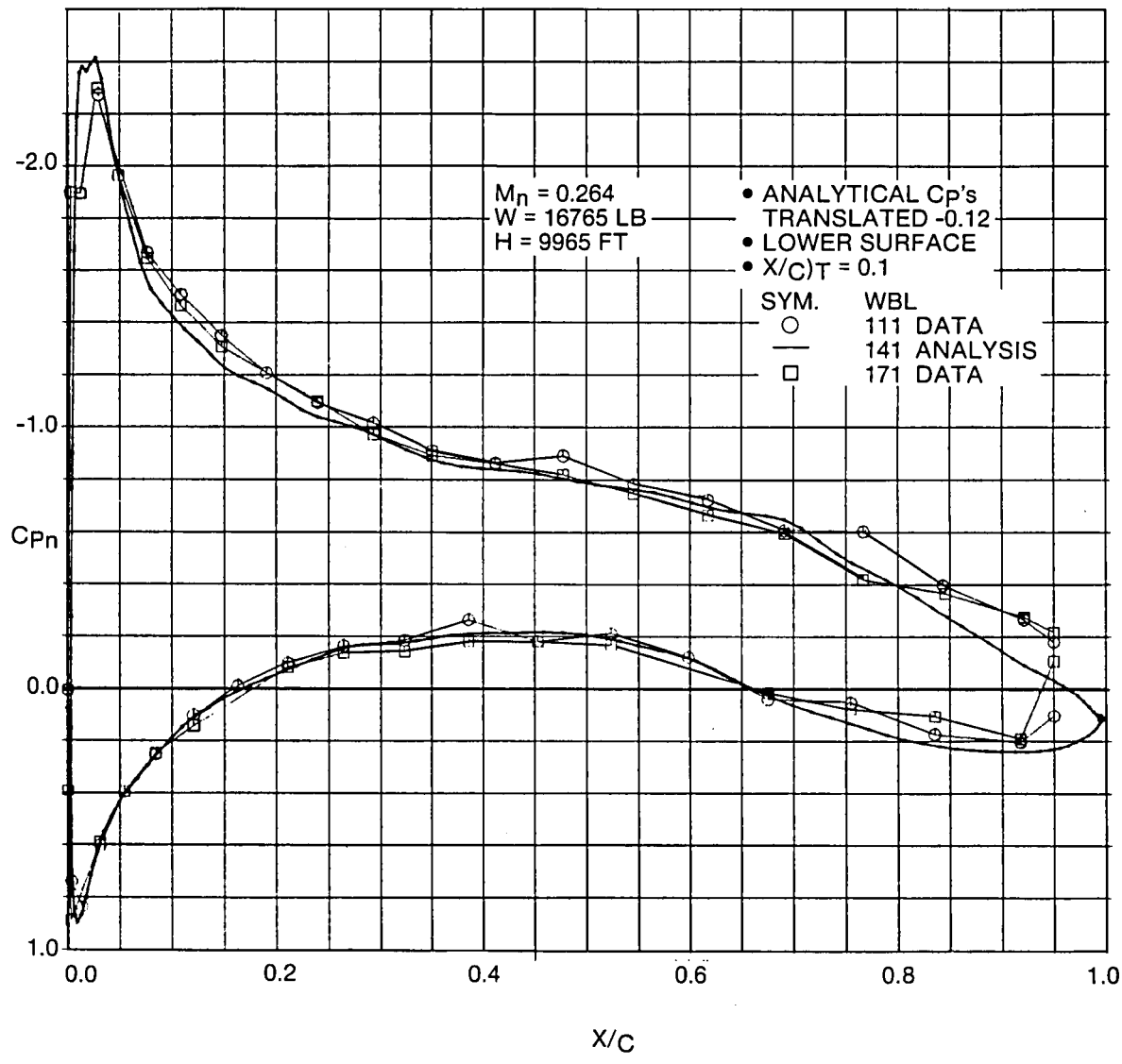

Fig. 5 Citation III Normal Wing Pressures -Transition Flight, Case 2

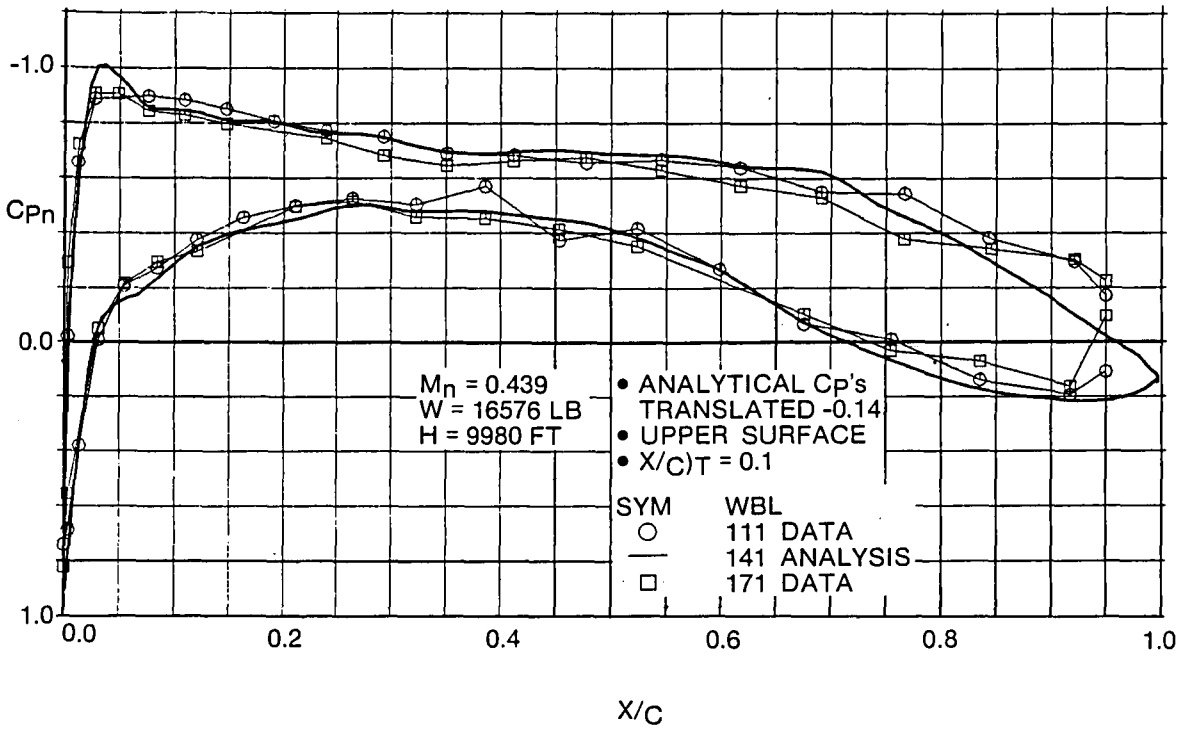

Fig. 6 Citation III Normal Wing Pressures -Transition Flight, Case 3

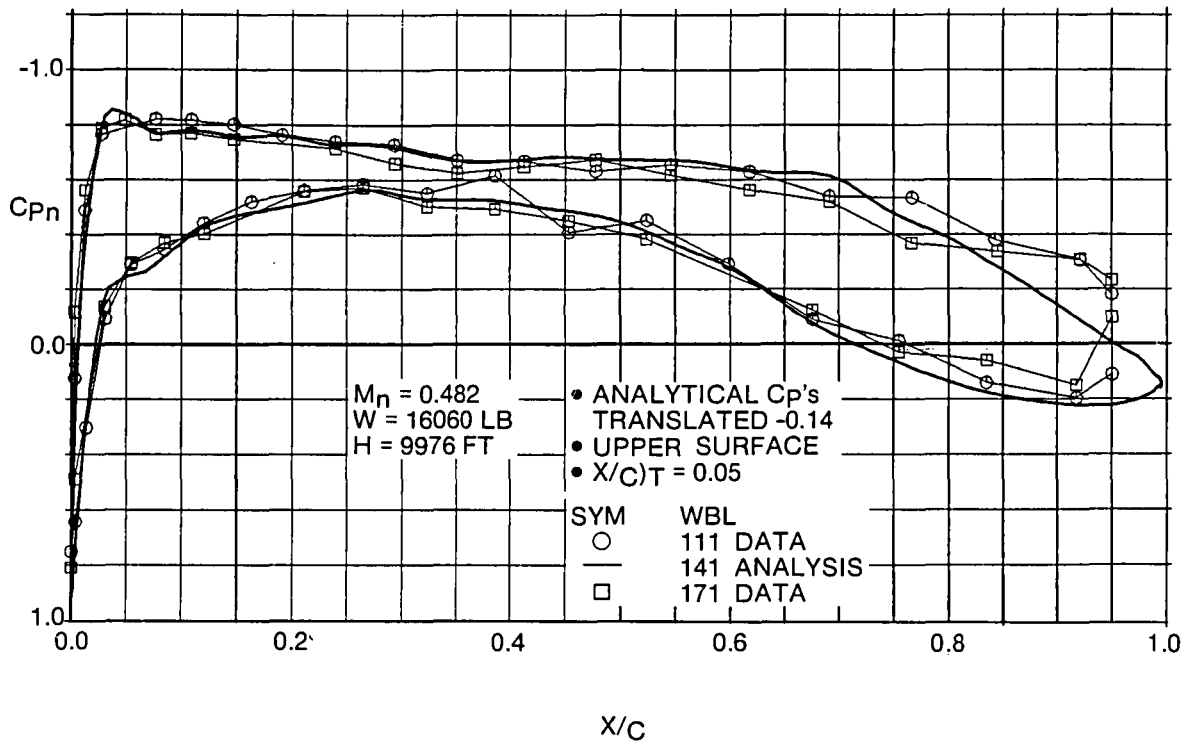

Fig. 7 Citation III Normal Wing Pressures -Transition Flight, Case 4

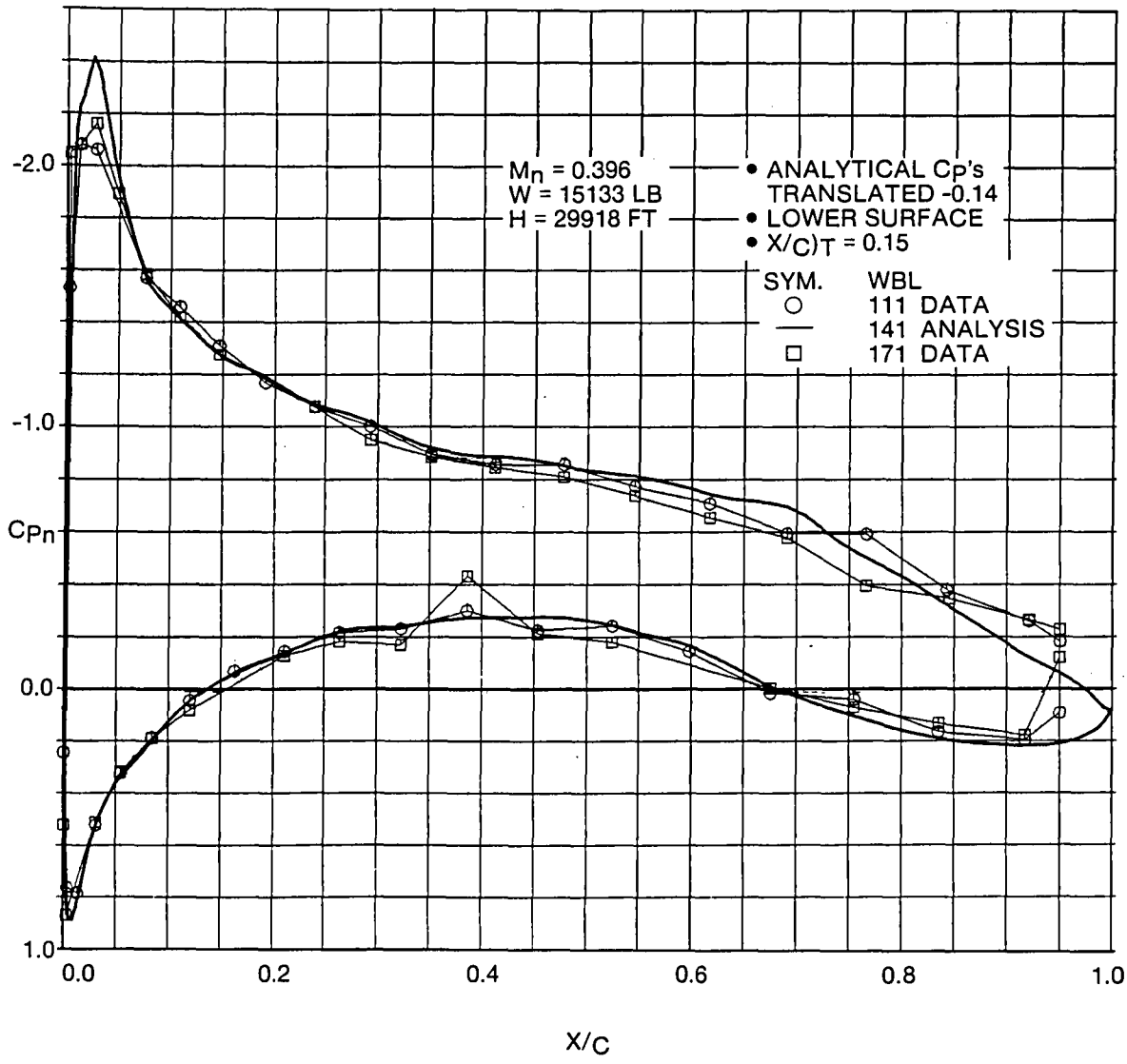

Fig. 8 Citation III Normal Wing Pressures -Transition Flight, Case 5

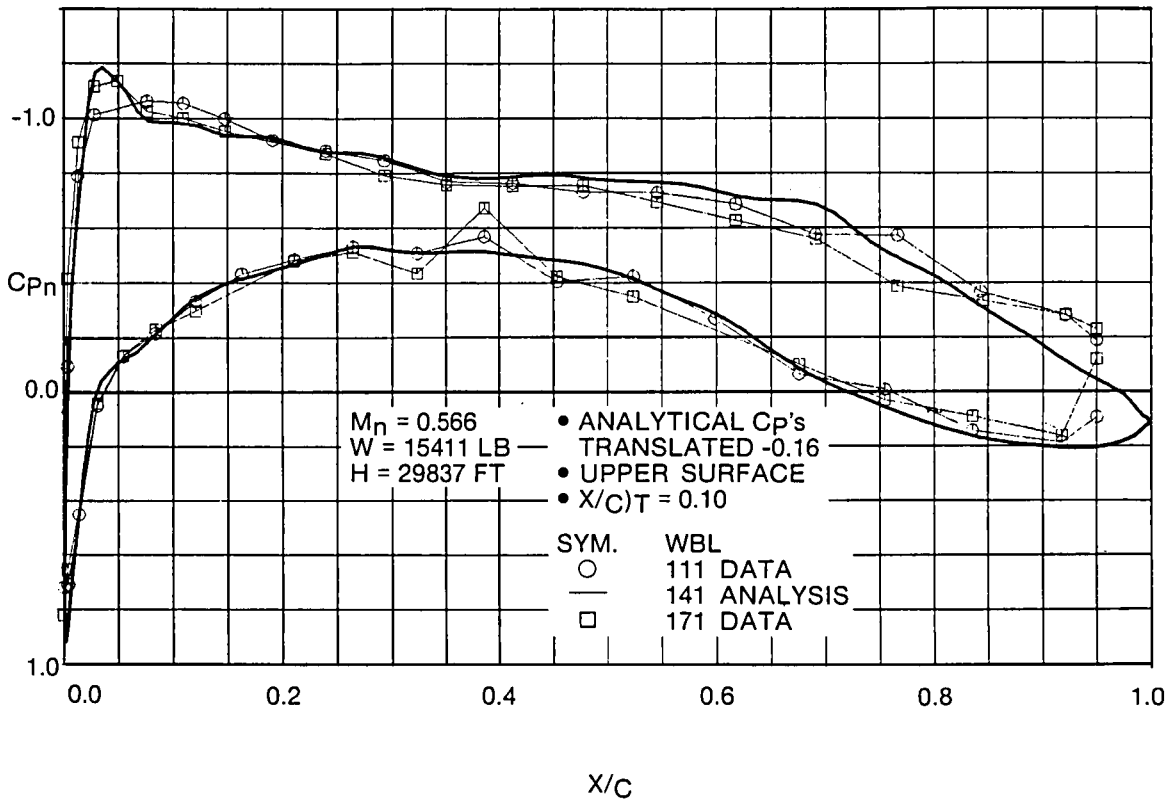

Fig. 9 Citation III Normal Wing Pressures -Transition Flight, Case 6

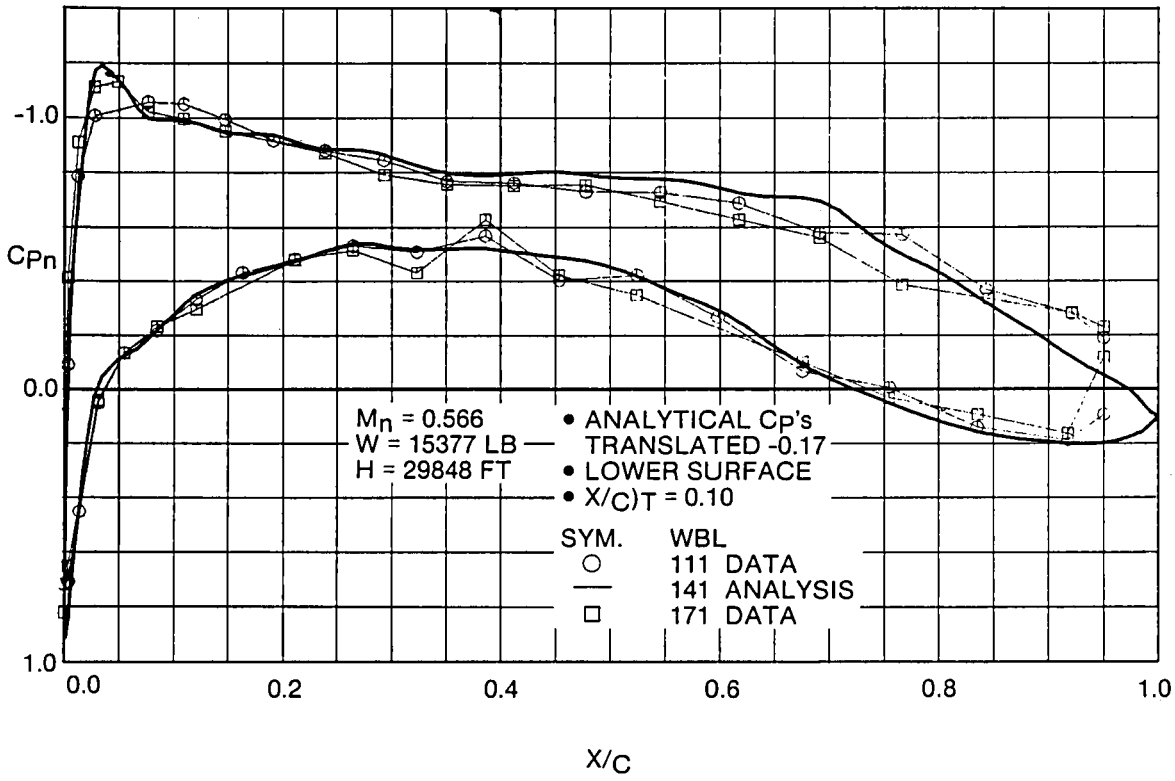

Fig. 10 Citation III Normal Wing Pressures -Transition Flight, Case 7

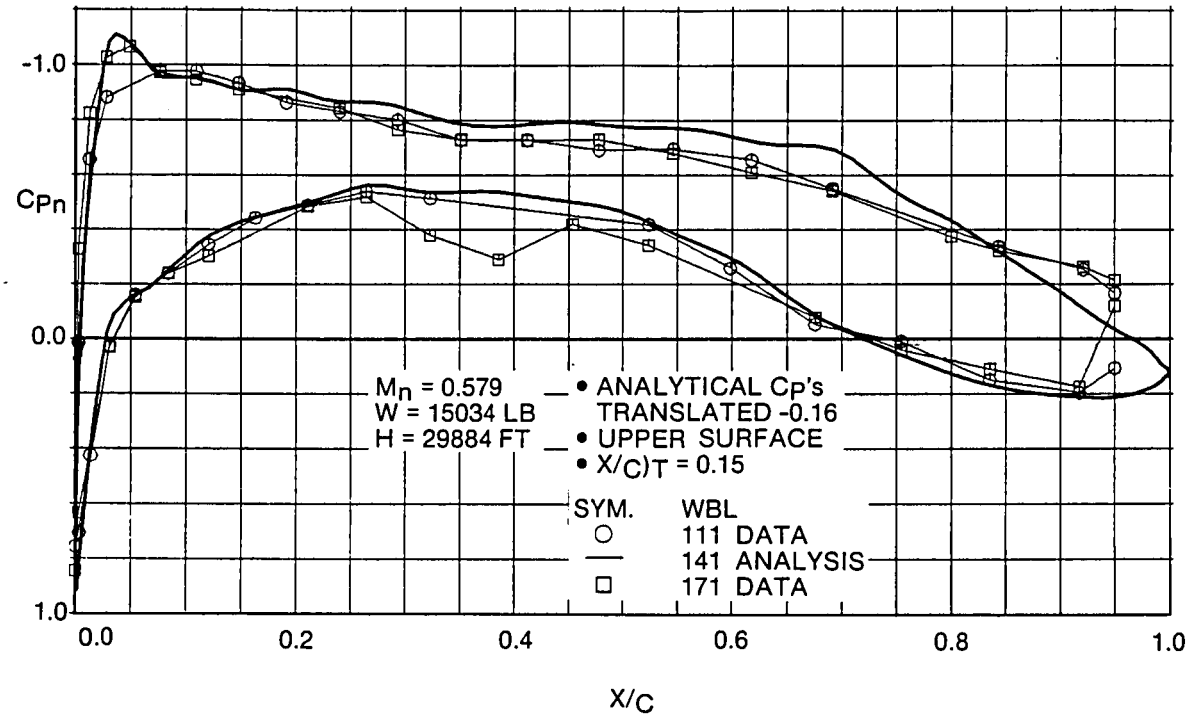

Fig. 11 Citation III Normal Wing Pressures -Transition Flight, Case 8

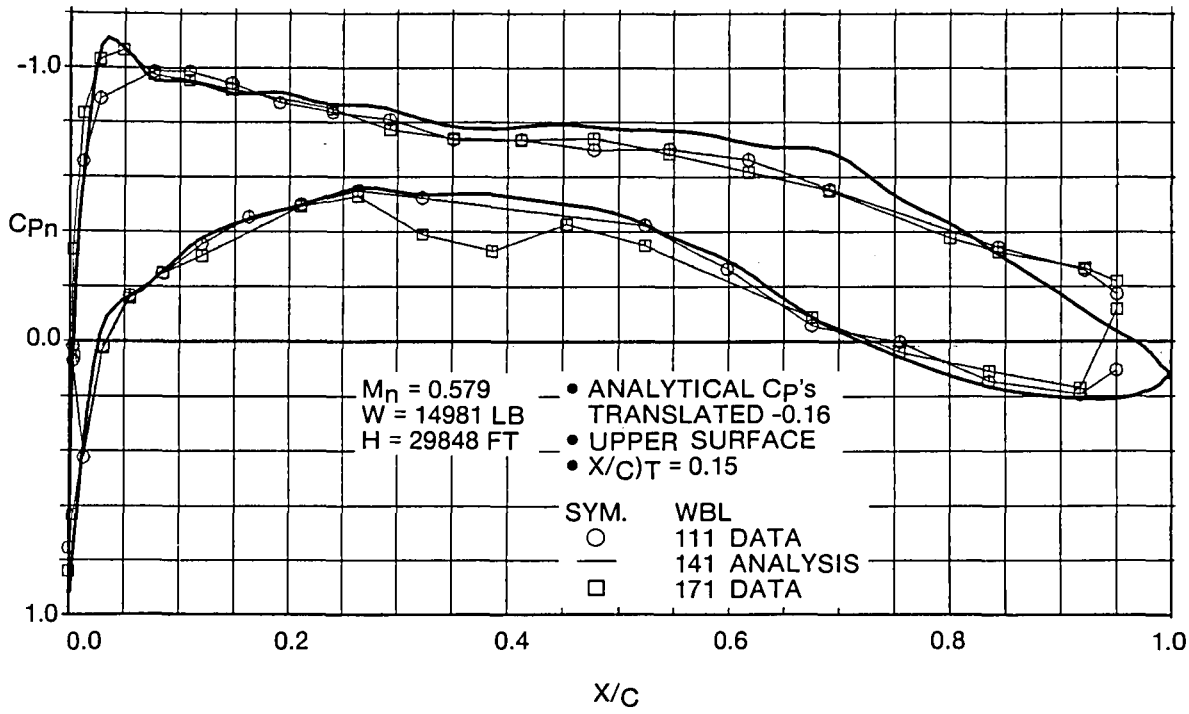

Fig. 12 Citation III Normal Wing Pressures -Transition Flight, Case 9

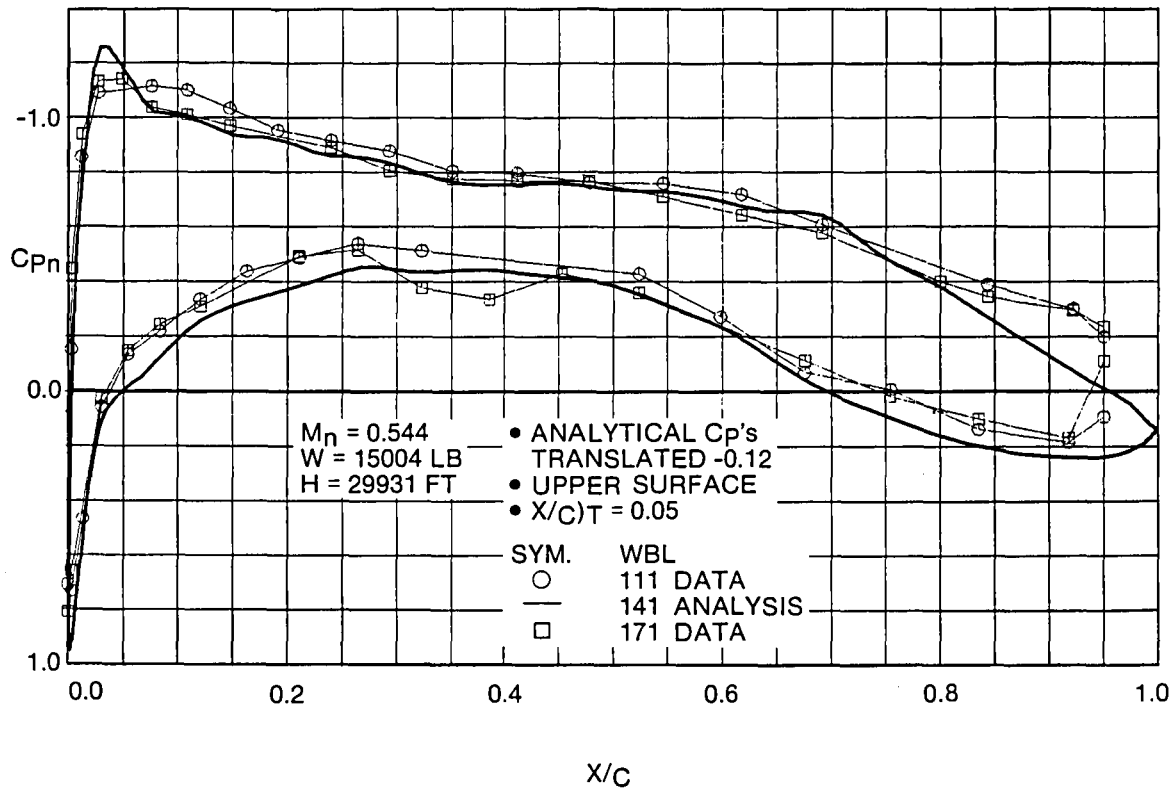

Fig. 13 Citation III Normal Wing Pressures -Transition Flight, Case 10

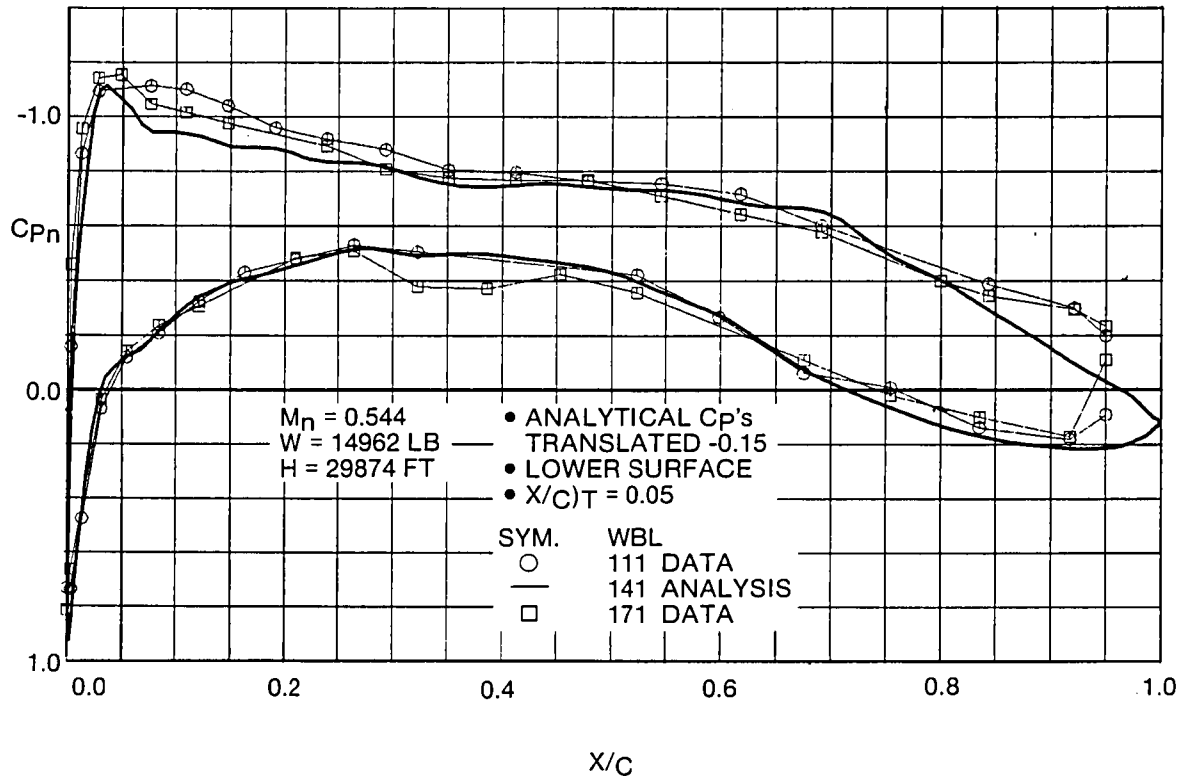

Fig. 14 Citation III Normal Wing Pressures -Transition Flight, Case 11

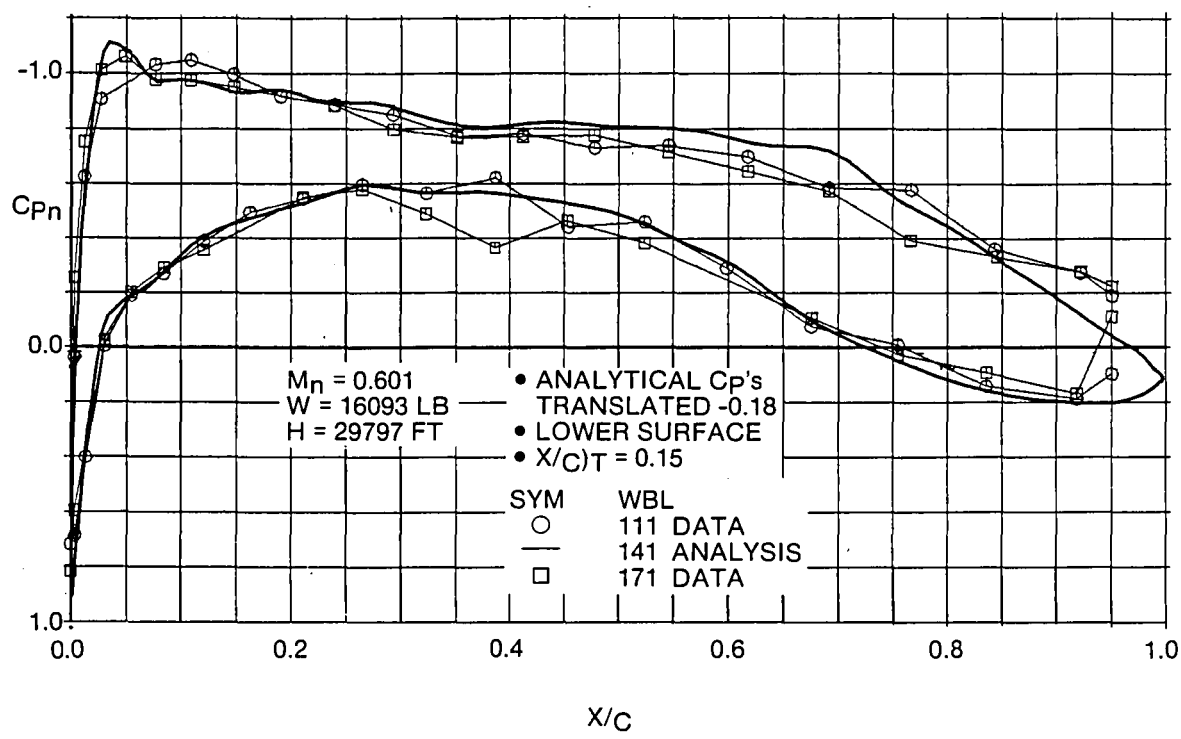

Fig. 15 Citation III Normal Wing Pressures -Transition Flight, Case 12

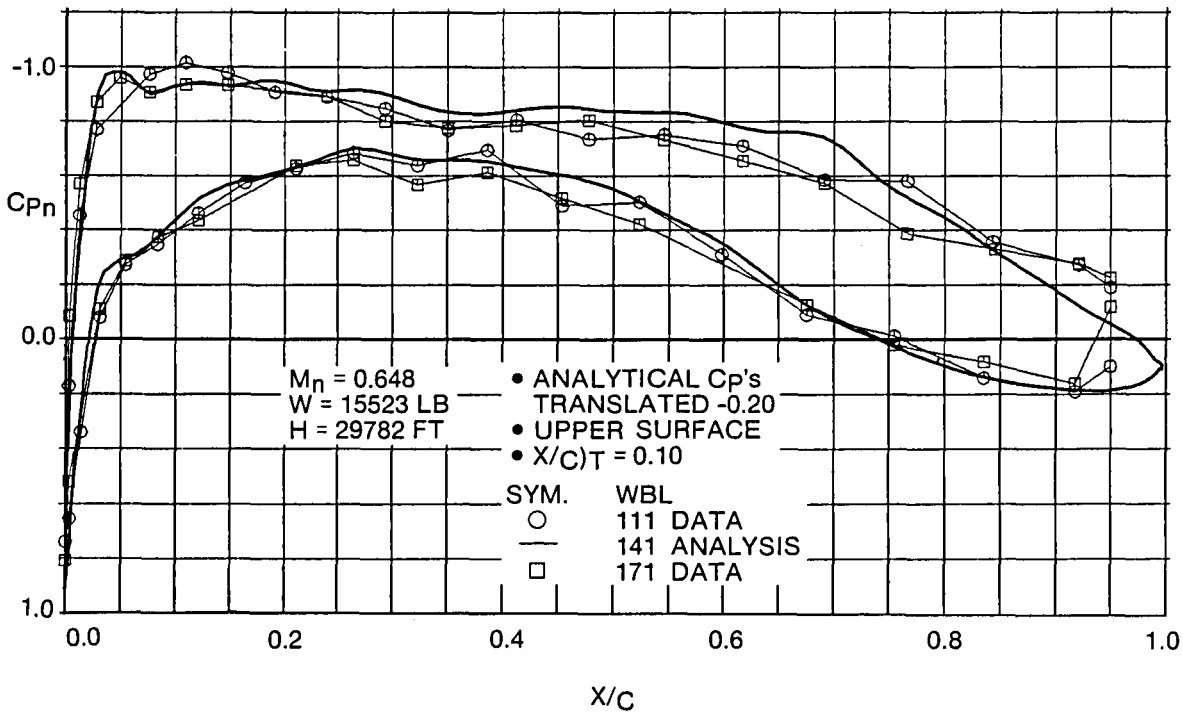

Fig. 16 Citation III Normal Wing Pressures -Transition Flight, Case 13

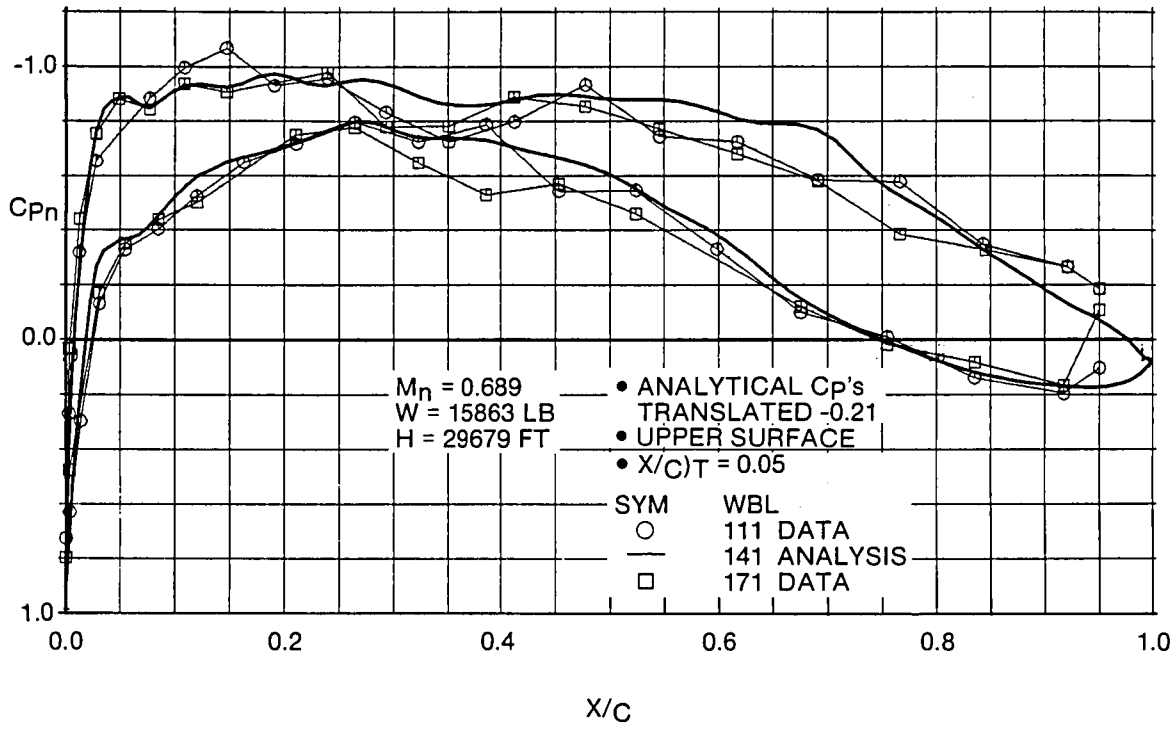

Fig. 17 Citation III Normal Wing Pressures -Transition Flight, Case 14

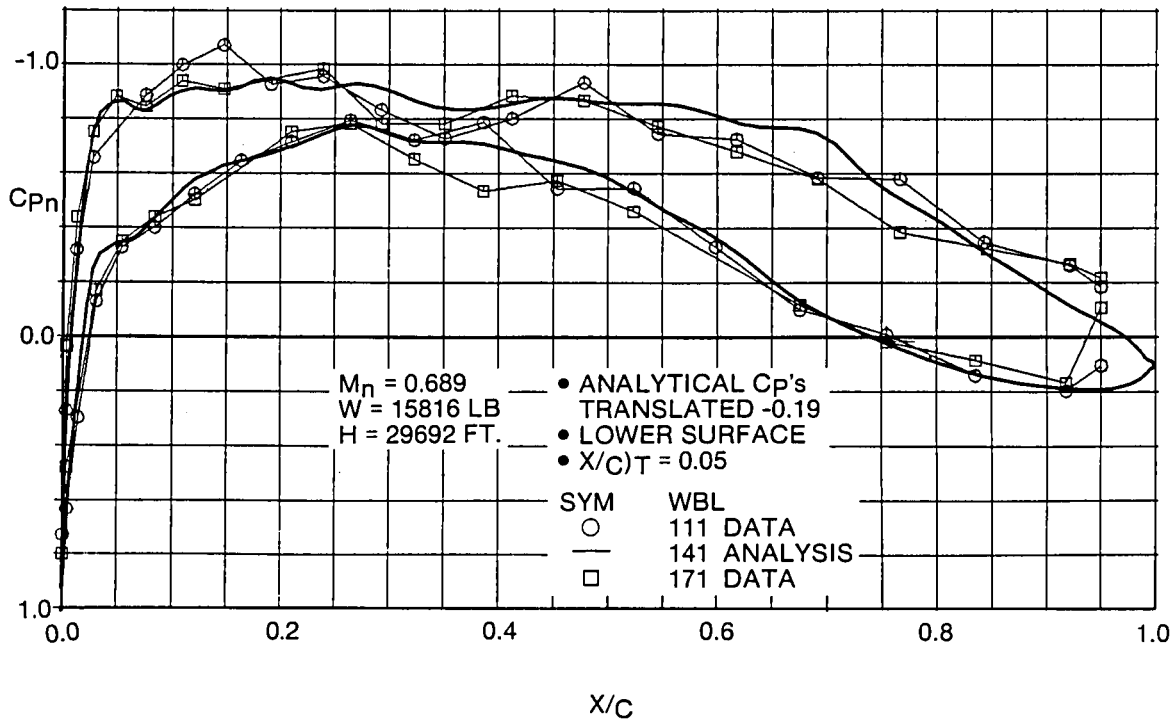

Fig. 18 Citation III Normal Wing Pressures -Transition Flight, Case 15

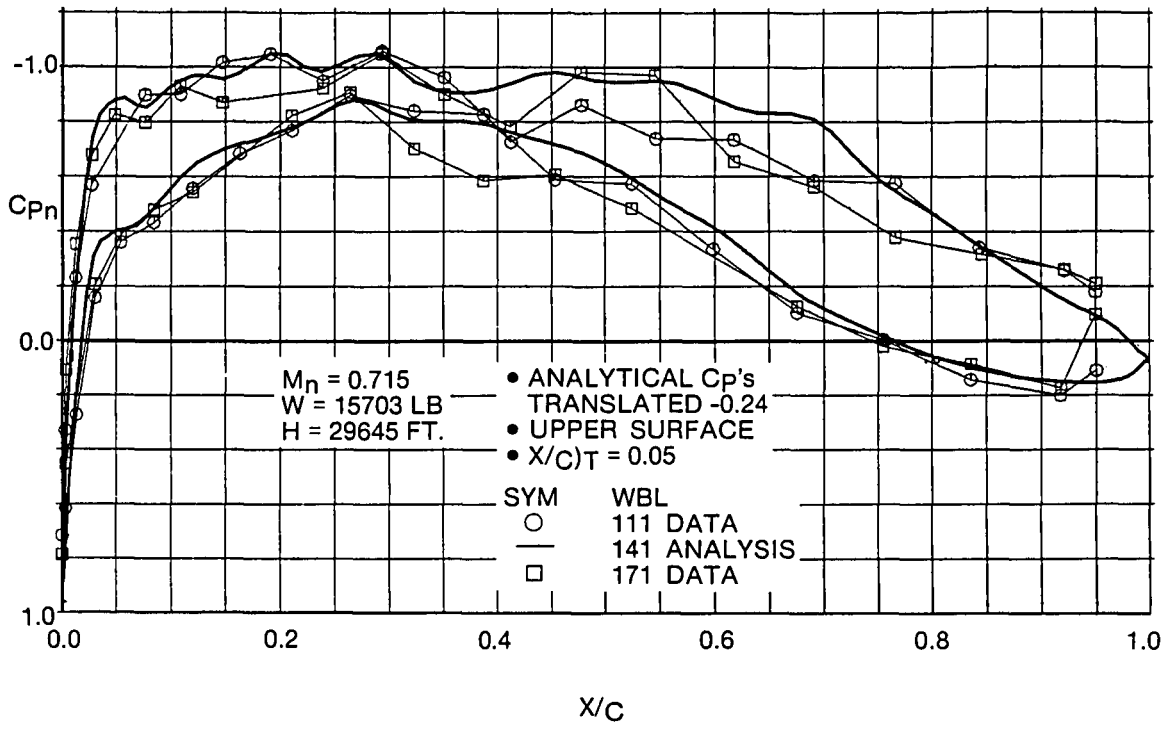

Fig. 19 Citation III Normal Wing Pressures -Transition Flight, Case 16

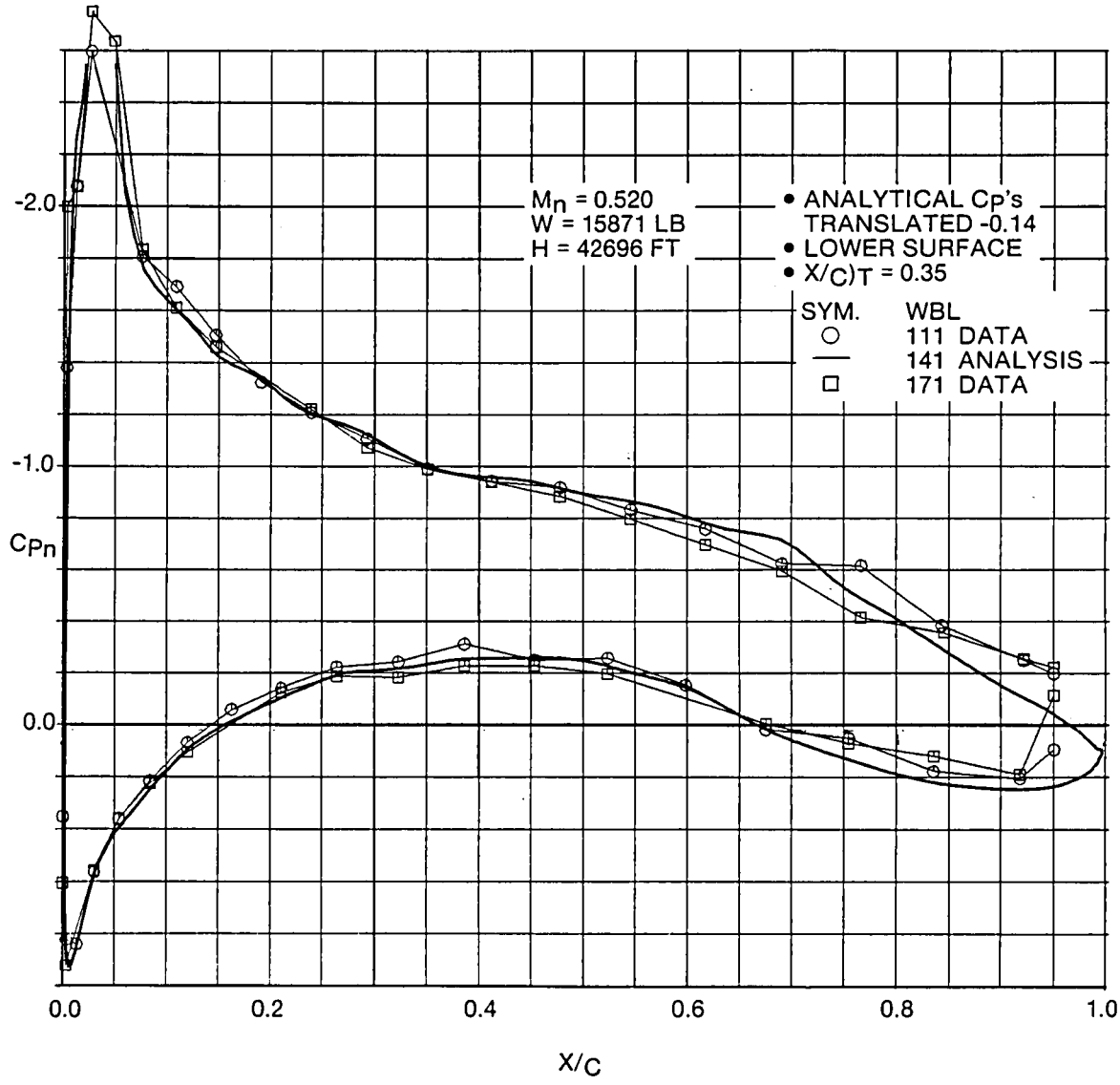

Fig. 20 Citation III Normal Wing Pressures -Transition Flight, Case 17

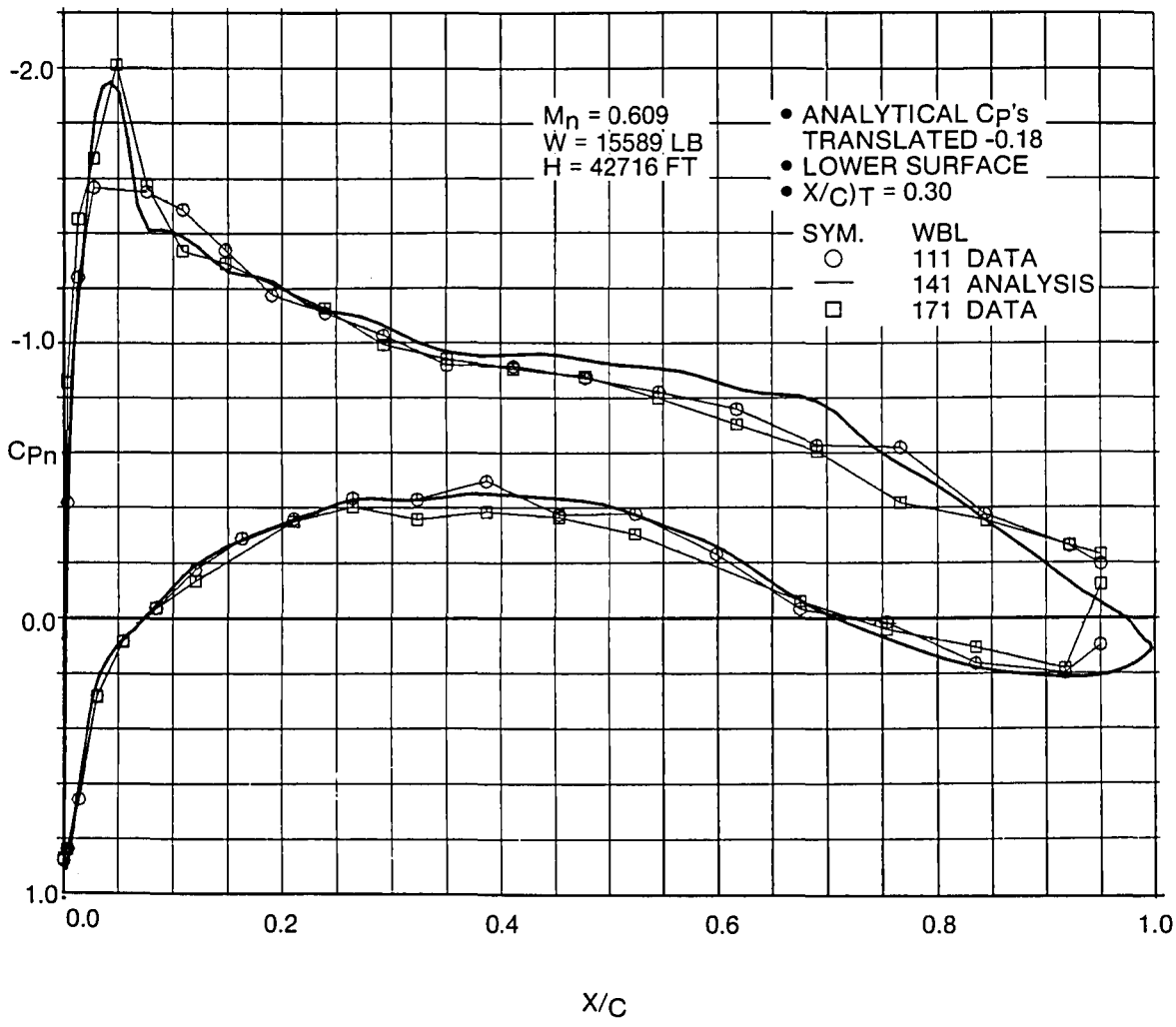

Fig. 21 Citation III Normal Wing Pressures -Transition Flight, Case 18

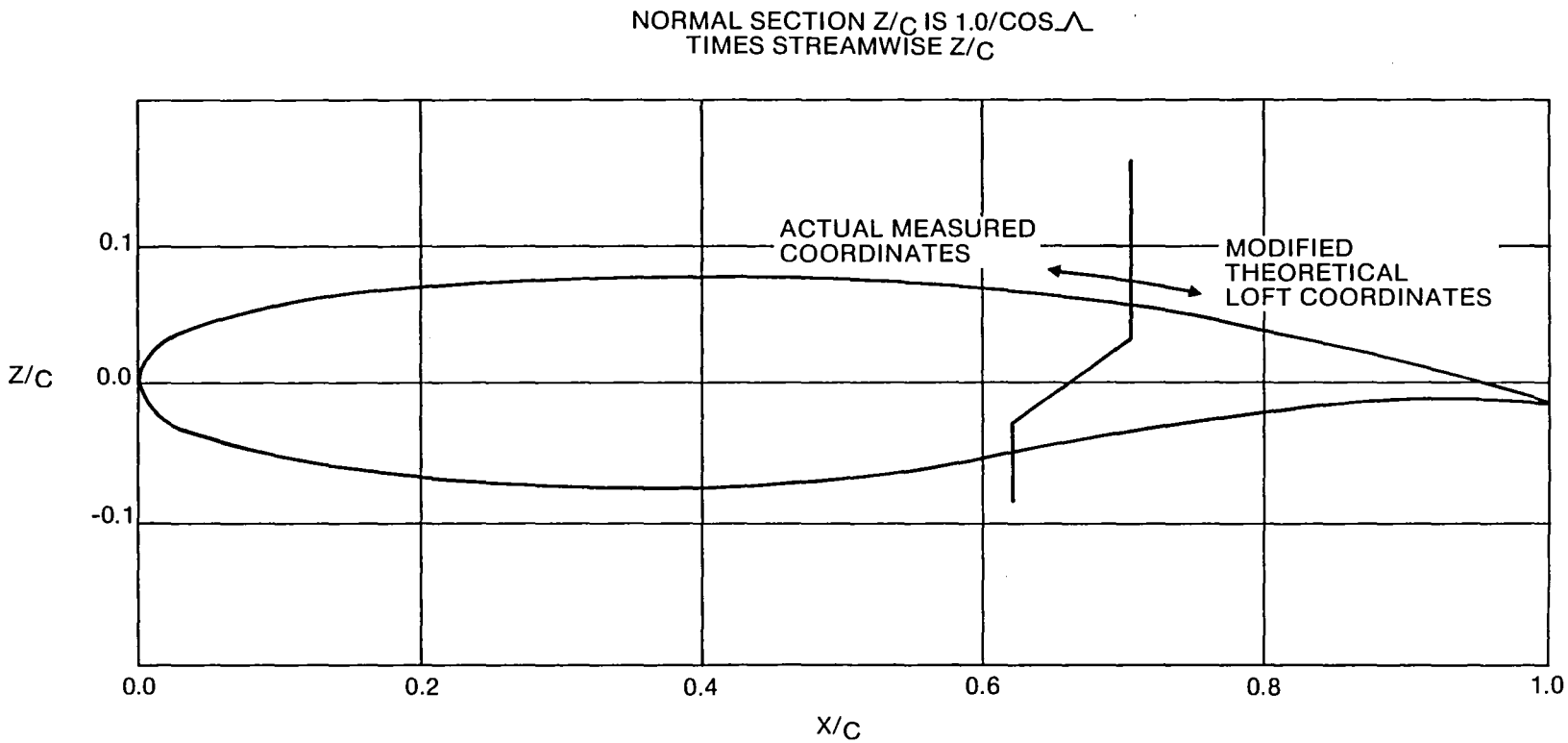

FIG. 22 Airfoil (Normal Section) Used For Theoretical Analyses

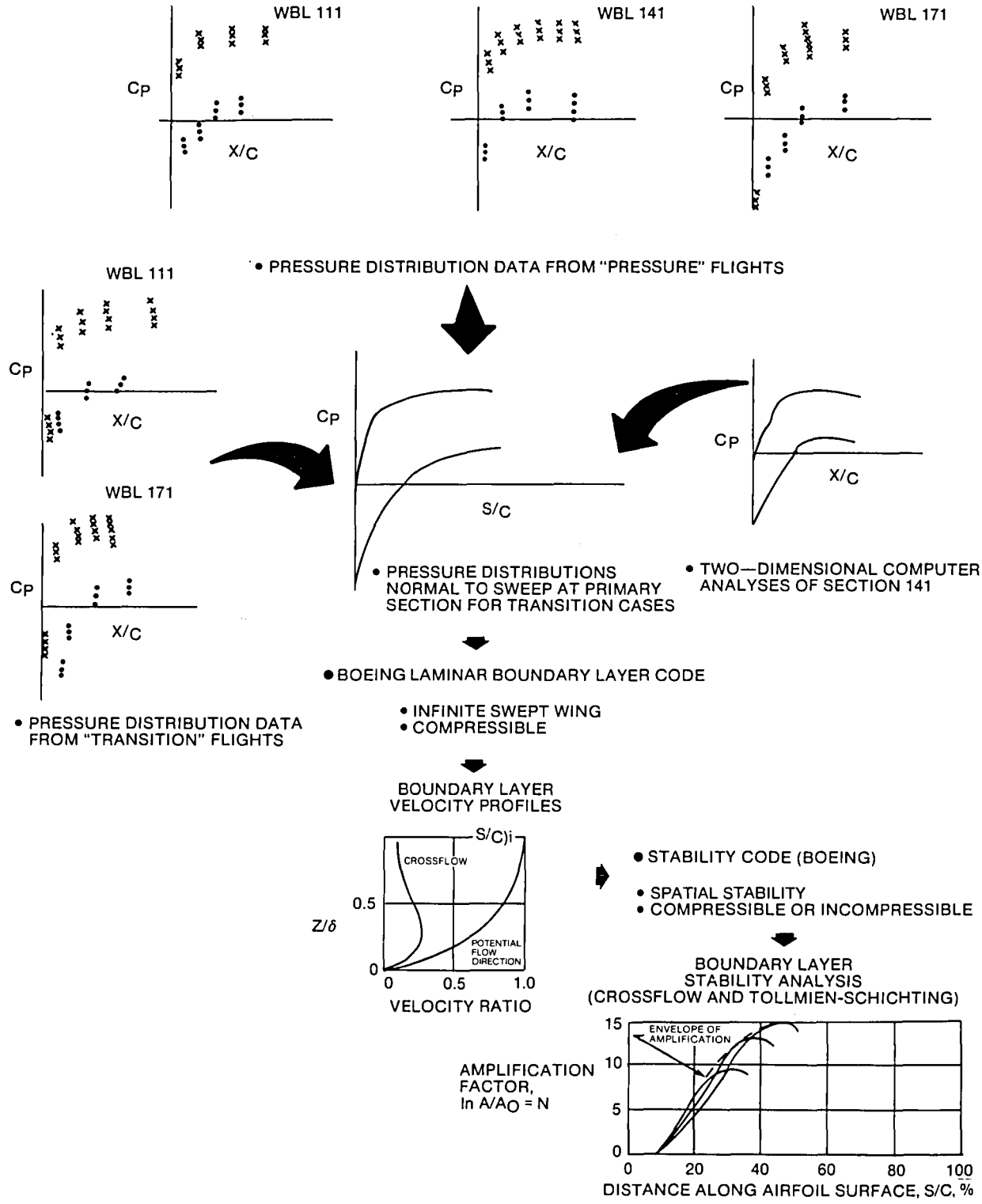

FIG. 23 Overall Stability Analysis Procedure

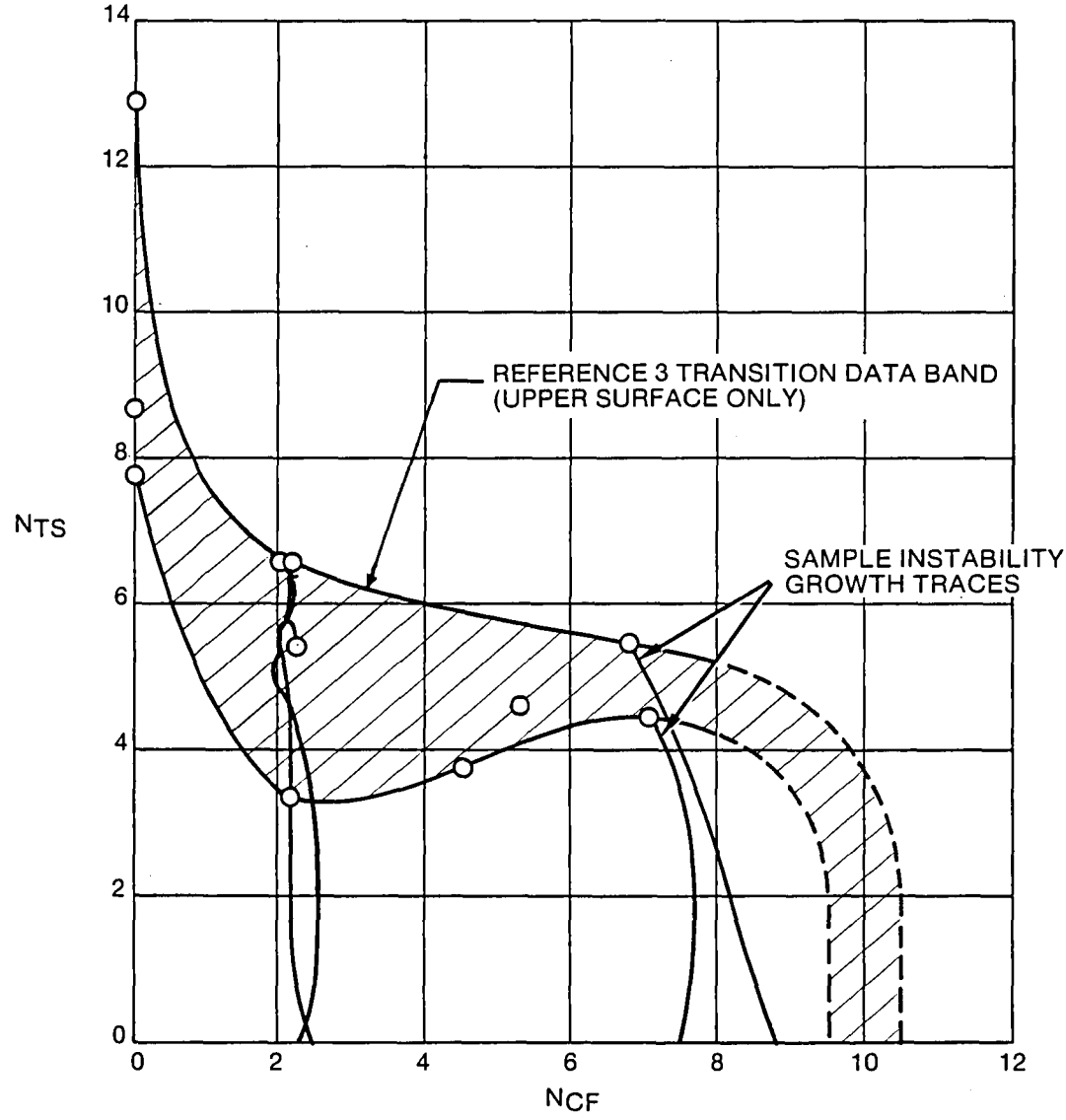

Fig. 24 F-111 Flight Data Transition N-Factors (Reference 3)

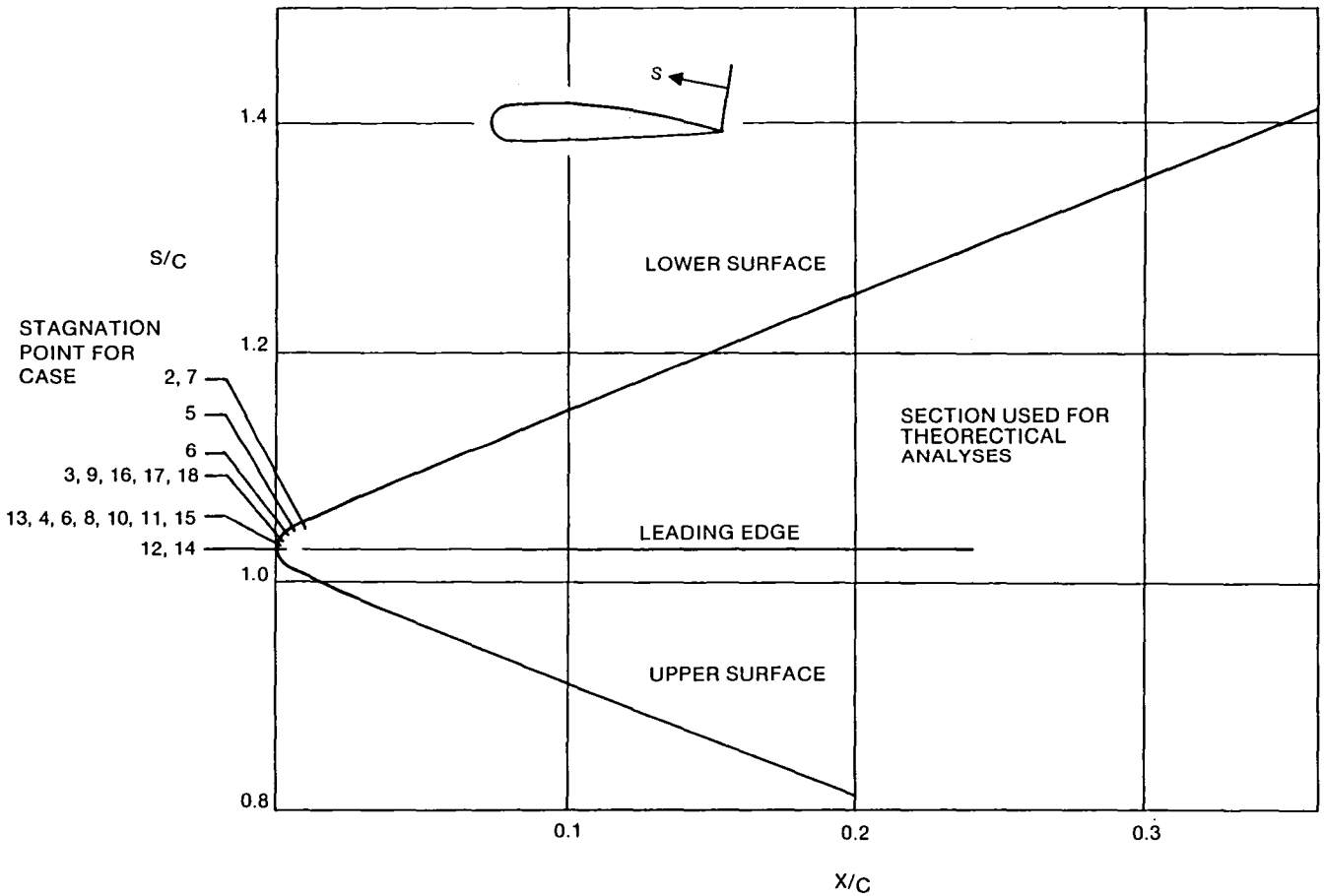

Fig. 25 Relationship of Surface and Chordwise Distance on "Normal" Test Section

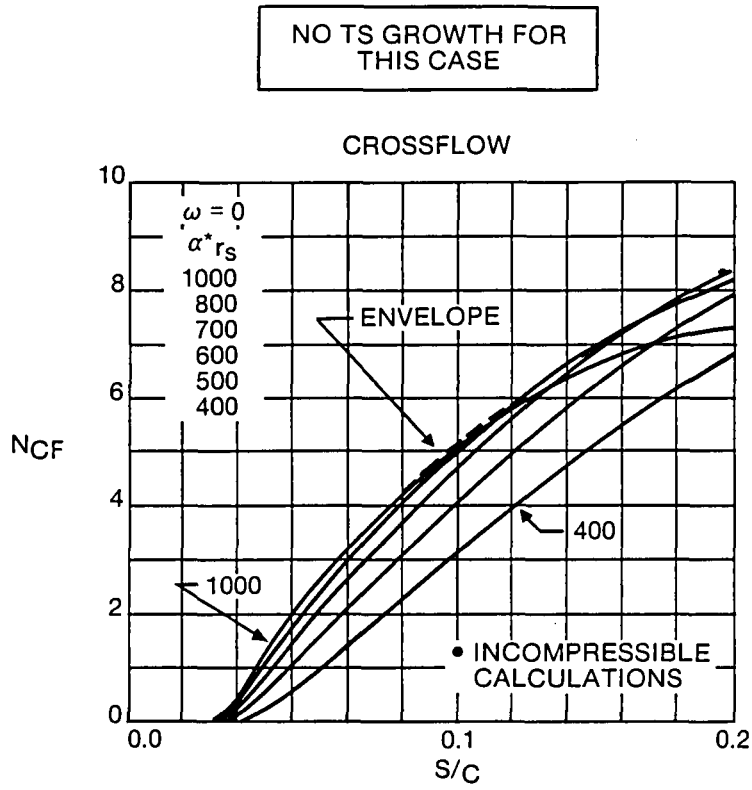

Fig. 26 Citation III Stability Analysis Results, Case 2,Lower Surface

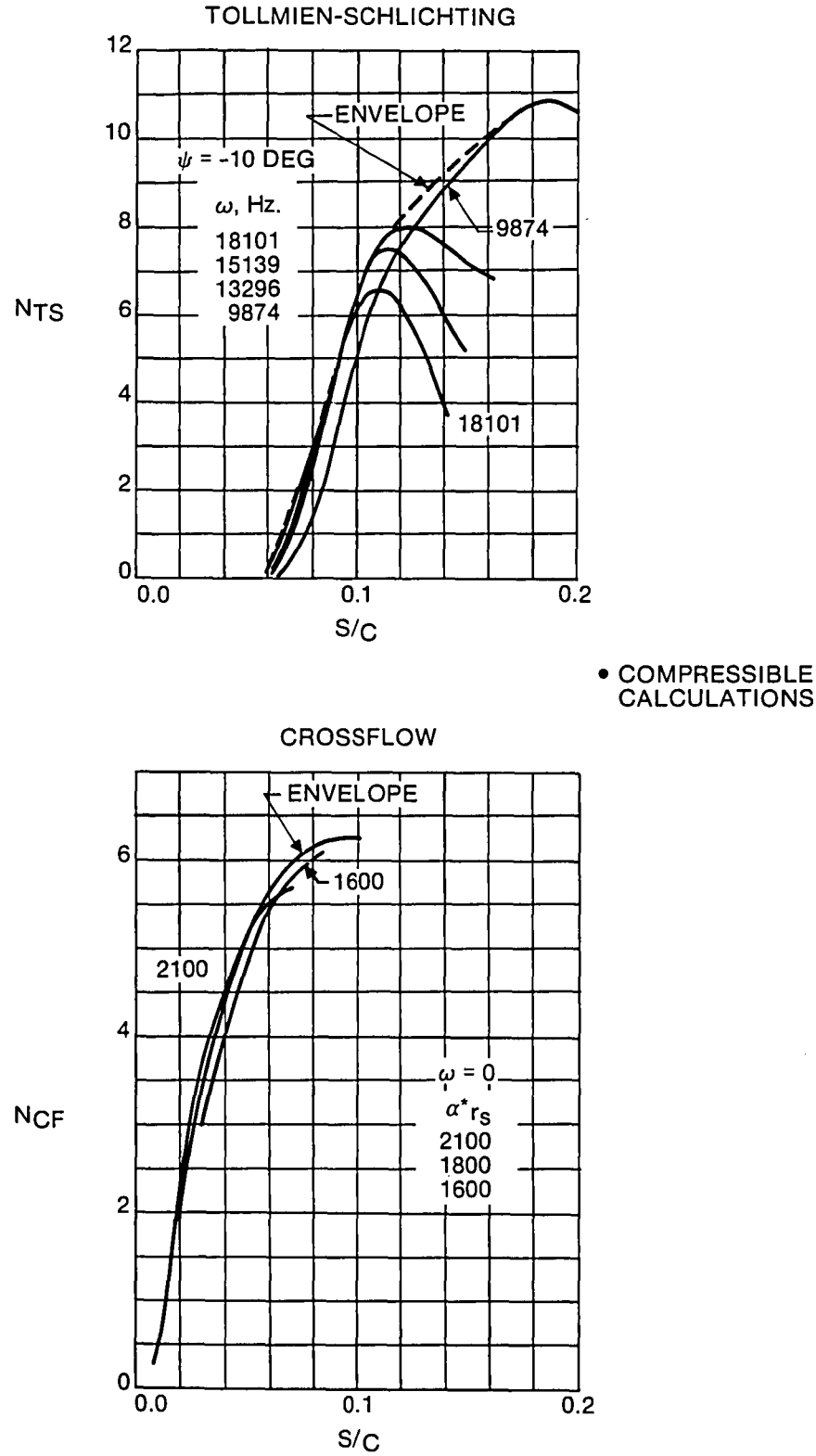

Fig. 27 Citation III Stability Analysis Results, Case 3,Upper Surface

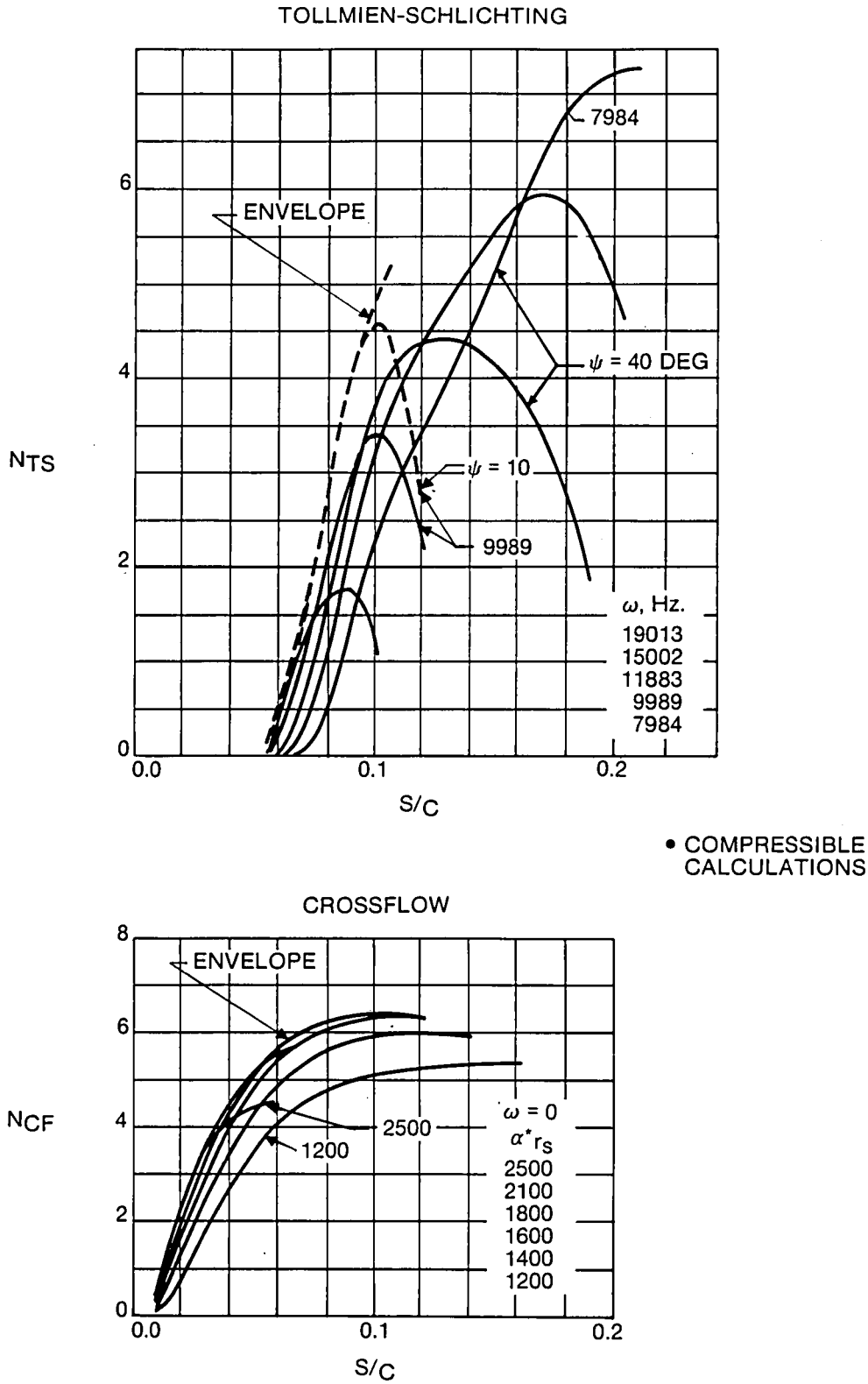

Fig. 28 Citation III Stability Analysis Results, Case 4, Upper Surface

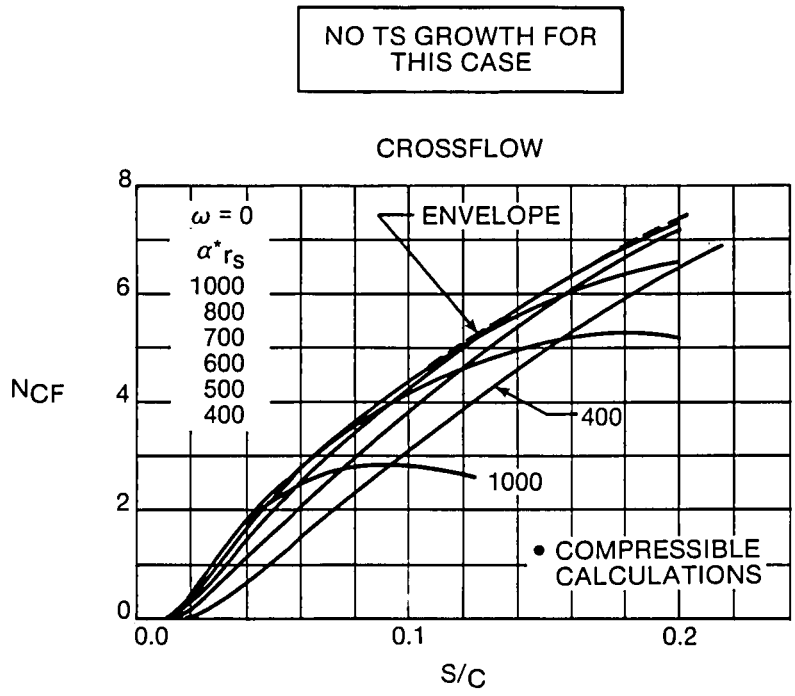

Fig. 29 Citation III Stability Analysis Results, Case 5,Lower Surface

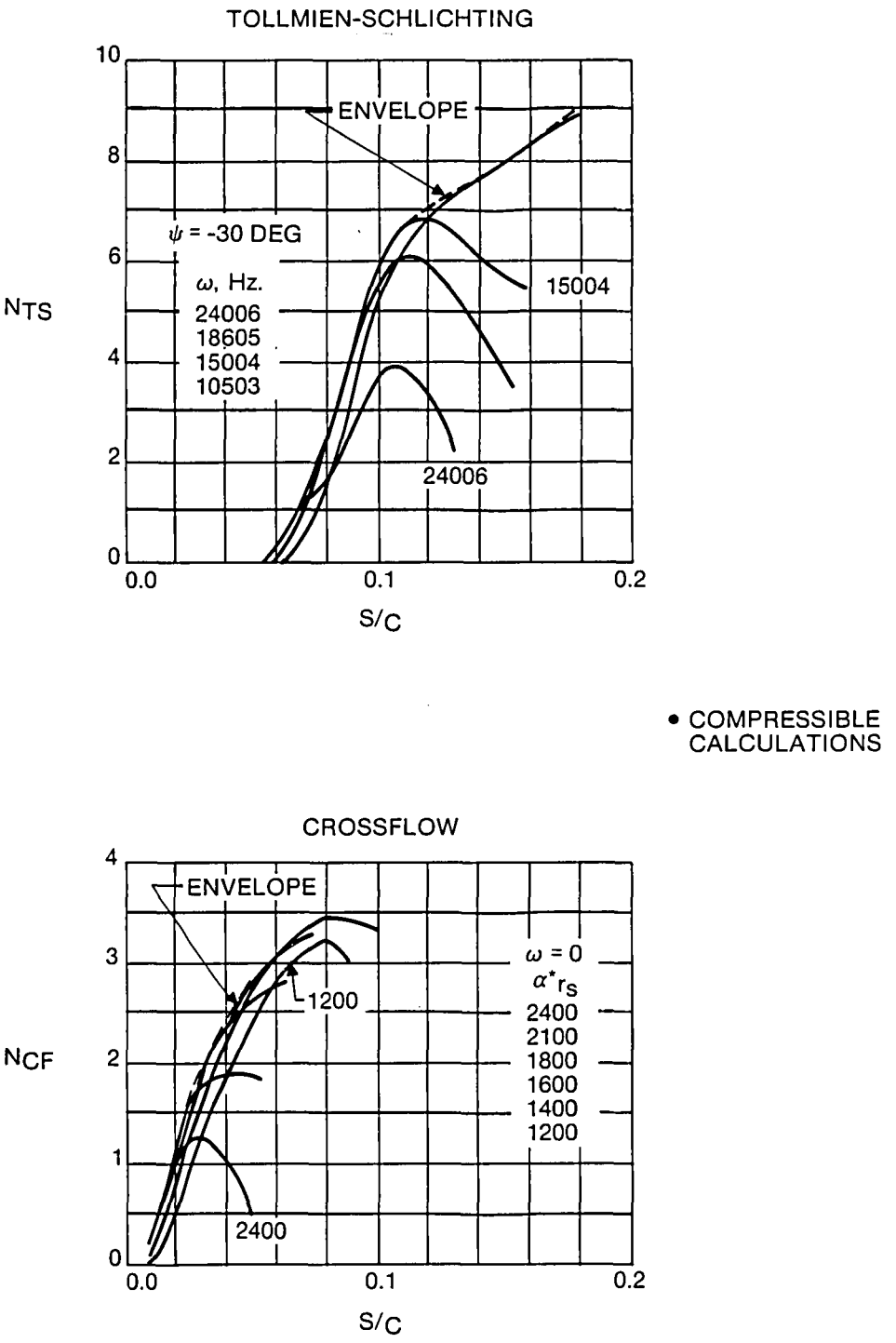

Fig. 30 Citation III Stability Analysis Results, Case 6,Upper Surface

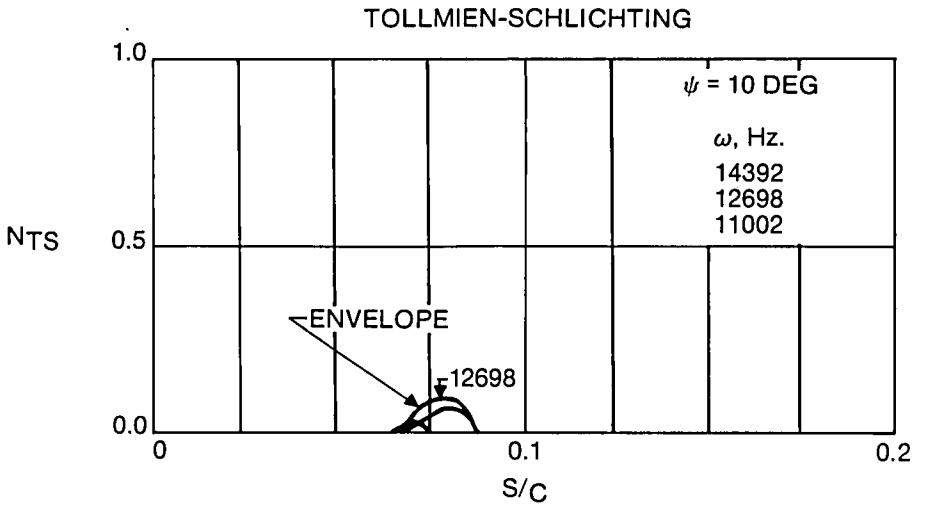

• COMPRESSIBLE CALCULATIONS

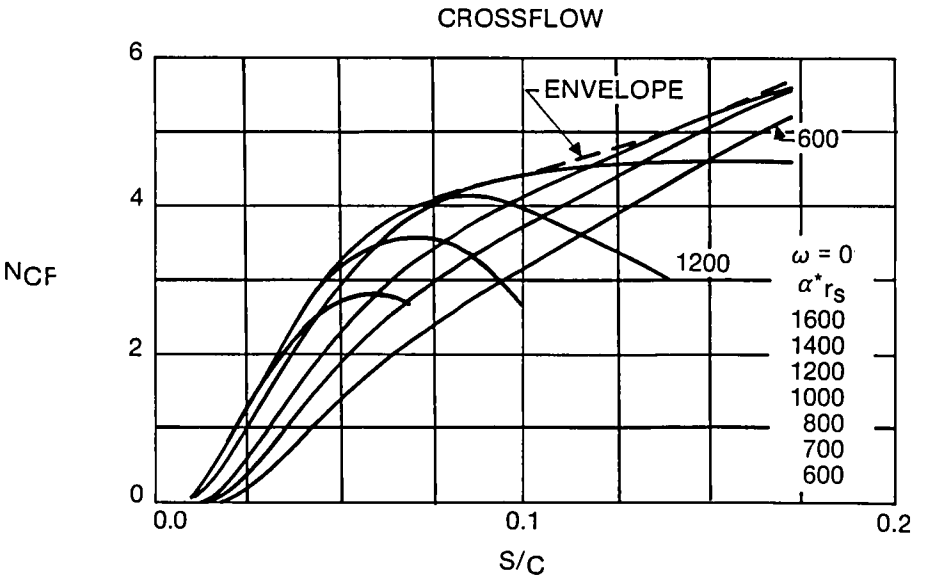

Fig. 31 Citation III Stability Analysis Results, Case 7, Lower Surface

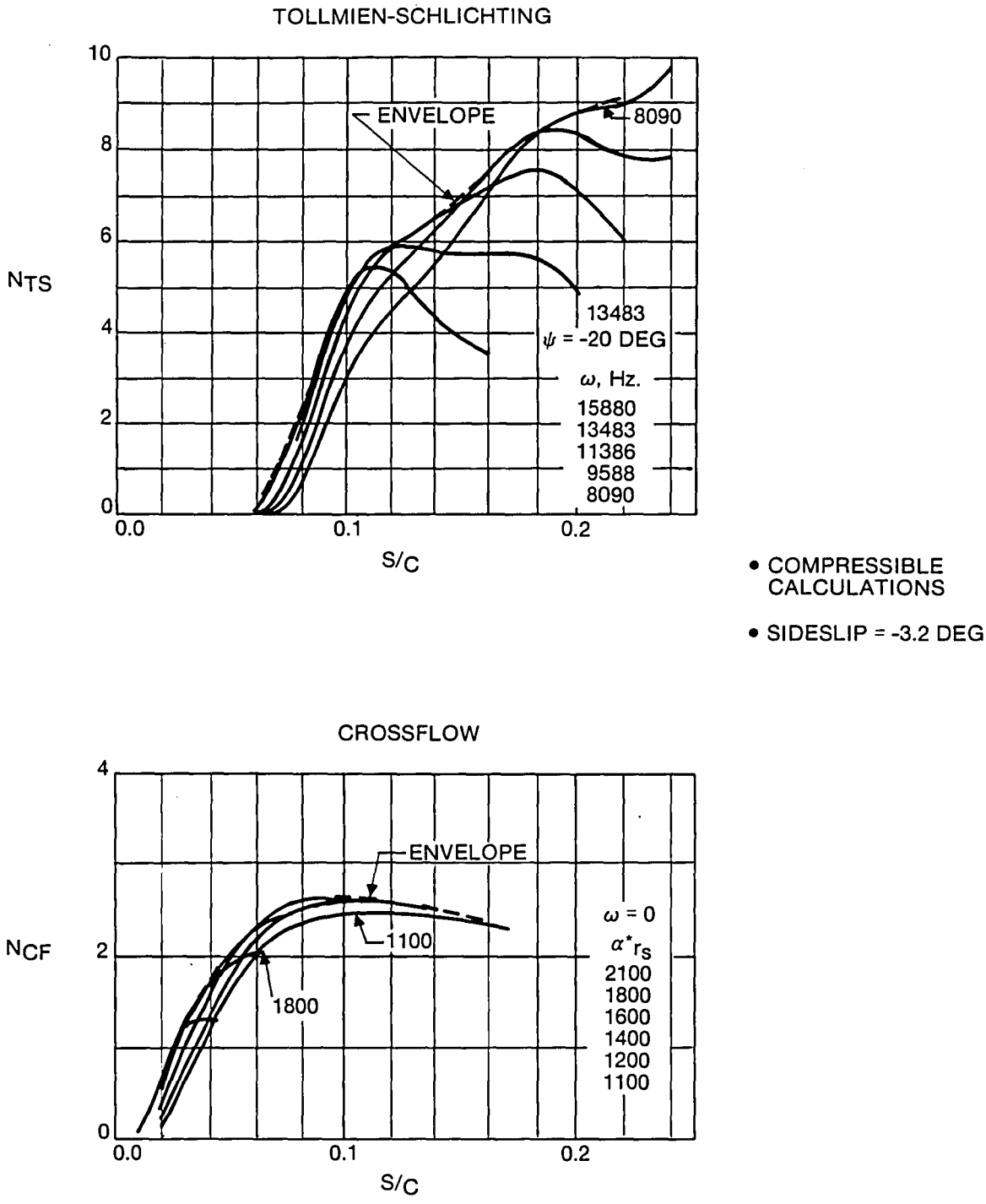

Fig. 32 Citation III Stability Analysis Results, Case 8, Upper Surface

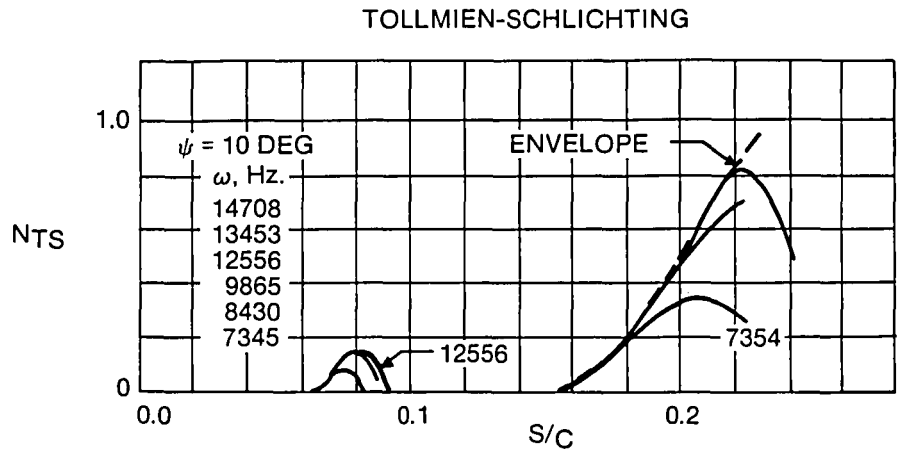

- COMPRESSIBLE CALCULATIONS
- SIDESLIP = -2.5 DEG.

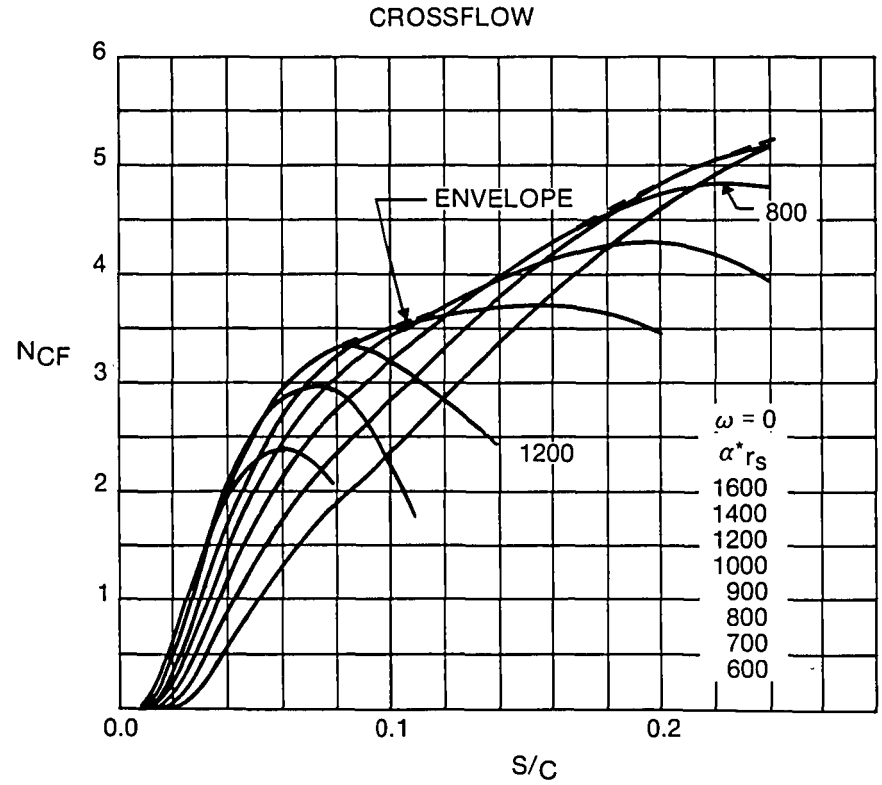

Fig. 33 Citation III Stability Analysis Results, Case 9 Lower Surface

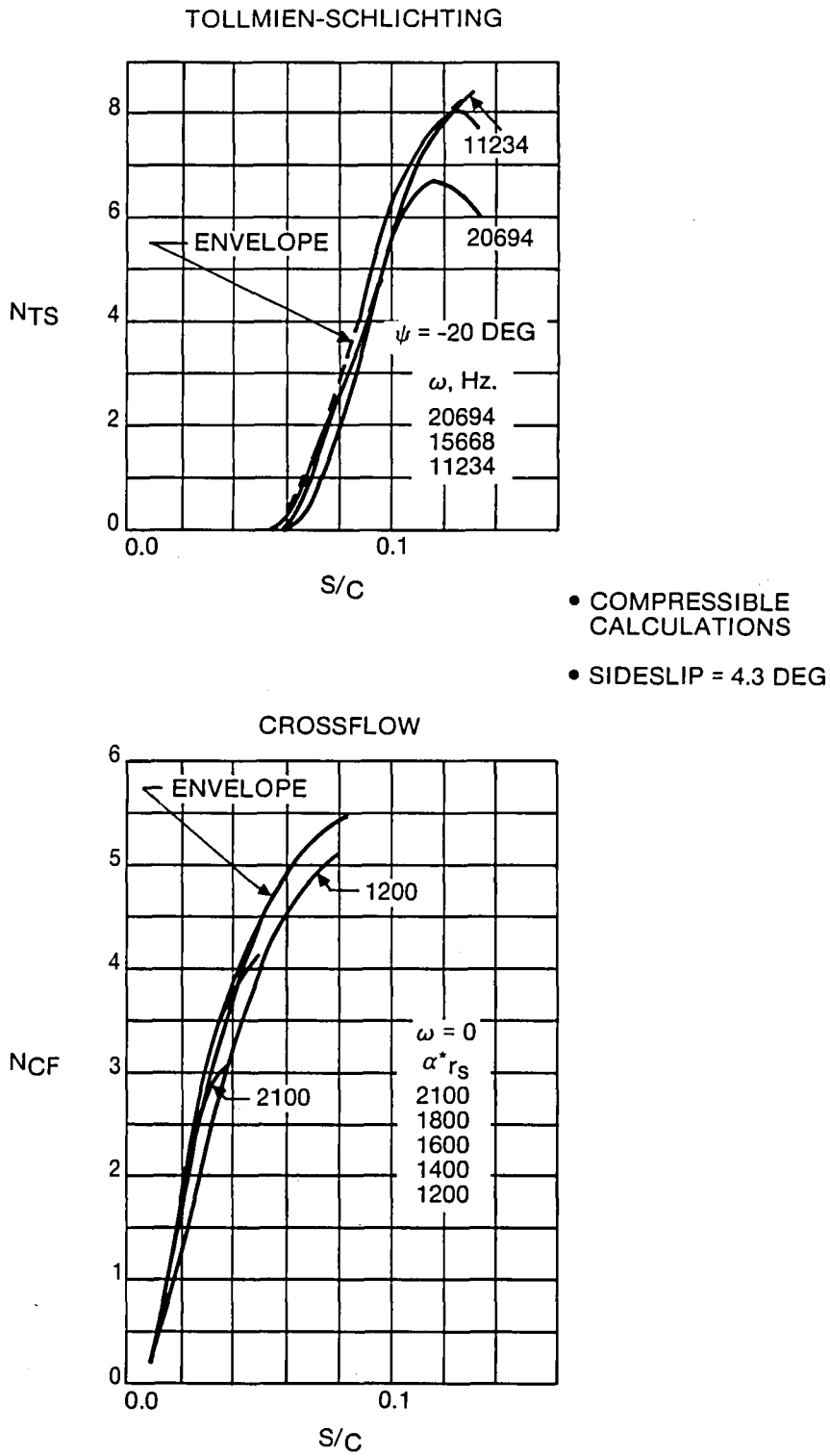

Fig. 34 Citation III Stability Analysis Results, Case 10, Upper Surface

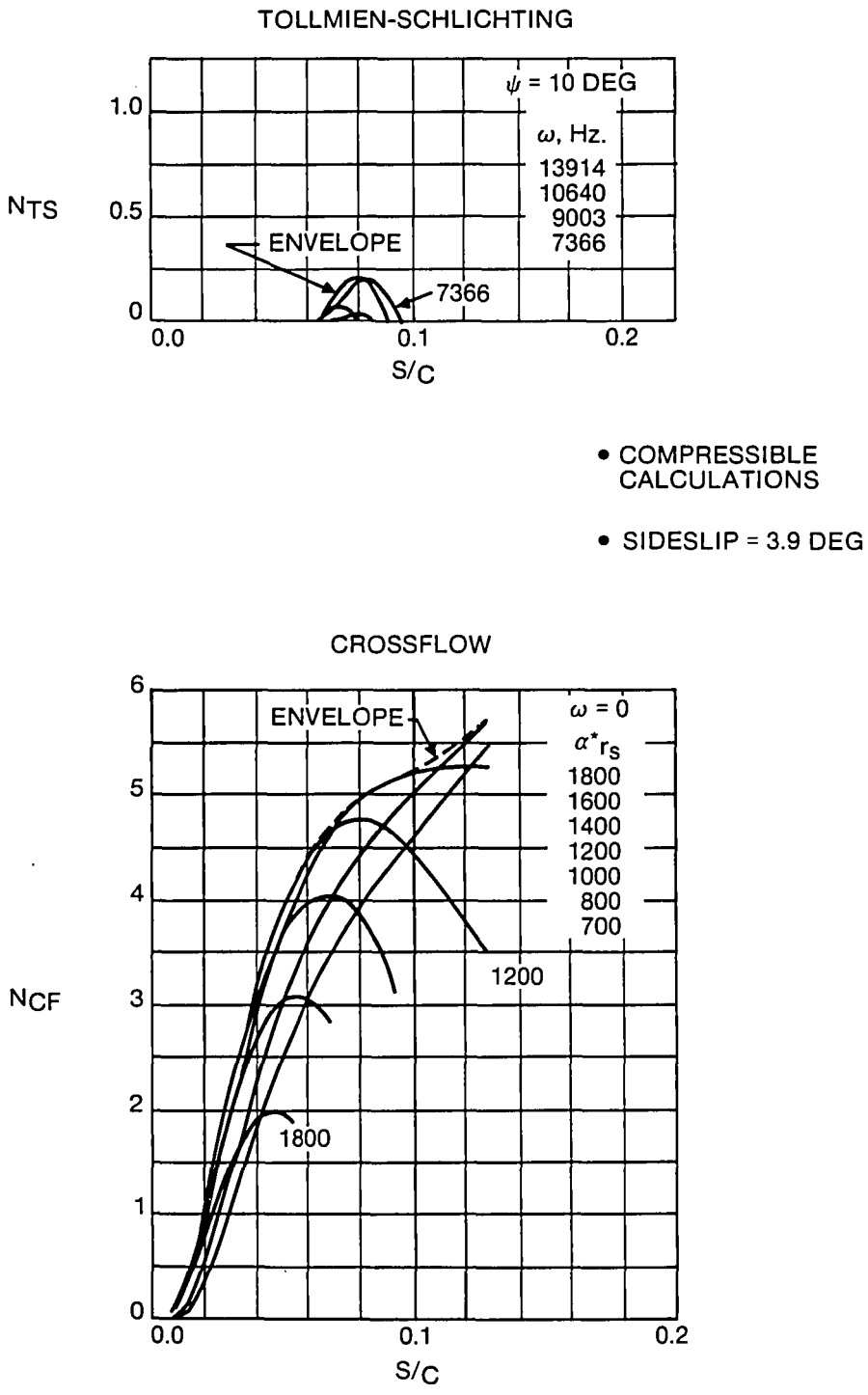

Fig. 35 Citation III Stability Analysis Results, Case 11, Lower Surface

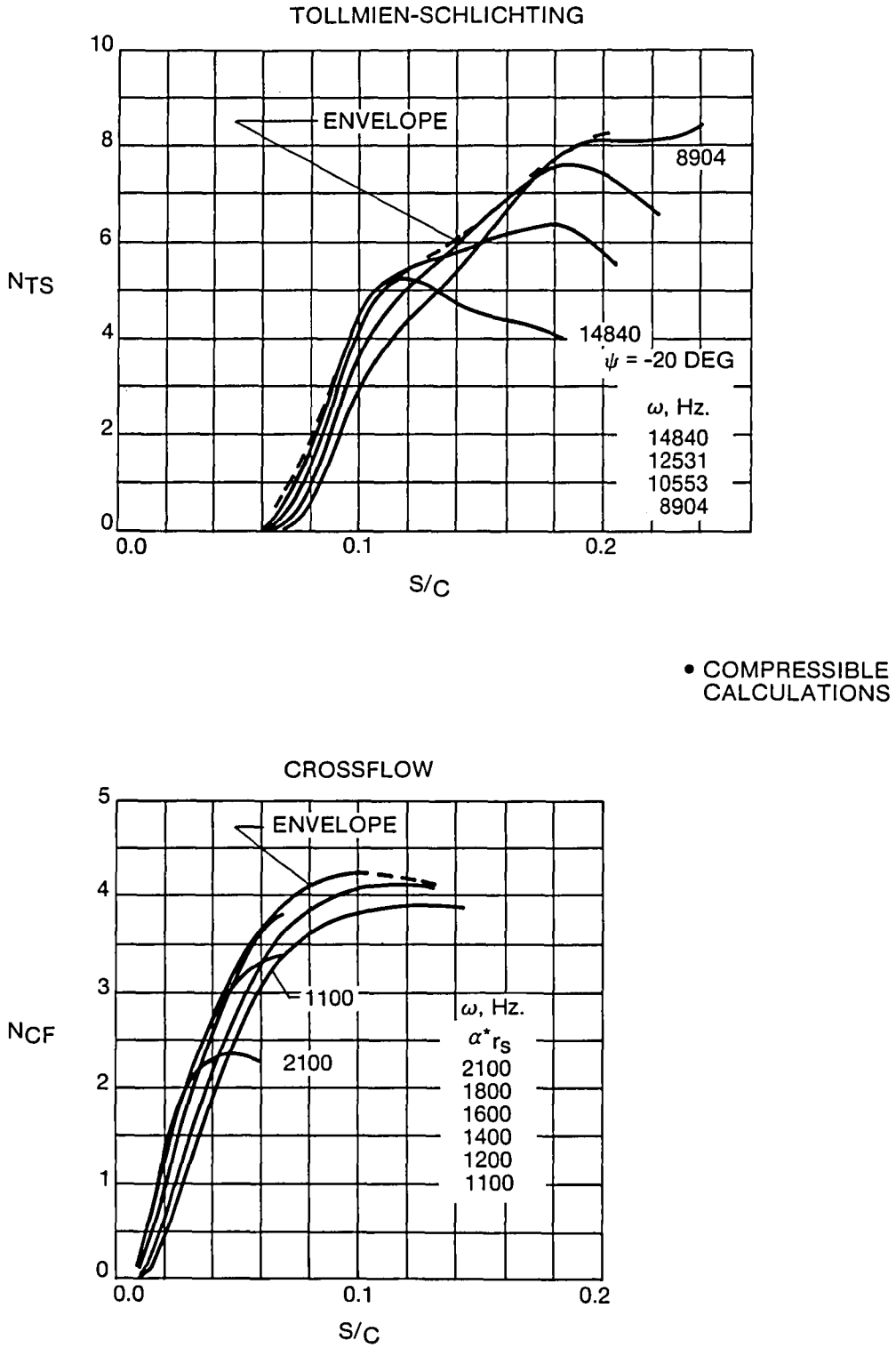

Fig. 36 Citation III Stability Analysis Results, Case 12, Upper Surface

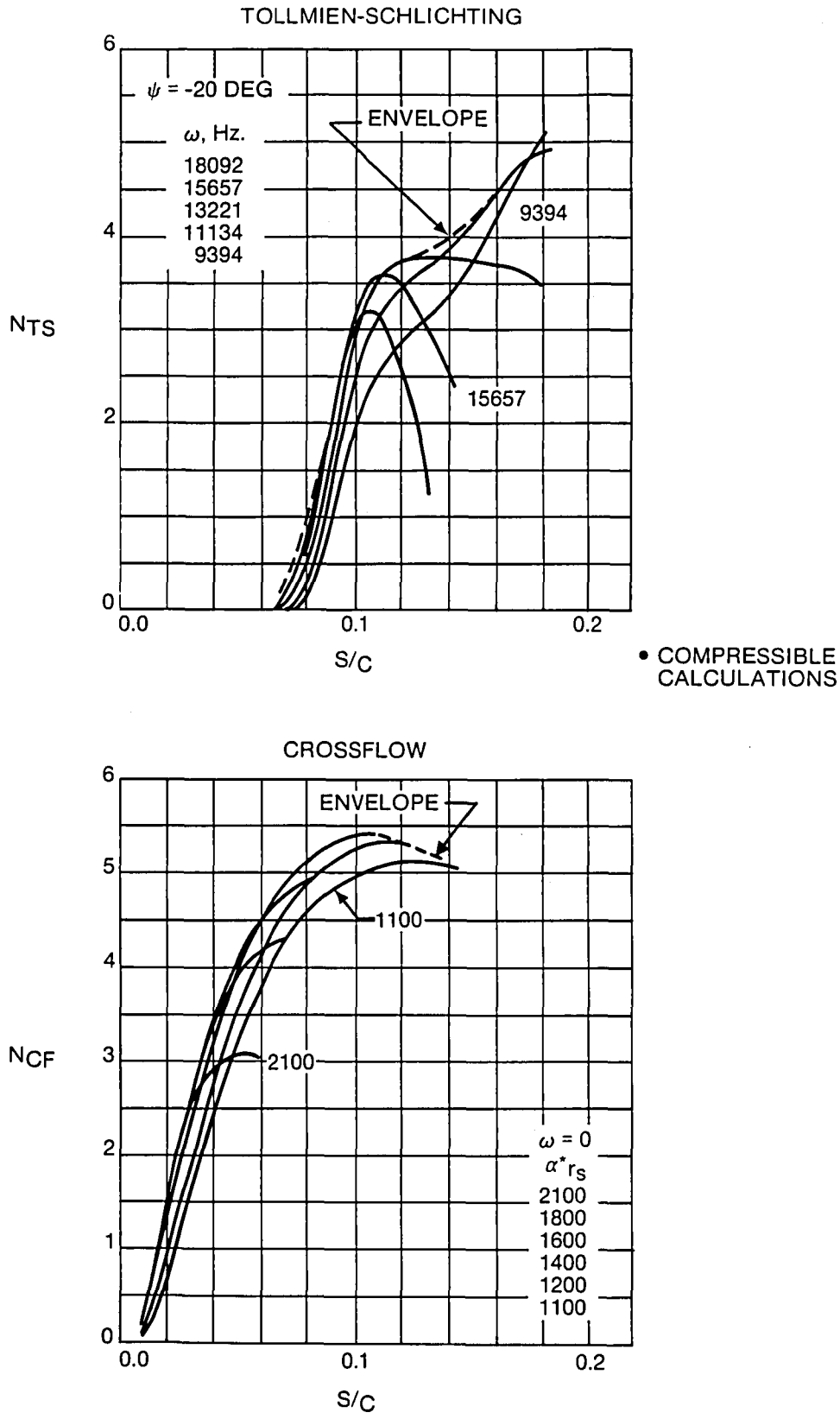

Fig. 37 Citation III Stability Analysis Results, Case 13, Upper Surface

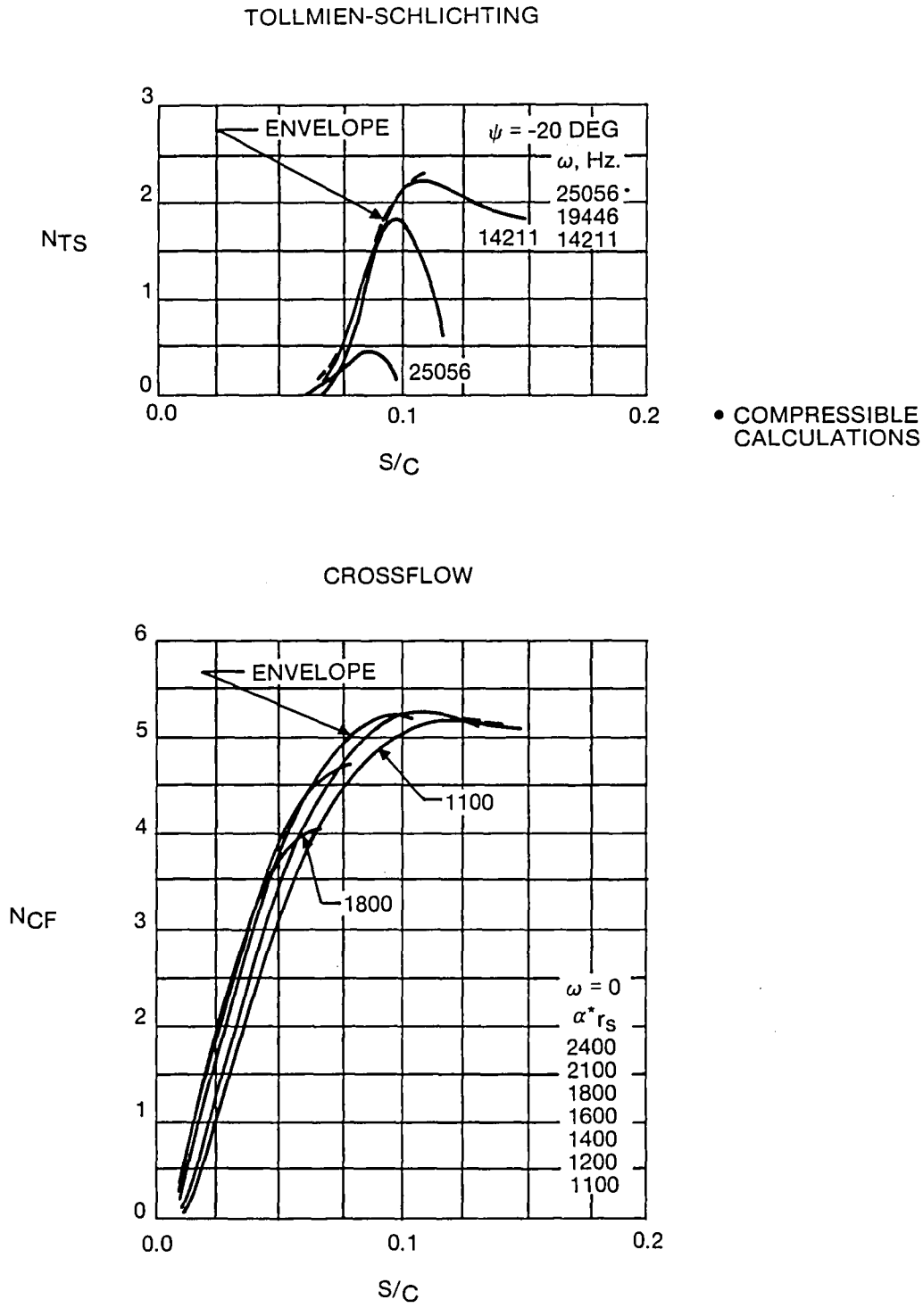

Fig. 38 Citation III Stability Analysis Results, Case 14, Upper Surface

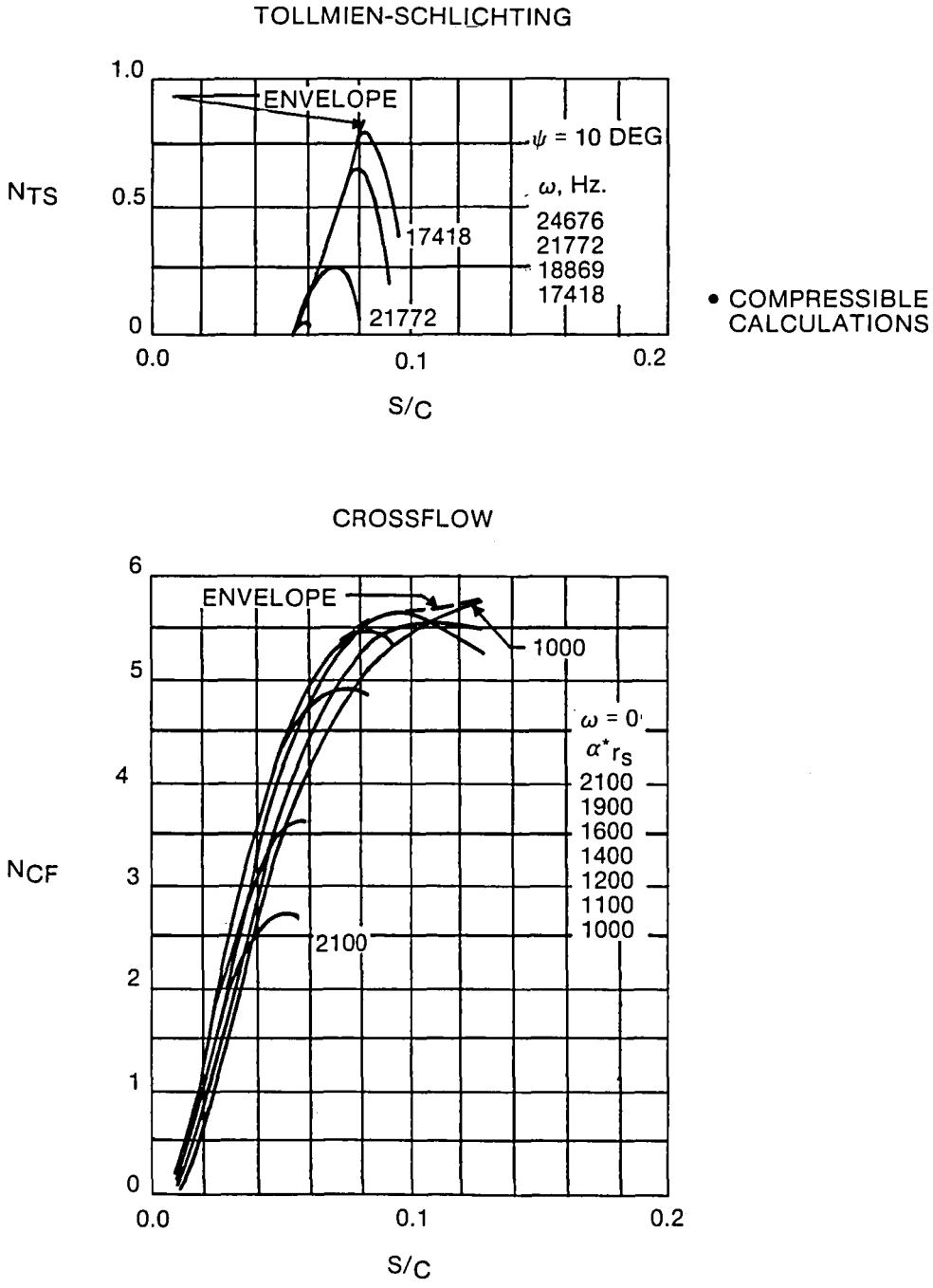

Fig. 39 Citation III Stability Analysis Results, Case 15, Lower Surface

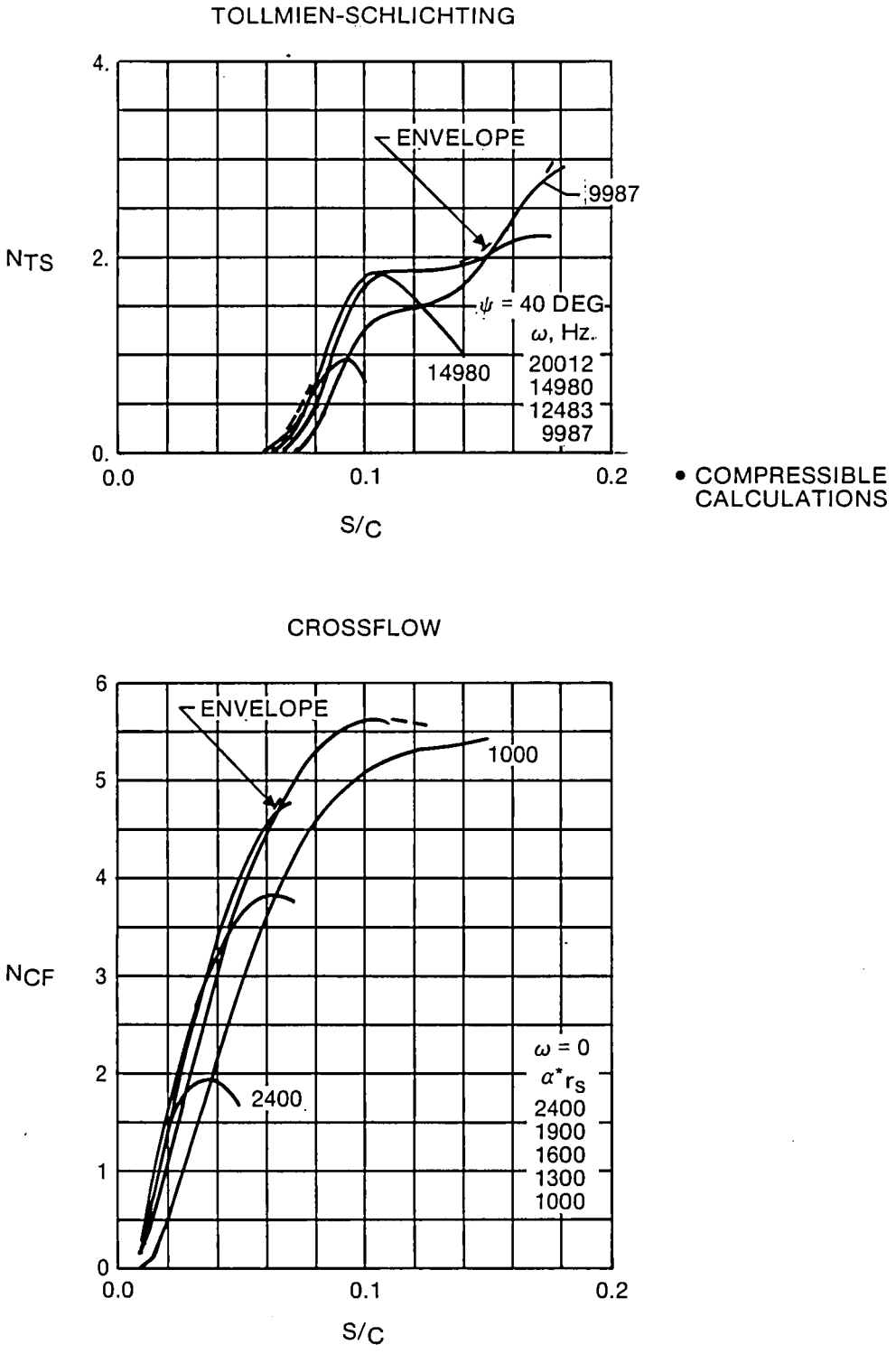

Fig. 40 Citation III Stability Analysis Results, Case 16,Upper Surface

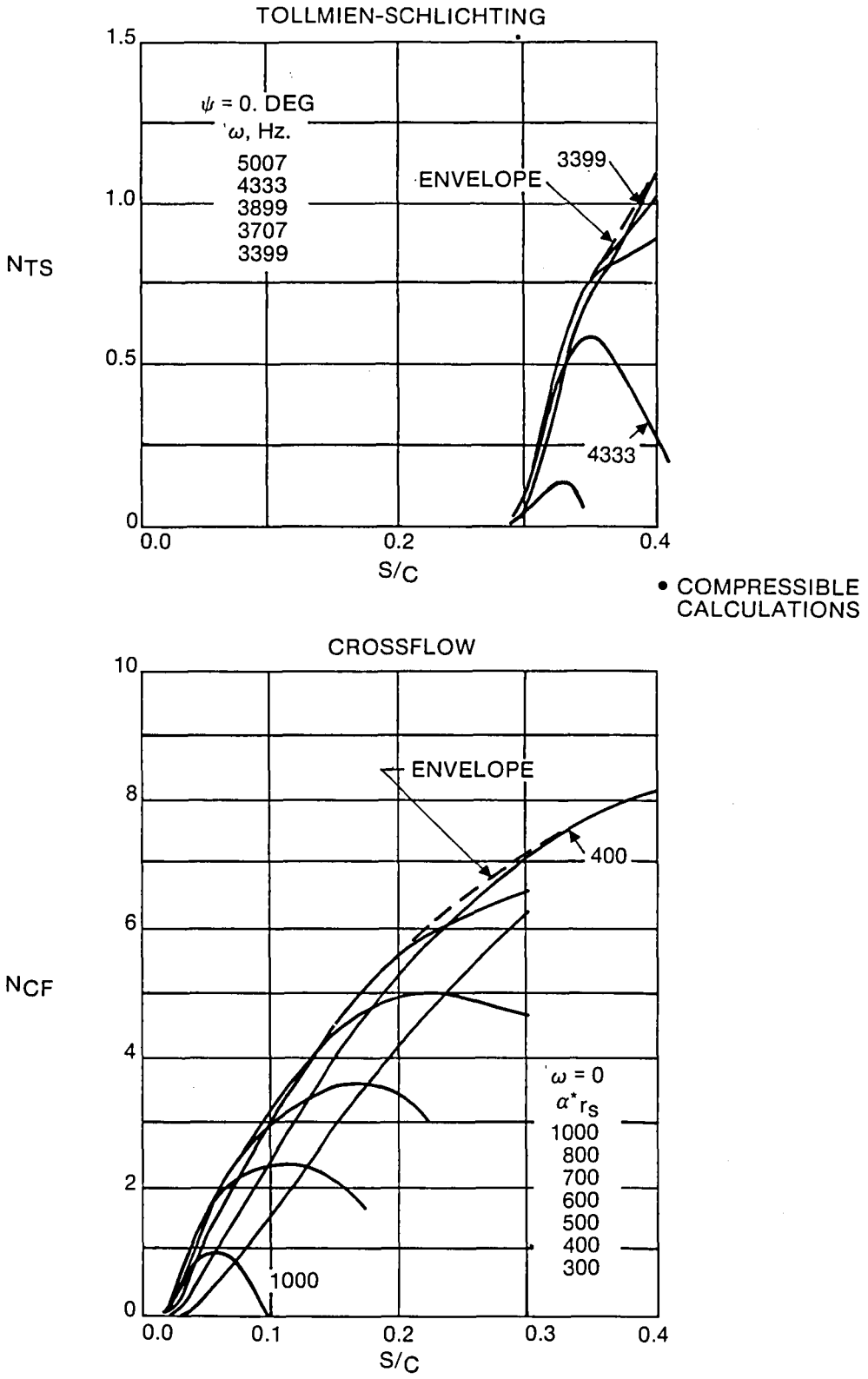

Fig. 41 Citation III Stability Analysis Results, Case 17, Lower Surface

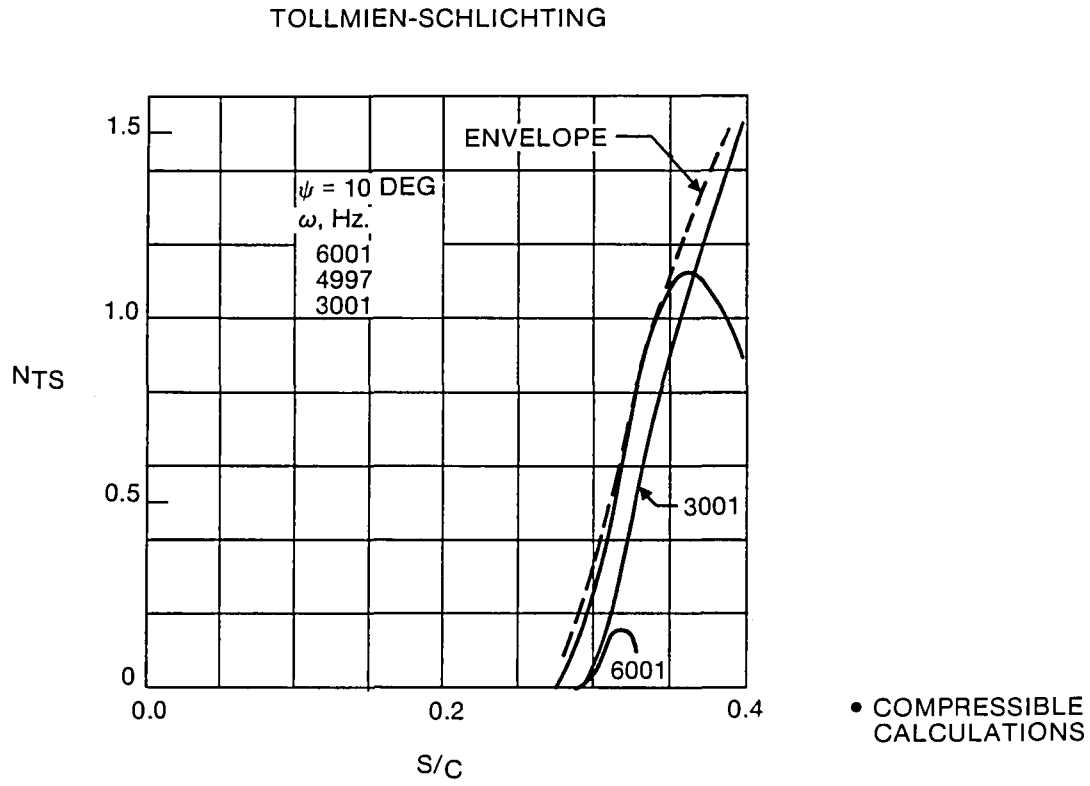

Fig. 42 Citation III Stability Analysis Results, Case 18, Lower Surface

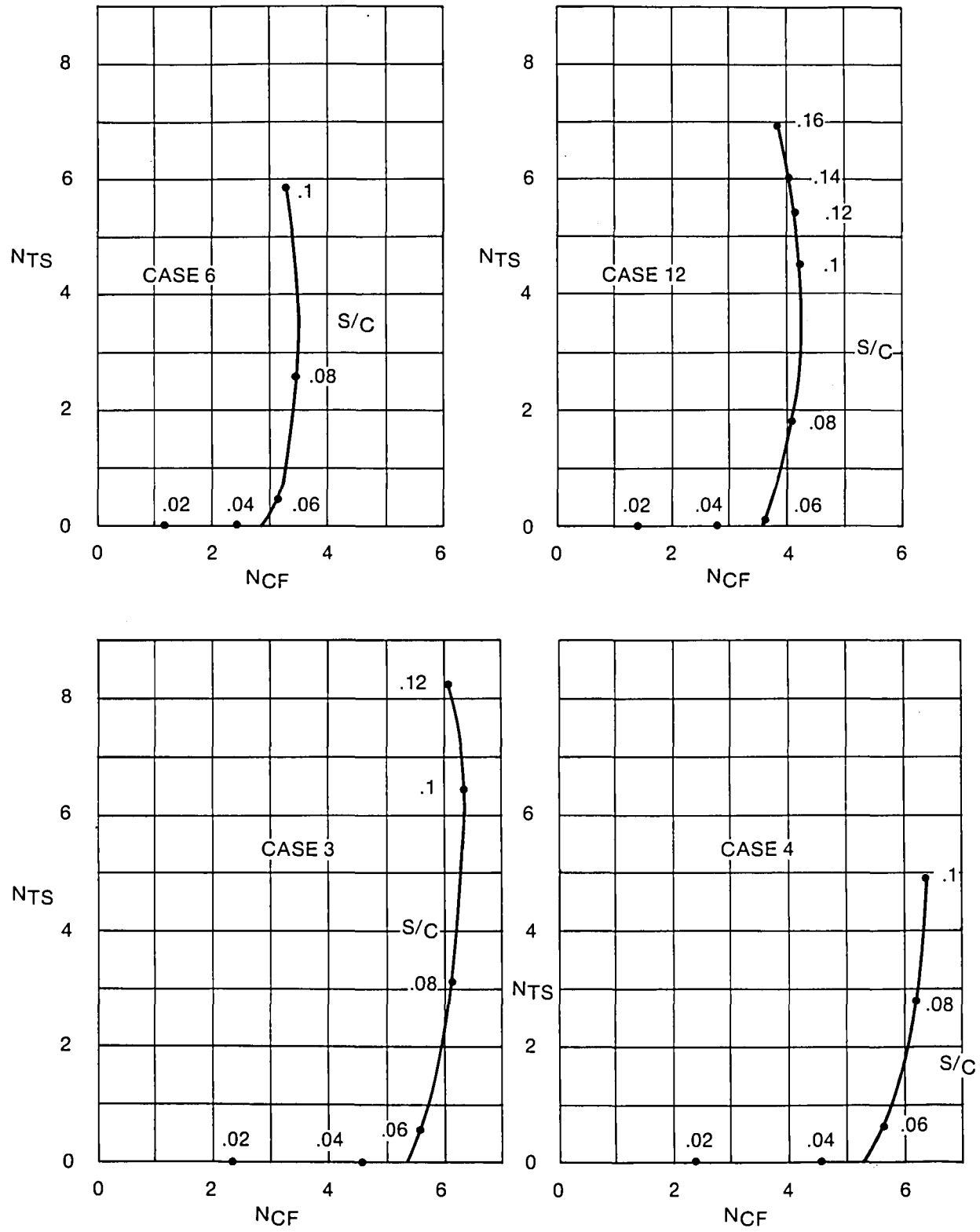

Fig. 43 Instability Growth Traces, Upper Surface

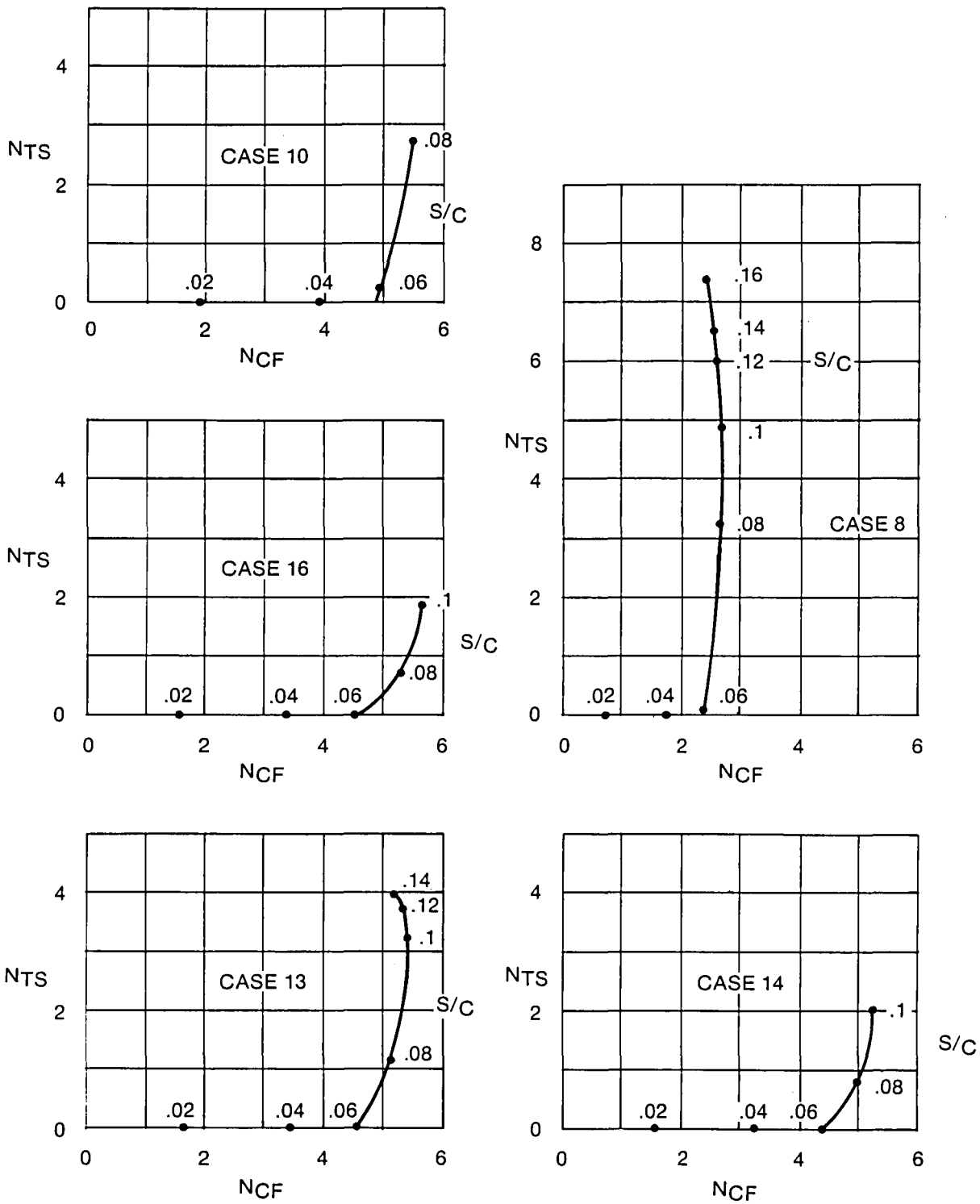

Fig. 43 Instability Growth Traces, Upper Surface

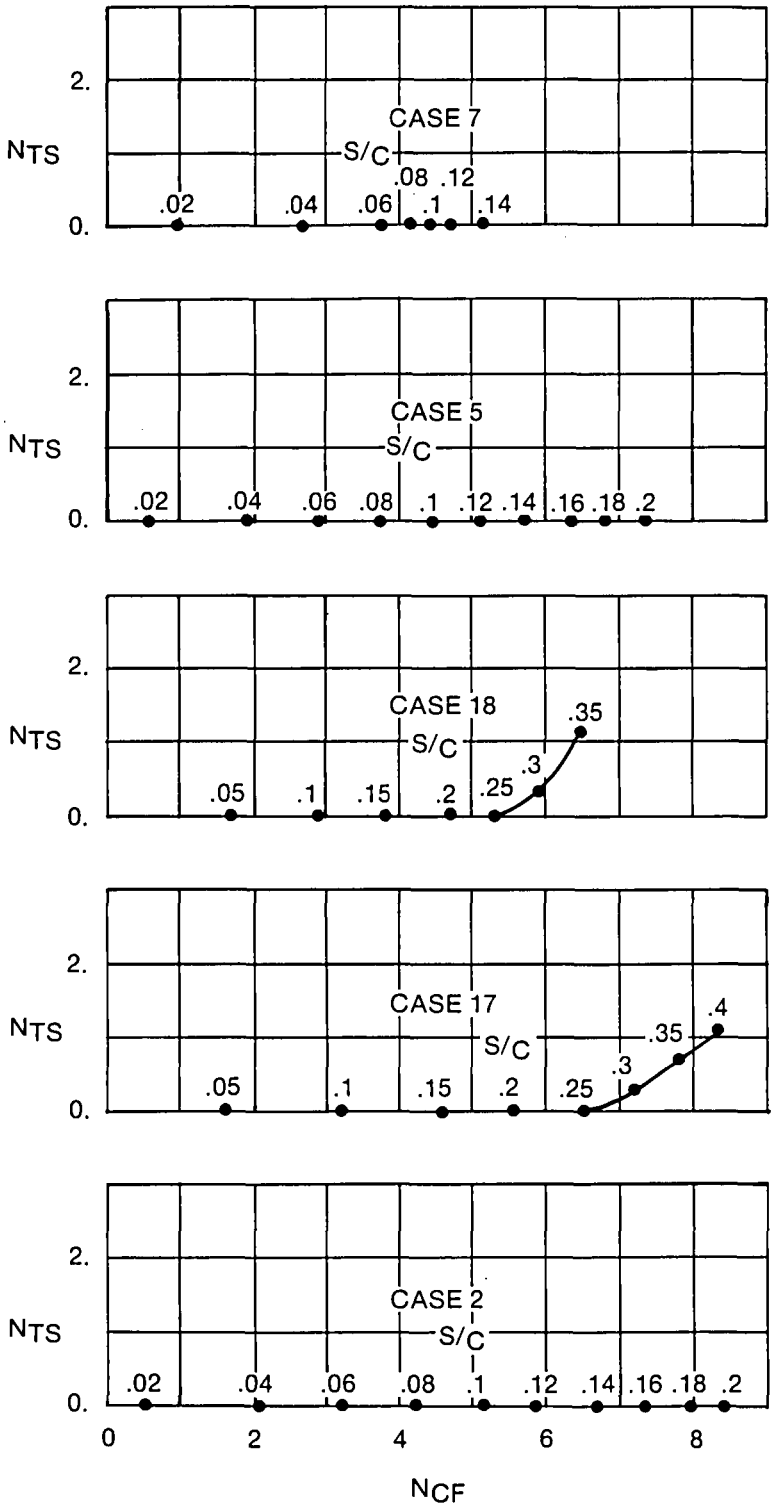

Fig. 44 Instability Growth Traces, Lower Surface

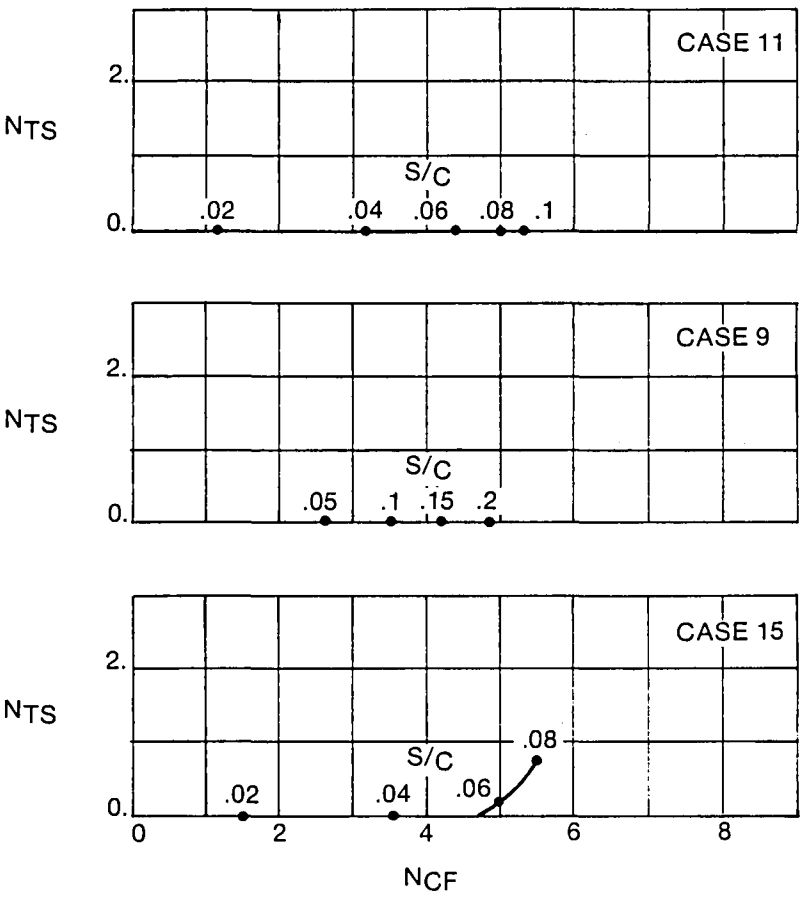

Fig. 44 Instability Growth Traces, Lower Surface

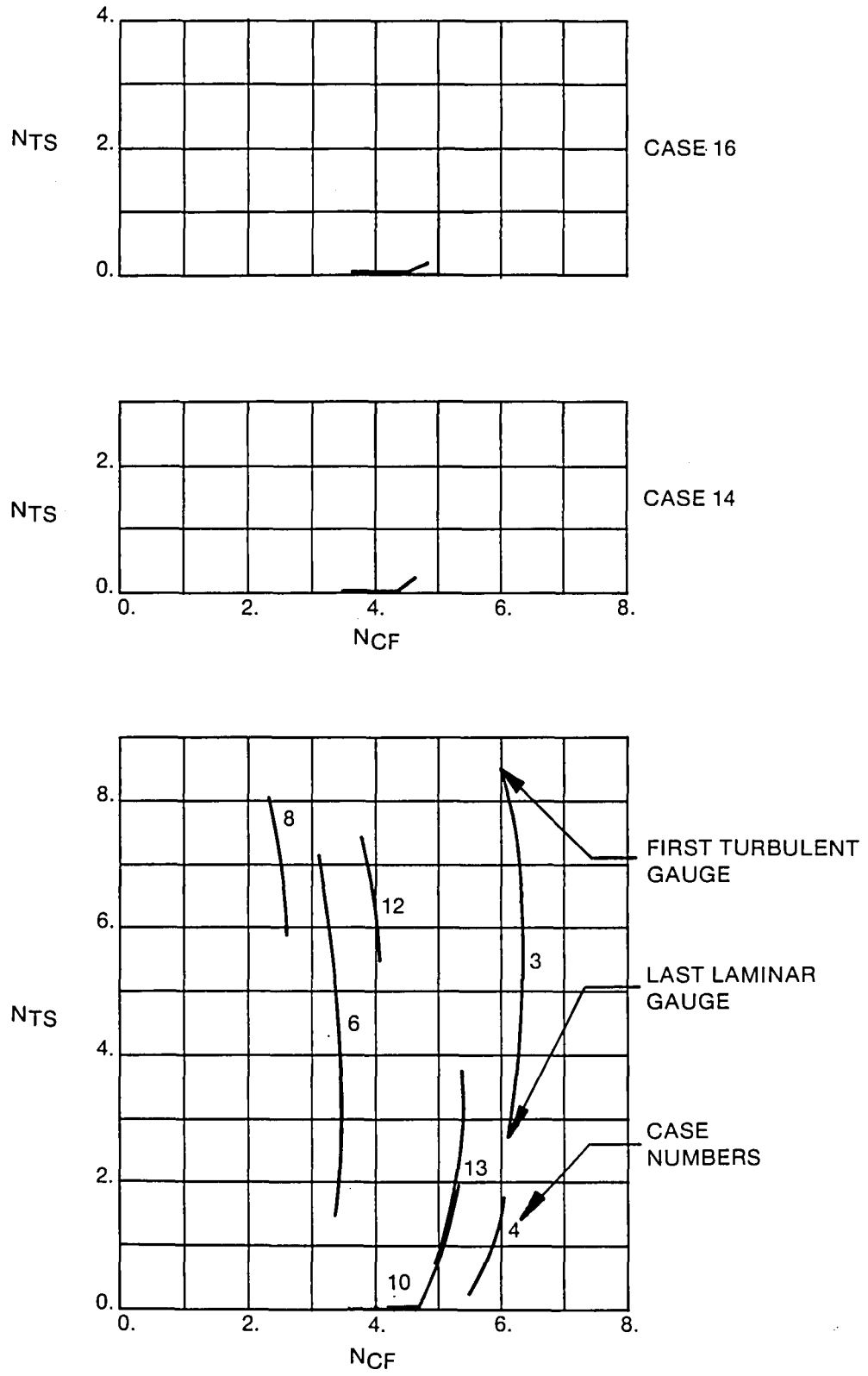

Fig. 45 Range of Instability Growth for Transition, Upper Surface

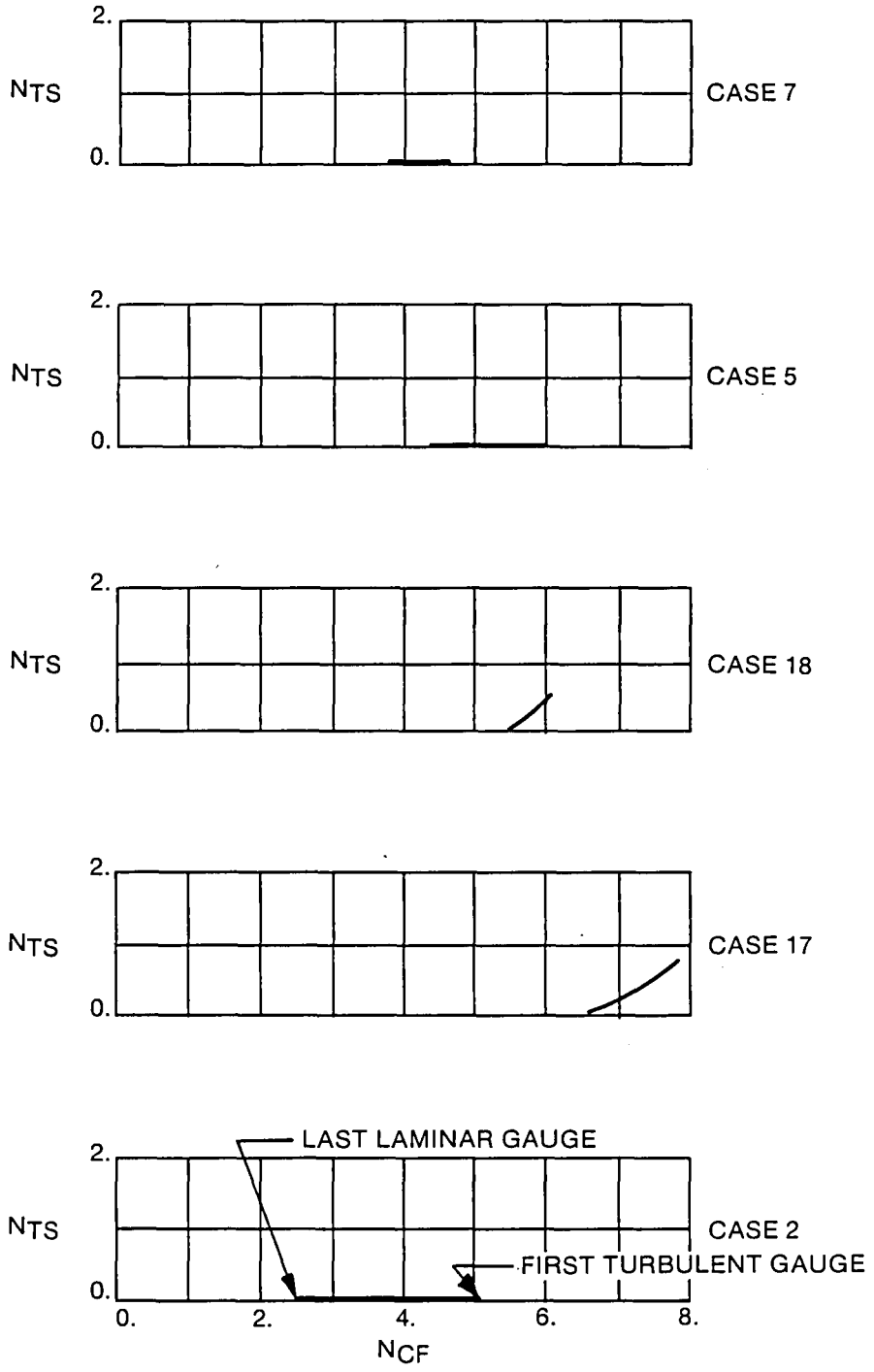

Fig. 46 Range of Instability Growth for Transition, Lower Surface

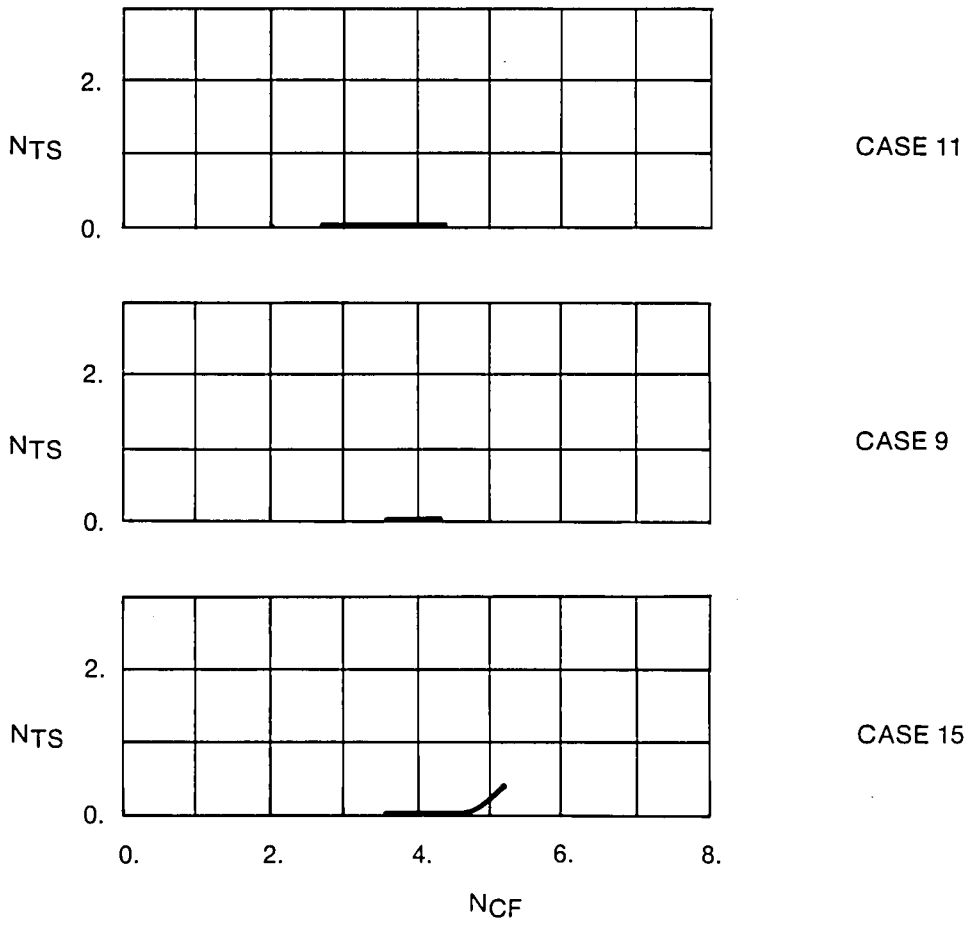

Fig. 46 Range of Instability Growth For Transition, Lower Surface

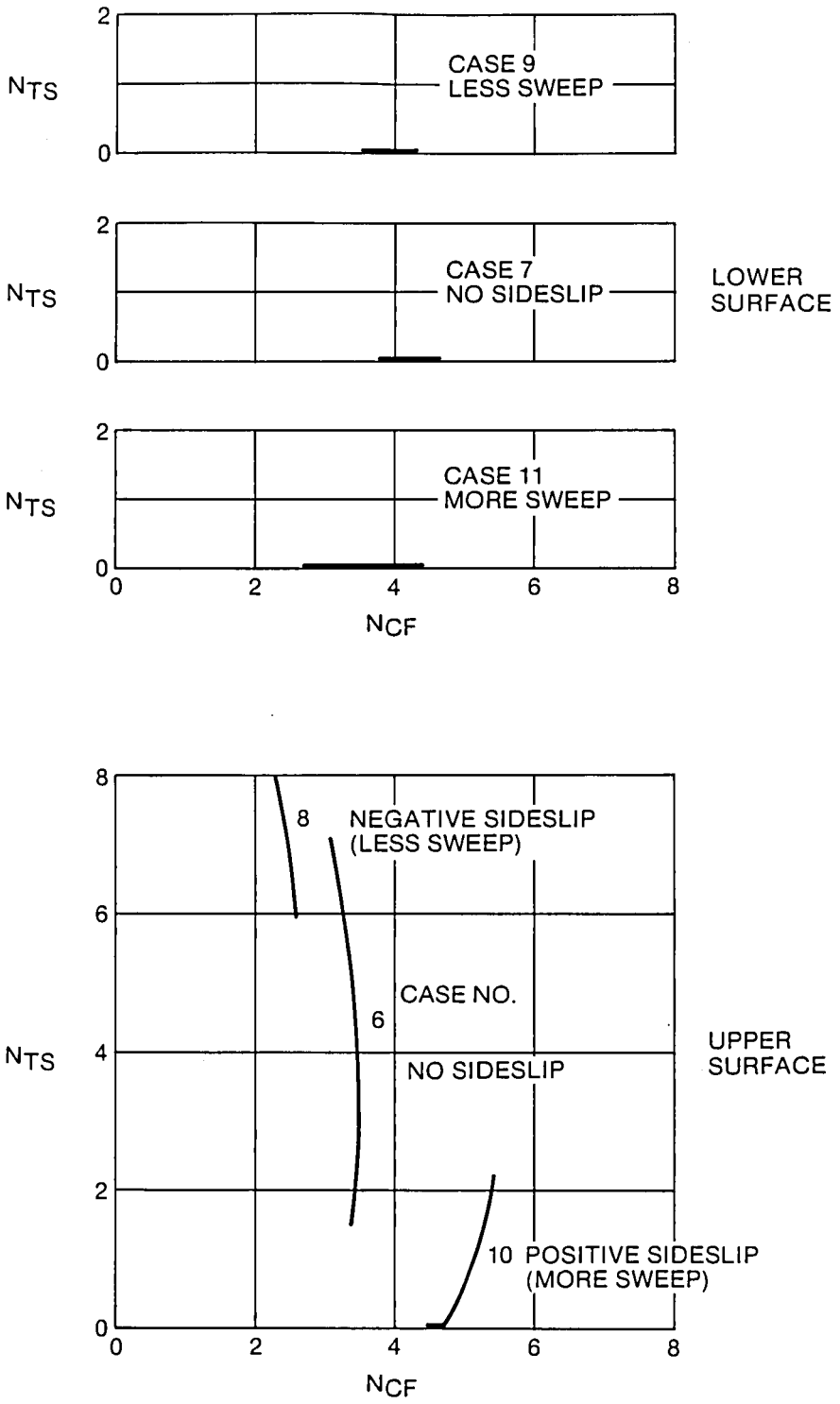

Fig. 47 Effect of Sideslip on Instability Growth at Transition

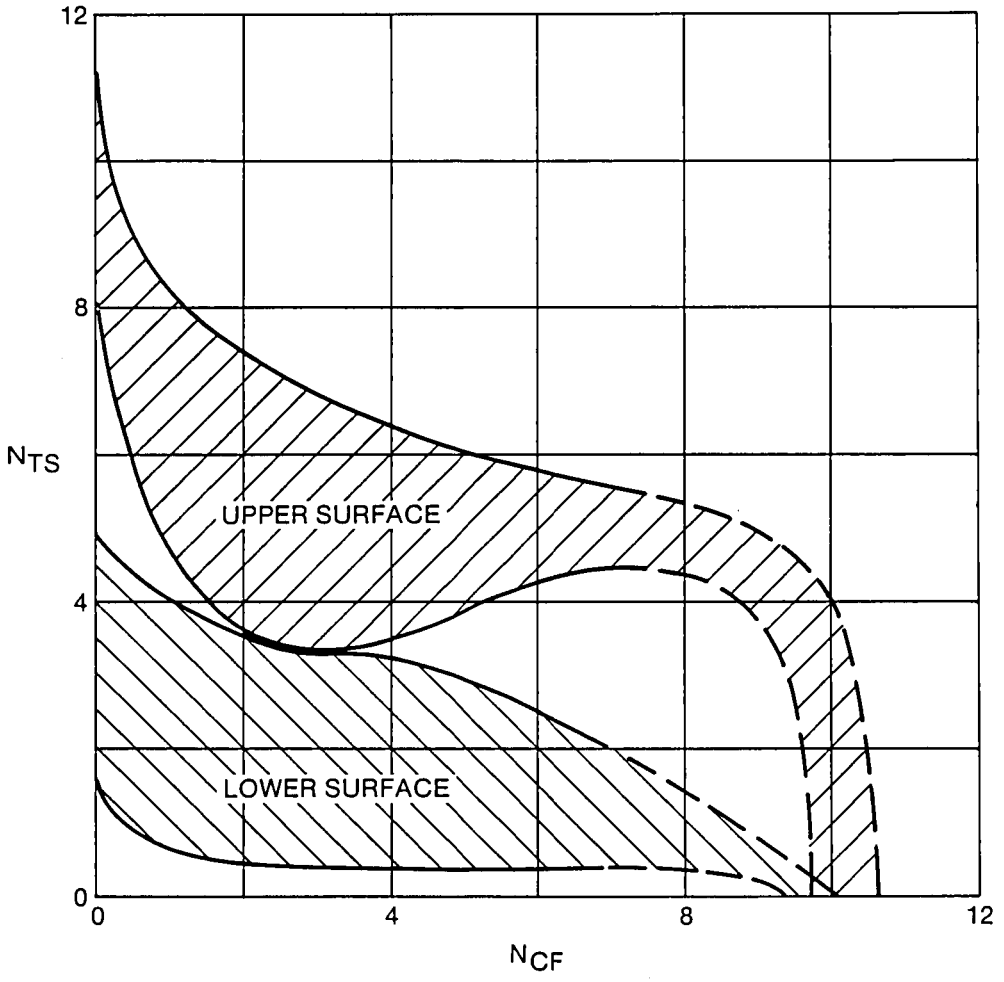

Fig. 48 F-111 Transition Data, Reference 3

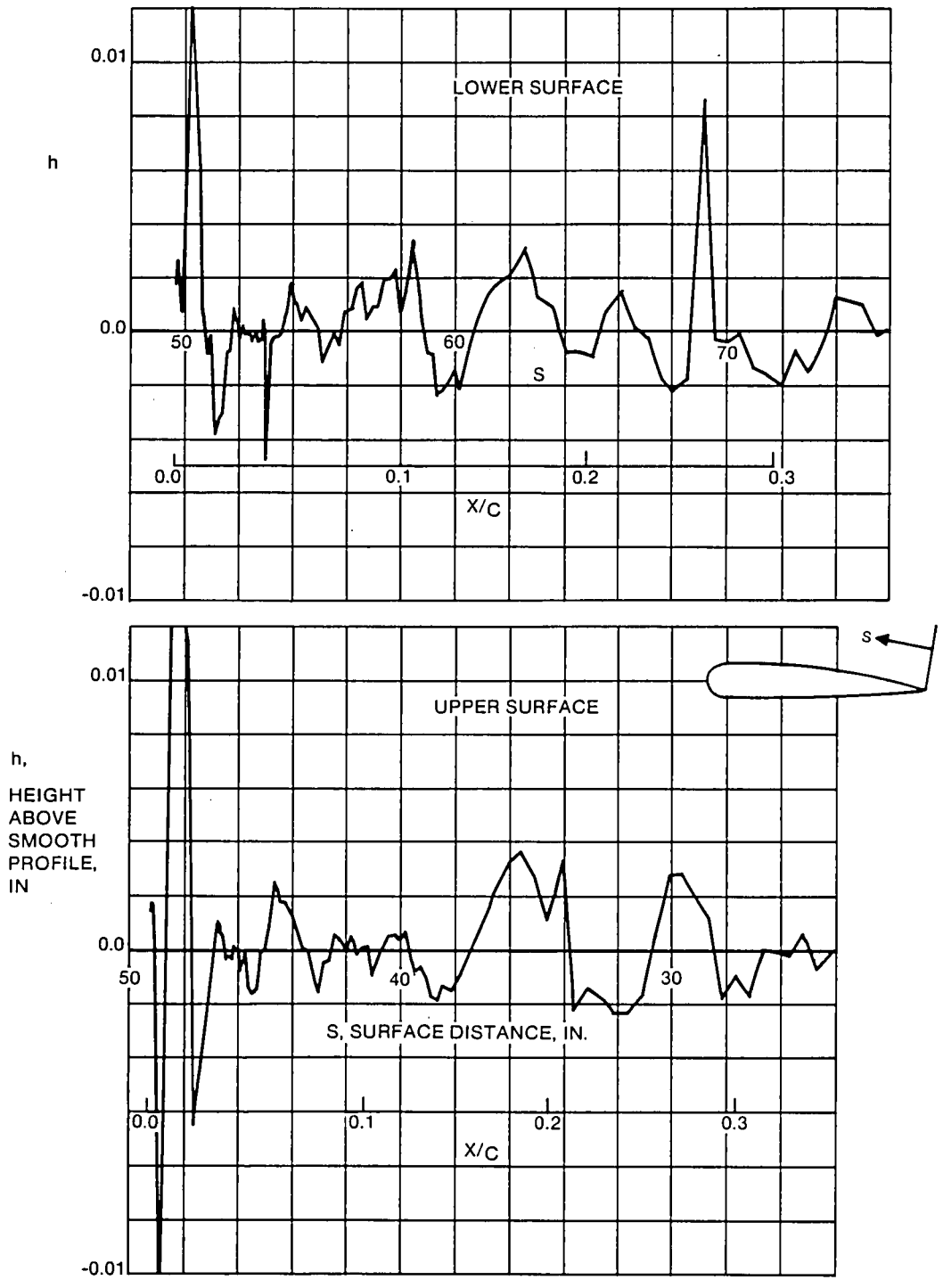

Figure 49. Waviness of Wing Section 141

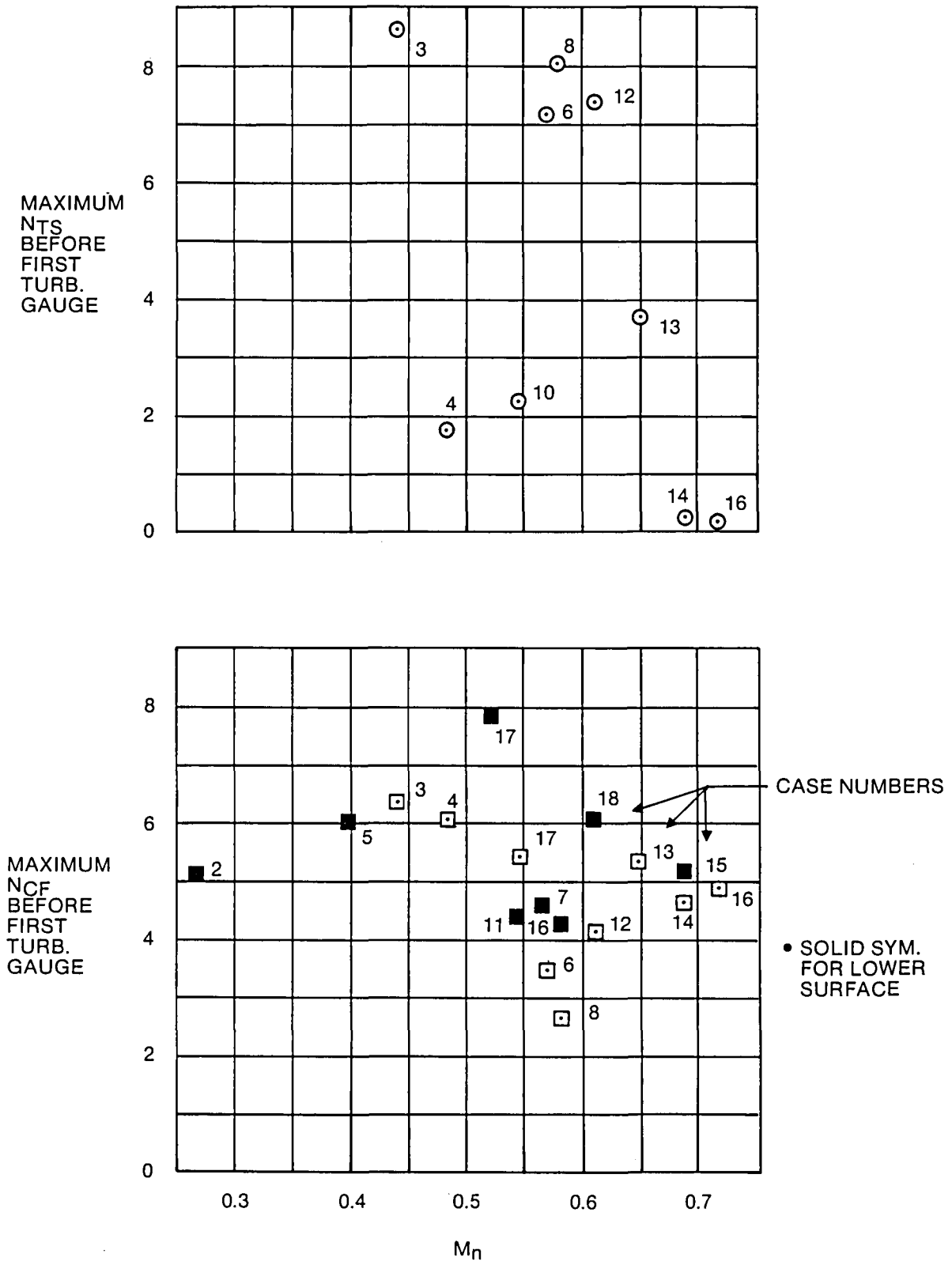

Fig. 50 Maximum Instability Growth Variation With Normal Mach Number

1. Report No.	2. Government Accession No.	3. Recipient's Catalog No.
NASA CR-3975		

4. Title and Subtitle	5. Report Date
Natural Laminar Flow Flight Experiments on a Swept Wing Business Jet—Boundary Layer Stability Analyses	May 1986
	6. Performing Organization Code
7. Author(s)	8. Performing Organization Report No.
Rodger A. Rozendaal, Boeing Commercial Airplane Co.	D6-53071
9. Performing Organization Name and Address	10. Work Unit No.
Wichita State University Wichita, KS 67208	
	11. Contract or Grant No.
	NAG1-401
	13. Type of Report and Period Covered
12. Sponsoring Agency Name and Address	Contractor Report, Sept. 1983 through March 1985
National Aeronautics and Space Administration Washington, DC 20546	14. Sponsoring Agency Code
	505-61-41-02

15. Supplementary Notes

This work was performed under subcontract to Boeing Commercial Airplane Company, Contract No. 84-151, Langley Technical Monitor: Bruce J. Holmes.

16. Abstract

This report contains the linear boundary layer stability analyses and their correlation with data of 18 cases from a natural laminar flow (NLF) flight test program using a Cessna Citation III business jet. The transition point varied from 5% to 35% chord for these conditions, and both upper and lower wing surfaces were included. Altitude varied from 10,000 to 43,000 ft and Mach number from 0.3 to 0.8. Four cases were at nonzero sideslip.

Although there was much scatter in the results, the analyses of boundary layer stability at the 18 conditions led to the conclusion that crossflow instability was the primary cause of transition. However, the sideslip cases did show some interaction of crossflow and Tollmien-Schlichting disturbances. The lower surface showed much lower Tollmien-Schlichting amplification at transition than the upper surface, but similar crossflow amplifications. No relationship between Mach number and disturbance amplification at transition could be found.

The quality of these results is open to question from questionable wing surface quality, inadequate density of transition sensors on the wing upper surface, and an unresolved pressure shift in the wing pressure data. The results of this study show the need for careful preparation for transition experiments. Preparation should include flow analyses of the test surface, boundary layer disturbance amplification analyses, and assurance of adequate surface quality in the test area. The placement of necessary instruments and usefulness of the resulting data could largely be determined during the pretest phase.

17. Key Words (Suggested by Author(s))	18. Distribution Statement
Boundary layer Crossflow disturbances Flight test Linear stability theory Natural laminar flow (NLF) Tollmien-Schlichting Disturbances	Subject Category 02 Unclassified—Unlimited

19. Security Classif. (of this report)	20. Security Classif. (of this page)	21. No. of Pages	22. Price
Unclassified	Unclassified	100	A05

For sale by the National Technical Information Service, Springfield, Virginia 22161

NASA-Langley, 1986

End of Document